

Contract No. NAS 7-505

(Period 5 July 1966 to 5 October 1967)

A STUDY TO ANALYZE THE PERMEATION OF HIGH DENSITY GASES
AND PROPELLANT VAPORS THROUGH SINGLE LAYER TEFLON OR
TEFLON STRUCTURE MATERIALS AND LAMINATIONS

INTERIM FINAL PROGRESS REPORT


25 October 1967

07282-6016-R000

Prepared for:


NASA Western Operations Office
Pasadena, California

Prepared by:


R. L. Johnson, Project Manager
Advanced Technology Department

Approved by:


P. G. Bhuta, Manager
Advanced Technology Department


M. V. Barton, Manager
Engineering Mechanics Laboratory

TRW Systems
One Space Park
Redondo Beach, California

ACKNOWLEDGMENT

The work reported herein was carried out by TRW Systems for the NASA Western Operations Office under Contract No. NAS 7-505. The contract was monitored for NASA Western Operations Office by the Jet Propulsion Laboratory, Pasadena, California. The Technical Manager for the Jet Propulsion Laboratory was Mr. Donald L. Young. Mr. Richard Weiner, also of the Jet Propulsion Laboratory, advised with the experimental aspects of the program.

The project manager for the contractor was Dr. R. L. Johnson of the Advanced Technology Department, Engineering Mechanics Laboratory. The analytical part of the program was carried out by Dr. Johnson with the assistance of Dr. F. W. Thomas, also of the Advanced Technology Department. The numerical programming was carried out by Mr. J. E. Melde and Mr. D. E. Coats of the Computation and Data Reduction Center. The experimental part of the program was under the direction of Mr. L. J. Van Nice of the Chemistry Department, Chemistry and Materials Laboratory. Mr. Van Nice was assisted by Mr. H. M. Hoffman in performance of the experiments and the interpretation of the data.

ABSTRACT

This report contains the results of a fifteen month analytical and experimental study of the leakage rate of the pressurant gases (N_2 , He) and the propellant vapors (N_2O_4 , N_2H_4) through bladder structures consisting of two layers of Teflon separated by a metallic foil diffusion barrier containing microscopic or larger holes.

Results were obtained for the steady state leakage rate through circular holes and long rectangular openings in the barrier for arbitrary thicknesses of the two Teflon layers. The effect of hole shape and relative hole position on the leakage rate were studied. The transient problem was analyzed and it was shown that steady state calculations are adequate for estimating the leakage rate. A computer program entitled "Diffusion Analyzer Program" was developed to calculate the leakage rate, both transient and steady state. Finally, the analytical results were compared to experimentally determined values of the leakage rate through a model laminated bladder structure. The results of the analysis are in good agreement with experiment.

The experimental effort (Part II of the Bladder Permeation Program) measured the solubility, diffusion coefficient and permeability of helium, nitrogen and nitrogen tetroxide vapor through Teflon TFE and FEP membranes. Data were obtained in the temperature range of 25 to 100°C at pressures ranging from near vacuum to about 20 atmospheres. Results of the experimental effort were compared with the limited data previously reported. As a verification to the applicability of results to actual bladder systems, counter diffusion tests were performed with a laminated sample containing aluminum foil with a selected group of holes.

TABLE OF CONTENTS

| | Page |
|--|------|
| 1.0 INTRODUCTION | 1-1 |
| 1.1 <u>Description of the Problem</u> | 1-1 |
| 1.2 <u>Multicomponent Counter Diffusion in Teflon</u> | 1-2 |
| 1.3 <u>Leakage Through Laminated Bladder Structures</u> | 1-5 |
| 1.4 <u>Investigations Carried Out Under Part I</u> <u>of the Study</u> | 1-9 |
| 2.0 STEADY STATE LEAKAGE THROUGH LAMINATED BLADDER STRUCTURES | 2-1 |
| 2.1 <u>Leakage Rate Through Two Layers of Permeable</u> <u>Material With One Circular Hole in the Barrier</u> | 2-1 |
| 2.2 <u>Leakage Rate Through Two Layers of Permeable</u> <u>Material With an Infinite Slit in the Barrier</u> | 2-11 |
| 2.3 <u>Effective Area of Influence of Holes</u> | 2-19 |
| 2.4 <u>Leakage Through Periodic Slits</u> | 2-23 |
| 2.5 <u>Effect of Hole Shape on Leakage Rate</u> | 2-28 |
| 3.0 STEADY STATE LEAKAGE THROUGH HOLES IN METAL FOIL BARRIERS | 3-1 |
| 3.1 <u>Leakage Through a Circular Hole in a Metal Foil</u> <u>Separating Pressurant Gas From Liquid Propellant</u> | 3-1 |
| 3.2 <u>Effect of the Teflon Coating on Leakage</u> | 3-8 |
| 4.0 TRANSIENT LEAKAGE THROUGH BLADDER STRUCTURES | 4-1 |
| 4.1 <u>Approximate Calculation of the Transient Period</u> <u>for a Laminated Bladder with a Circular Hole</u> <u>in the Barrier</u> | 4-2 |
| 4.2 <u>Further Remarks on the Transient Problem</u> | 4-9 |
| 5.0 INSPECTION TECHNIQUES FOR DETERMINING THE PRESENCE OF MICROSCOPIC HOLES IN METAL FOIL | 5-1 |
| 6.0 SUMMARY OF ANALYTICAL RESULTS | 6-1 |
| 6.1 <u>Summary of Results</u> | 6-1 |
| 6.2 <u>Comparison of Calculated with the Experimentally</u> <u>Measured Leak Rate</u> | 6-2 |
| 6.3 <u>Suggestions for Further Study</u> | 6-6 |
| 7.0 EXPERIMENTAL EFFORT | 7-1 |

TABLE OF CONTENTS (cont)

| | | |
|-------|--|------|
| 8.0 | TECHNICAL DISCUSSION | 8-1 |
| 8.1 | <u>Adsorption Tests</u> | 8-1 |
| 8.2 | <u>Permeation Tests</u> | 8-5 |
| 8.2.1 | <u>Unidirectional Permeation</u> | 8-8 |
| 8.2.2 | <u>Counter Diffusion</u> | 8-12 |
| 9.0 | RESULTS | 9-1 |
| 9.1 | <u>Solubility Data</u> | 9-2 |
| 9.2 | <u>Diffusion Coefficients</u> | 9-5 |
| 9.3 | <u>Permeability Constants</u> | 9-10 |
| 9.4 | <u>Summary of Results</u> | 9-18 |
| 9.4.1 | <u>Helium Permeation</u> | 9-18 |
| 9.4.2 | <u>Nitrogen Permeation</u> | 9-20 |
| 9.4.3 | <u>Nitrogen Tetroxide Permeation</u> | 9-21 |
| 9.5 | <u>Leakage Through Holes</u> | 9-25 |
| 10.0 | REFERENCES | 10-1 |
| | Appendix A | A-1 |
| | Appendix B | B-1 |
| | Appendix C | C-1 |

1.0 INTRODUCTION

1.1 Description of the Problem

The objective of this program was to study the leakage of pressurant gases and propellant vapors through bladder structures composed of laminates of Teflon and thin sheets of stainless steel or aluminum foil serving as a diffusion barrier. As a result of pin-holes developed during manufacture and cracks which appear due to failure during flexure, the barriers are never perfect. If the barrier had no openings there would not be any leakage since the common pressurant gases as well as propellant vapors are not soluble to any degree in aluminum or stainless steel. Consequently, the purpose of the study can be stated as the calculation of the leakage rate through laminated bladder structures having holes in the diffusion barrier.

A typical such laminated bladder structure consists of one layer of Teflon exposed to the pressurant gas, another exposed to the propellant, with a sheet of aluminum or stainless steel about 1 mil thick placed between. When there is an opening in the barrier, pressurant gas dissolves in the Teflon layer on the gas side and diffuses through the Teflon to the opening. It streams through the opening, or diffuses through, depending on whether or not the opening is filled with Teflon and dissolves in the other layer of Teflon. Subsequently, it diffuses through this layer of Teflon to the liquid side. Assuming no formation of gas between the liquid and the Teflon, the gas leaving the Teflon is dissolved in the liquid propellant and is transported by diffusion to the far reaches of the propellant. The driving force for this process is the gradient of the chemical potential, or the Gibbs free energy of the gas in solution. It can usually be stated as being merely due to the existence of a concentration gradient. Simultaneously, and by the same process, the propellant diffuses through the bladder into the pressurant gas space.

Obviously, the problem, if taken in all its complexity, is quite difficult. A complete solution to the problem would require that one consider diffusion in the gas space, in the first Teflon layer, and through more than one irregularly shaped and spaced opening in the

barrier, followed by diffusion through the other Teflon layer, and then finally through the liquid propellant. In addition one must consider that propellant in molecular form simultaneously diffuses in the opposite direction, and that in general, the two diffusion processes are coupled, that is, the mass flux vector for the flow of the gas through the Teflon depends not only on the gradient of the concentration of the gas in Teflon but on that of the propellant as well. It seems reasonable to assume, however, that adequate engineering results can be obtained using a somewhat simplified model. The model adopted is discussed in the following sections along with its justification.

1.2 Multicomponent Counter Diffusion in Teflon

The flow of one chemical component (the solute) in dilute solution in a second component (the solvent) obeys Ficks' Law⁽¹⁾, as is well known. According to this law, the mass flux vector of the solute or the net amount of solute crossing unit area in unit time is proportional to the gradient of the concentration of the solute in the solution composed of the mixture of solute and solvent. Thus

$$\hat{j} = -\rho D \nabla c \quad (1.2.1)$$

where \hat{j} denotes the mass flux vector, ρ the density of the solution, c the concentration of the solute in the solution, and D is the diffusion coefficient. The units of concentration chosen are those of mass fraction, i.e., $c_i = \rho_i / \rho$, where ρ_i is the grams/cm³ of species i present and ρ is the total gms/cm³ of the mixture, $\rho = \sum_i \rho_i$. Combining eq. (1.2.1) with the law of conservation of the mass of the solute

$$\rho \frac{\partial c}{\partial t} = -\nabla \cdot \hat{j} \quad (1.2.2)$$

leads to the diffusion equation for a two component mixture

$$\rho \frac{\partial c}{\partial t} = \nabla \cdot \rho D \nabla c \quad (1.2.3)$$

Equation (1.2.1) is valid for dilute solutions, in the absence of temperature gradients, pressure gradients, and chemical reactions. Thus eq. (1.2.3) is subject to the same restrictions. In fact both temperature gradient diffusion and pressure gradient diffusion are very small effects so that for practical purposes eq. (1.2.3) is valid in the presence of quite large temperature and pressure gradients. The presence of a chemical reaction leads to a source term on the right side of eq. (1.2.3).

When there are more than two components present, eq. (1.2.1) is more complex. The flow of component i depends on the gradient of the concentration of the other components present as well as that of component i ⁽²⁾.

$$\hat{j}_i = -\sum_{j=1}^{n-1} \rho D_{ij} \nabla c_j \quad (1.2.4)$$

Thus in a mixture composed of pressurant gas with concentration c_1 , propellant with concentration c_2 , and solid of concentration $1 - c_1 - c_2$, we have

$$\hat{j}_1 = -\rho D_{11} \nabla c_1 - \rho D_{12} \nabla c_2 \quad (1.2.5)$$

$$\hat{j}_2 = -\rho D_{21} \nabla c_1 - \rho D_{22} \nabla c_2 \quad (1.2.6)$$

where \hat{j}_1 is the mass flux vector for pressurant gas, \hat{j}_2 that for propellant. The law of conservation of mass then requires two equations

$$\rho \frac{\partial c_1}{\partial t} = \nabla \cdot \rho D_{11} \nabla c_1 + \nabla \cdot \rho D_{12} \nabla c_2 \quad (1.2.7)$$

$$\rho \frac{\partial c_2}{\partial t} = \nabla \cdot \rho D_{21} \nabla c_1 + \nabla \cdot \rho D_{22} \nabla c_2 \quad (1.2.8)$$

The coefficients D_{12} and D_{21} are called cross diffusion coefficients by some writers. The numbers D_{11} and D_{22} are the direct diffusion coefficients.

It is not possible to demonstrate theoretically the relative magnitudes of the cross diffusion and the direct diffusion effects. This can only be done by the actual measurement of all four coefficients which would be an expensive and time consuming task. Instead, it will be assumed that the coupling between the two diffusive flows is negligible so that the concentration of each component obeys an equation of the form of (1.2.3). Thus we assume that the pressurant gas diffuses through the Teflon in one direction entirely independent of the presence of the pressurant diffusing in the opposite direction and conversely. Physically, one would expect a coupling to exist when the two components compete to a significant degree for the available lattice vacancies. Thus for dilute solutions, neglect of coupling effects should not lead to any serious error.

This assumption can be tested experimentally by measuring the permeation rate for a given component in the absence of any counter-diffusing component and when one is present and comparing the two results. This was carried out as part of the experimental part of this program. It was found that the permeation rate of the pressurant gases was increased by the presence of counter diffusing N_2O_4 , while that of N_2O_4 decreased. The direct diffusion coefficients can, however, be adjusted to account for the effect to within the accuracy of the data.

In the diffusion of N_2O_4 through Teflon some chemical reaction apparently take place leading to swelling and discoloration of the Teflon. This effect could probably be accounted for by a direct diffusion coefficient which depends both on time and concentration of N_2O_4 in Teflon. No effort was made under this contract to include these effects in measured values of the diffusivity. However, the span of time over which D varies is probably small compared to times of interest for long term space missions so that sufficiently accurate calculations can be made using the asymptotic value of D (the diffusivity).

Finally it should be noted that leakage through the Teflon could be due to leakage through capillaries in the Teflon, that is, Knudsen's flow, in addition to diffusion. Such a transport process would not

obey the diffusion equation. Experiments carried out under this program, however, have found no evidence for the occurrence of such a process. (See Part II)

1.3 Leakage Through Laminated Bladder Structures

Suppose that a plane laminated bladder structure separates the gas and propellant spaces within a tank as shown in figure (1.1).

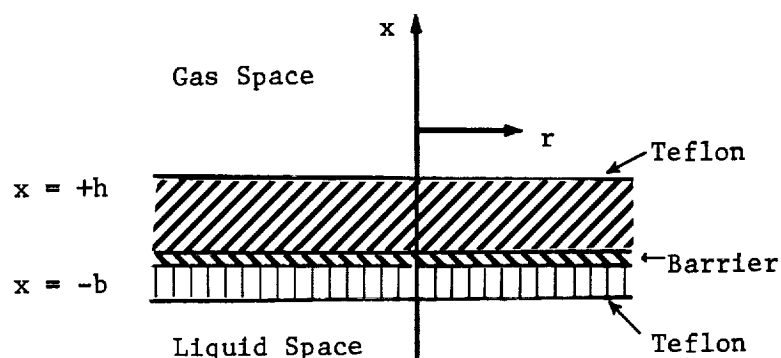


Figure (1.1)

Let subscript 1 denote the diffusing component under consideration, for example, pressurant gas, leaking through the bladder into the propellant. As a result of the above assumptions concerning the diffusion of gas through the Teflon, we can write the following differential equations for the concentration c_1 of the diffusing component.

In the gas space:

$$\frac{\partial c_1}{\partial t} = D_g \nabla^2 c_1 \quad h < x < \infty \quad (1.3.1)$$

In the first Teflon layer:

$$\frac{\partial c_1}{\partial t} = D_1 \nabla^2 c_1 \quad 0 < x < h \quad (1.3.2)$$

In the second Teflon layer:

$$\frac{\partial c_1}{\partial t} = D_2 \nabla^2 c_1 \quad -b < x < 0 \quad (1.3.3)$$

In the liquid propellant:

$$\frac{\partial c_1}{\partial t} = D_\ell \nabla^2 c_1 \quad -\infty < x < -b \quad (1.3.4)$$

Here subscript D_g refers to the diffusion coefficient of pressurant gas through a solution of pressurant gas and propellant molecules which have leaked through the bladder. D_1 is that for gas through the first layer of Teflon, D_2 for the second and D_ℓ is that for pressurant gas through liquid propellant. The barrier, for convenience, is considered to have zero thickness. This assumption will not affect the accuracy of the calculations provided eqs. (1.3.2) and 1.3.3) are connected by the correct boundary conditions across the openings in the barrier.

For finite gas and propellant spaces, the above equations have, strictly speaking, no non-trivial steady state solution. The pressurant gas, for example, leaks through the bladder structure into the liquid space, its concentration in the liquid space constantly increasing with time, until the entire liquid body becomes saturated with propellant gas. That is, the entire system reaches thermodynamic equilibrium, after which there is no longer any mass flux of either pressurant or propellant. However, for the nearly perfect barriers in which we are primarily interested, the openings are small and the leakage rate is also small. Quasi-steady state solutions are then possible which give a finite leak rate because the change in the concentration of the solute with time in either the pressurant or propellant space is very slow compared to the relaxation time of the bladder structure itself. Further, for small (microscopic) openings in the barrier, the region over which the distribution of concentration varies is very small compared with the volume of either the pressurant gas space or the liquid propellant space. These spaces may then, for purposes of calculation, be considered as semi-infinite space separated by a permeable bladder structure.

In Part I - Appendix A, it is shown that under certain conditions the gas and liquid spaces are ignorable in solving eqs. (1.3.1 - 1.3.4). The total system is then replaced by one which considers only diffusion within the two Teflon layers, the concentration of solute being held at

a constant value on one surface and at zero value on the other. The conditions required are essentially that the permeation rates through the gas and liquid of the solute be much larger than that through the Teflon. Based on order of magnitude estimates of the diffusion parameters of gas through gas and gas through liquid and the values measured under this program for Teflon, the conditions seem to be well satisfied. The above system of equations are then replaced by

$$\frac{\partial c_1}{\partial t} = D_1 \nabla^2 c_1 \quad 0 < x < h \quad (1.3.5)$$

$$\frac{\partial c_2}{\partial t} = D_2 \nabla^2 c_2 \quad -b < x < 0 \quad (1.3.6)$$

where we now denote by c_2 the concentration of solute in Teflon layer two for convenience. The boundary conditions can now be chosen as

$$c_1 = c_0 = \kappa_1 p_0 \quad (x = h) \quad (1.3.7)$$

and

$$c_2 = 0 \quad (x = -b) \quad (1.3.8)$$

and the conditions of thermodynamic equilibrium⁽³⁾ and conservation of diffusing particles across any opening in the barrier. κ_1 is the solubility of solute in material 1 and p_0 is the total system pressure. Outside the openings in the barrier the diffusive fluxes must vanish. The last condition is stated mathematically as

$$\left. \frac{\partial c_1}{\partial x} \right|_{x=0} = \left. \frac{\partial c_2}{\partial x} \right|_{x=0} = 0 \quad (1.3.9)$$

whenever (x,y) the coordinates in the plane lie outside the region of an opening in the barrier. Conservation of diffusing particles within the opening requires

$$\rho_1 D_1 \left. \frac{\partial c_1}{\partial x} \right|_{x=0} = \rho_2 D_2 \left. \frac{\partial c_2}{\partial x} \right|_{x=0} \quad (1.3.10)$$

whenever (x,y) lies inside the region of the opening. Here ρ_1 and ρ_2 refer to the total density of materials 1 and 2 respectively.

The condition of thermodynamic equilibrium at the interface between the two materials requires that the thermodynamic potential of the solute be equal at the interface. For dilute solutions of pressurant gas or propellant in solids the thermodynamic potential takes the form⁽⁴⁾

$$\mu = RT \ln c + f(p, T) \quad (1.3.11)$$

when μ is the thermodynamic potential (Gibbs' Free Energy), R is the gas constant, T the temperature and $f(p, T)$ denotes a function of the pressure and temperature. From eq. (1.3.11) the condition of equilibrium is

$$RT \ln c_1 + f_1(p, T) = RT \ln c_2 + f_2(p, T)$$

or

$$\frac{c_1}{c_2} = e^{-\{f_1(p, T) - f_2(p, T)\}/RT} = \frac{e^{-f_1/RT}}{e^{-f_2/RT}} \quad (1.3.12)$$

The right side of eq. (1.3.12) is however just the ratio of the Henry Law solubility of component 1 in material 1 to that in material 2. Denoting the solubility by κ we have

$$\frac{c_1}{c_2} = \frac{\kappa_1}{\kappa_2} = \gamma \quad (1.3.13)$$

as the condition of thermodynamic equilibrium at the interface between materials 1 and 2.

Equations (1.3.7) through (1.3.13) indicate that the physical parameters needed to specify the leakage rate through a structure composed of two laminates of Teflon are the solubility and the diffusivity of the solute in each Teflon laminate. Since these quantities were not available in the literature, it was one of the objectives of this program to experimentally obtain these quantities as a function of pressure and temperature. The results of that phase of the program are reported in Part II.

2.0 STEADY STATE LEAKAGE THROUGH LAMINATED BLADDER STRUCTURES

As was stated in section 1.3 steady state calculations of the leak rate through a laminated bladder structure are meaningful because for small leak rates the mean concentration of the diffusing species in either the pressurant or propellant tank changes significantly only over periods of the order of days whereas the transient period for a typical bladder structure is of the order of a few hours. Thus over long periods of time the concentration on the boundary of the bladder does not change appreciably so that the leakage rate can be calculated by assuming the concentration is constant. By assuming a maximum value of the concentration on one side, zero on the other, an upper bound for the steady state leak rate is obtained. Such results will be useful for engineering purposes and have the advantage of being conservative, that is, they give the maximum leak rate.

2.1 Leakage Rate Through Two Layers of Permeable Material With One Circular Hole in the Barrier

This problem was worked out and reported in great detail in references 5 and 6 and will therefore only be outlined here. Consider Figure 2.1 which is a schematic of the cross-section of a laminated bladder structure containing a circular hole in the barrier foil of radius a . The concentration of the solute is held at c_0 everywhere on the upper boundary, $c_2 = 0$ everywhere on the lower boundary.

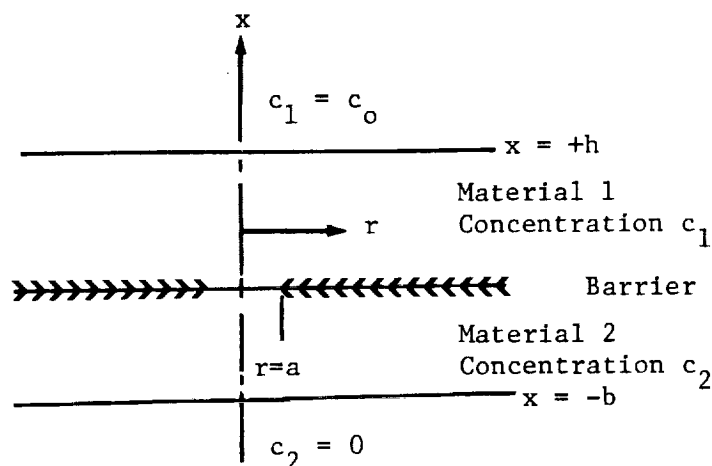


Figure 2.1

As a consequence of the assumption of independent diffusion of the various species through the bladder material, the steady state concentration of any given species obeys Laplace's Equation. This follows from the usual diffusion equation by setting the time derivative equal to zero. If $c_1(r,x)$ is the concentration of the diffusing species in medium 1, $c_2(r,x)$ that in medium 2, then in cylindrical coordinates

$$\nabla^2 c_1 = \frac{\partial^2 c_1}{\partial r^2} + \frac{1}{r} \frac{\partial c_1}{\partial r} + \frac{\partial^2 c_1}{\partial x^2} = 0 \quad (0 \leq x \leq h) \quad (2.1.1)$$

and

$$\nabla^2 c_2 = \frac{\partial^2 c_2}{\partial r^2} + \frac{1}{r} \frac{\partial c_2}{\partial r} + \frac{\partial^2 c_2}{\partial x^2} = 0 \quad (-b \leq x \leq 0) \quad (2.1.2)$$

On the surface, $x = h$, the concentration $c_1(r,h)$ must go to a constant value, while on $x = -b$, $c_2(r,-b)$ is to vanish. Thus,

$$c_1(r,h) = c_o \quad (\text{all } r) \quad (2.1.3)$$

$$c_2(r,-b) = 0 \quad (\text{all } r) \quad (2.1.4)$$

At the interface between the two materials there must be no diffusive flow except within the radius of the hole. Thus the presence of the barrier is simulated by

$$\frac{\partial c_1}{\partial x} = 0 \quad x = 0, r > a \quad (2.1.5)$$

and

$$\frac{\partial c_2}{\partial x} = 0 \quad x = 0, r > a \quad (2.1.6)$$

Within the radius of the hole the conditions to be satisfied are

$$c_1(r,0) = \gamma c_2(r,0) \quad (x = 0, r < a) \quad (2.1.7)$$

$$D_1 \frac{\partial c_1(r,0)}{\partial x} = D_2 \frac{\partial c_1(r,0)}{\partial x} \quad (x = 0, r < a) \quad (2.1.8)*$$

Equations (2.1.7) and (2.1.8) state, respectively, that the concentrations in the adjoining materials within the radius of the hole are proportional, and that the number of particles is conserved (conservation of mass). The proportionality of c_1 and c_2 requires the assumption of thermodynamic equilibrium at the interface between the two materials. The proportionality constant, γ , is known as Nernst's constant and is equal to the ratio κ_1/κ_2 of the solubilities of the solute in the two materials. It is not strictly constant but depends on temperature and pressure, principally the temperature⁽⁴⁾. Finally, note that c_0 in eq. (2.1.3) is not the concentration of diffusing component (i.e., He gas) in the space above $x = h$, but is the equilibrium concentration of this substance in material 1 when it is exposed to a bath of pure diffusing component. Thus, c_0 must be calculated from thermodynamic equilibrium data which will be obtained experimentally.

For convenience, we solve not for $c_1(r,x)$ in region 1, but for the function $\psi(r,x)$ defined by

$$\psi(r,x) = c_0 - c_1(r,x) \quad (2.1.9)$$

This function has the advantage of vanishing at $x = h$, and enables one to avoid the use of non-convergent integrals. Obviously, it satisfies Laplace's equation,

$$\frac{\partial^2 \psi}{\partial r^2} + \frac{1}{r} \frac{\partial \psi}{\partial r} + \frac{\partial^2 \psi}{\partial x^2} = 0 \quad 0 < x < h \quad (2.1.10)$$

*We assume the two Teflon materials have the same density, $\rho_1 = \rho_2$. The results are easily modified to include the more general case.

Taking the zero-order Handel Transform of Equation (2.1.10) removes the r dependence. The transform is defined as

$$\psi(k, x) = \int_0^{\infty} \psi(r, x) r J_0(kr) dr \quad (2.1.11)$$

Using eq. (2.1.11) in eq. (2.1.10) gives as the differential equation obeyed by $\psi(k, x)$

$$\frac{d^2 \psi}{dx^2} - k^2 \psi(k, x) = 0 \quad (2.1.12)$$

The solution to this equation which vanishes at the boundary $x = h$ is

$$\psi(k, x) = A_1(k) \frac{\sinh k(h-x)}{\sinh kh} \quad (2.1.13)$$

where $A_1(k)$ is an unknown function of k . Of course, the denominator of eq. (2.1.13) can be absorbed in the function $A_1(k)$ if desired. By the inversion theorem for Hankel transforms,

$$\psi(r, x) = \int_0^{\infty} k A_1(k) \frac{\sinh k(h-x)}{\sinh kh} J_0(kr) dk \quad (2.1.14)$$

so that

$$c_1(r, x) = c_0 - \int_0^{\infty} k A_1(k) \frac{\sinh k(h-x)}{\sinh kh} J_0(kr) dk \quad (2.1.15)$$

In the same manner it is found that the solution for $x < a$ is given by

$$c_2(r, x) = \int_0^{\infty} k A_2(k) \frac{\sinh k(b+x)}{\sinh kb} J_0(kr) dk \quad (2.1.16)$$

The two sets of boundary conditions (2.1.5), (2.1.6) and (2.1.8) can be combined to state that

$$D_1 \frac{\partial c_1}{\partial x} = D_2 \frac{\partial c_2}{\partial x}, \quad x = 0 \quad (2.1.17)$$

for all r . Application of this condition to eqs. (2.1.15) and (2.1.16) then gives

$$D_1 \int_0^\infty k^2 A_1(k) \operatorname{ctnh} kh J_0(kr) dk = D_2 \int_0^\infty k^2 A_2(k) \operatorname{ctnh} kb J_0(kr) dk \quad (2.1.18)$$

Since this equation is valid for all r , the Hankel inversion theorem states that

$$D_1 A_1(k) \operatorname{ctnh} kh = D_2 A_2(k) \operatorname{ctnh} kb$$

or

$$A_2(k) = \frac{D_1}{D_2} \frac{\operatorname{ctnh} kh}{\operatorname{ctnh} kb} A_1(k) \quad (2.1.19)$$

for all k . Using now the condition, eq. (2.1.7) and eq. (2.1.19) we find that for $r < a$,

$$\int_0^\infty \frac{k A_1(k)}{\tanh kh} \left(\tanh kh + \frac{\gamma D_1}{D_2} \tanh kb \right) J_0(kr) dk = c_0 \quad (2.1.20)$$

while for $r > a$, from eq. (2.1.5),

$$\int_0^\infty \frac{k^2 A_1(k)}{\tanh kh} J_0(kr) dk = 0 \quad (2.1.21)$$

The latter equation being required in order that the current vanish for $r > a$. Putting

$$\frac{k^2 A_1(k)}{\tanh kh} = f(k)$$

reduces eqs. (2.1.20) and (2.1.21) to the pair

$$\int_0^\infty \frac{f(k)}{k} \left(\tanh kh + \frac{\gamma D_1}{D_2} \tanh kb \right) J_0(kr) dk = c_0, \quad (r < a) \quad (2.1.22)$$

$$\int_0^\infty f(k) J_0(kr) dk = 0, \quad r > a \quad (2.1.23)$$

Substituting $\rho = \frac{r}{a}$, $k = \frac{u}{a}$, $\alpha = \frac{h}{a}$ and $\beta = \frac{b}{a}$ we have the set

$$\int_0^\infty \frac{f(u)}{u} \left(\tanh \alpha u + \frac{\gamma D_1}{D_2} \tanh \beta u \right) J_0(\rho u) du = c_0 \quad \rho < 1 \quad (2.1.24)$$

and

$$\int_0^\infty f(u) J_0(\rho u) du = 0 \quad \rho > 1 \quad (2.1.25)$$

These two equations are of the form

$$\int_0^\infty G(u) f(u) J_0(\rho u) du = c_0 \quad \rho < 1 \quad (2.1.26)$$

$$\int_0^\infty f(u) J_0(\rho u) du = 0 \quad \rho > 1 \quad (2.1.27)$$

where

$$G(u) = \frac{1}{u} \left(\tanh \alpha u + \frac{\gamma D_1}{D_2} \tanh \beta u \right) \quad (2.1.28)$$

A general method of solution, due to Tranter⁽⁷⁾, is available for this type of dual integral equations. It is based on the fact that if $f(u)$ is expanded as a series of Bessel functions of ascending order, eq. (2.1.27) is identically satisfied. The coefficients in the expansion have then to be chosen so that eq. (2.1.26) is satisfied. The procedure is complex, however, and can only be carried out to yield closed form solutions in a few cases. Putting

$$f(u) = u^{1-k} \sum_{m=0}^{\infty} a_m J_{2m+k}(u) \quad (2.1.29)$$

eq. (2.1.27) is satisfied due to the discontinuous nature of the resulting integrals. The substitution of eq. (2.1.29) into eq. (2.1.26) leads to an infinite set of linear inhomogeneous equations for the expansion coefficients a_m . Tranter presents an iterative technique for solving these equations which works well in some cases. A slight modification of his technique works well in this case also so long as α and β are large. Large α and β corresponds to the case where the thickness of the permeable laminate is much greater than the hole radius. This is a practically important case.

The details of the calculation of the coefficients a_m and subsequently the leak rate are given in reference 6. Here we quote and discuss the result for the total flow rate W which is given by

$$\begin{aligned}
W = & 4D_1 a \rho \left(\frac{c_o}{1 + (\gamma D_1/D_2)} \right) \left\{ 1 + \frac{2 \ell n 2}{\pi} \frac{1}{1 + (\gamma D_1/D_2)} \left(\frac{a}{h} + \frac{\gamma D_1}{D_2} \frac{a}{b} \right) \right. \\
& + \left(\frac{2 \ell n 2}{\pi} \right)^2 \left(\frac{1}{1 + (\gamma D_1/D_2)} \right)^2 \left[\frac{a^2}{h^2} + \left(\frac{\gamma D_1}{D_2} \right)^2 \frac{a^2}{b^2} \right] \\
& + \left[\left(\frac{2 \ell n 2}{\pi} \right)^3 \left(\frac{1}{1 + (\gamma D_1/D_2)} \right)^3 - \frac{\zeta(3)}{4\pi} \frac{1}{1 + (\gamma D_1/D_2)} \right] \frac{a^3}{h^3} \\
& + \frac{\gamma D_1}{D_2} \left[\left(\frac{2 \ell n 2}{\pi} \right)^3 \left(\frac{1}{1 + (\gamma D_1/D_2)} \right)^3 \left(\frac{\gamma D_1}{D_2} \right)^2 - \frac{\zeta(3)}{4\pi} \frac{1}{1 + (\gamma D_1/D_2)} \right] \frac{a^3}{b^3} \\
& + 2 \left(\frac{2 \ell n 2}{\pi} \right)^2 \left(\frac{1}{1 + (\gamma D_1/D_2)} \right)^2 \frac{\gamma D_1}{D_2} \frac{a^2}{hb} \\
& \left. + 3 \left(\frac{2 \ell n 2}{\pi} \right)^3 \left(\frac{1}{1 + (\gamma D_1/D_2)} \right)^3 \frac{\gamma D_1}{D_2} \left(\frac{a^3}{h^2 b} + \frac{\gamma D_1}{D_2} \frac{a^3}{hb^2} \right) \right\} \quad (2.1.30)
\end{aligned}$$

accurate to terms of third degree.

The quantity $W/4D_1 a c_o \rho$ depends on three parameters. These are the ratios a/h , a/b , and the factor $\gamma D_1/D_2$. Figure 2.2 shows a typical set of curves for various values of $y = b/h$, the ratio of the thickness of the two slabs and for $\gamma D_1/D_2 = 0.5$. The parameter $\gamma D_1/D_2$ is, in fact, the ratio of the permeability of material 1 to material 2. A more complete set of curves is available in the Design Guide⁽⁹⁾.

The result is expected to be valid for ratios of hole diameter to laminate thickness as large as 0.5, perhaps even larger. The reason for this is that eq. (2.1.30) is not very sensitive to the terms nonlinear in a/h or a/b since the coefficient of these terms is small compared to that of the linear terms. The quantity $\zeta(3)$ in eq. (2.1.30) denotes the Riemann Zeta function of argument 3.0 and has the value 1.202 nearly.

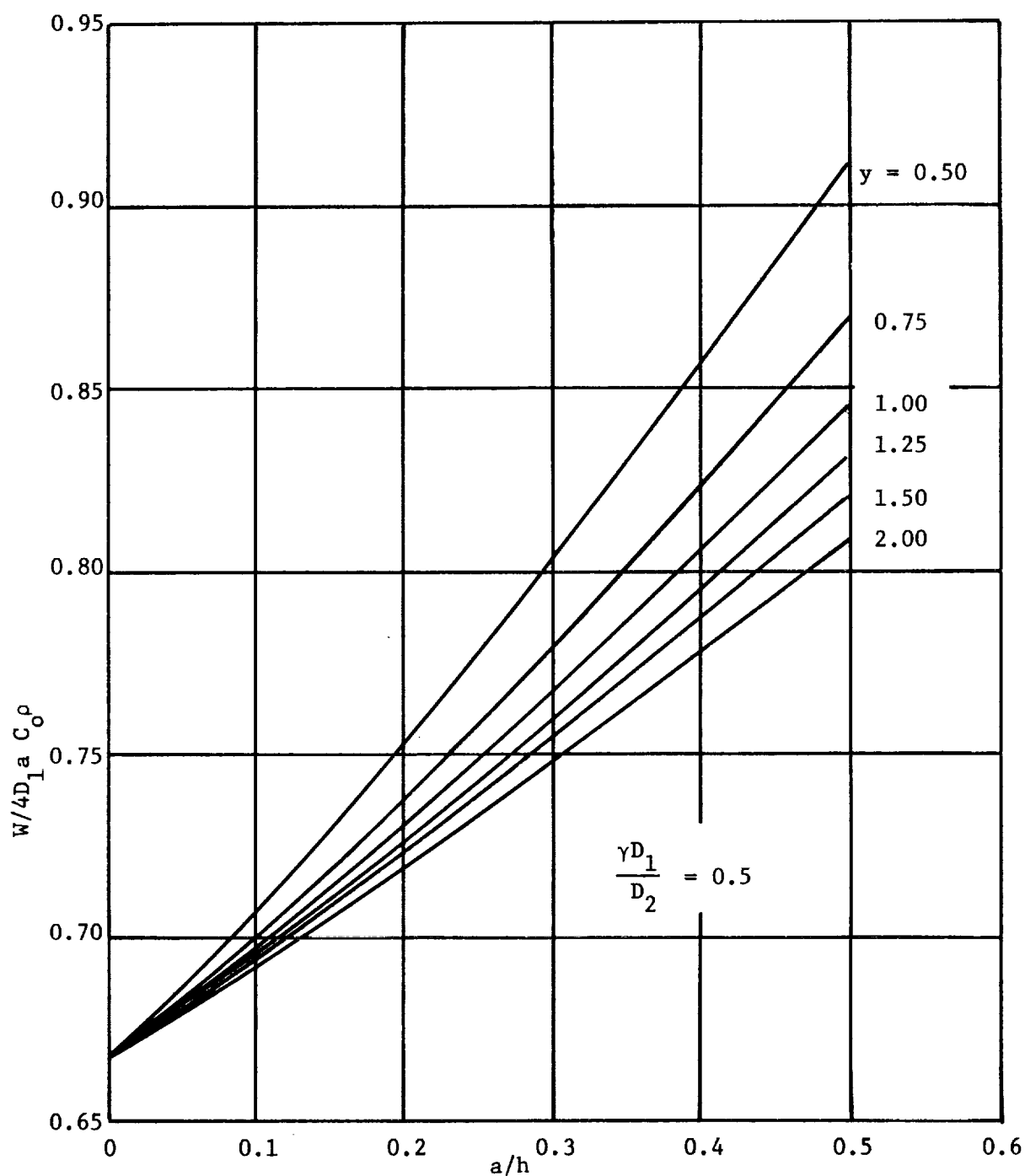


Figure 2.2 Dependence of Flow Rate on the Ratio of Hole Radius to Slab Thickness

Nomenclature:

| | | | |
|------------|-----------------------------|--------|--|
| a | hole radius | W | mass flow rate |
| h | Teflon thickness, side 1 | ρ | Teflon density |
| b | Teflon thickness, side 2 | C_0 | Concentration of diffusion gas absorbed by Teflon at Teflon-gas space interface, dimensions of mass of gas per unit mass of Teflon |
| y | ratio of Teflon thicknesses | | |
| D_1, D_2 | diffusion coefficients | | |
| γ | ratio solubility constants | | |

To use the results to calculate W , the total flow rate per unit time, one must have the value of γ , the two diffusion coefficients, the hole radius, and the thickness of the two slabs. In addition, one needs to know the value of the concentration c_0 , on one surface. If, for example, it is desired to calculate the leakage of Nitrogen pressurant gas through the bladder structure to the propellant side, the value of c_0 is obtained from the Henry law constant and the pressure of the gas by $c_0 = \kappa_1 p$, where κ_1 is the Henry law constant for material 1 and p is the pressure of the gas pressurant. The constant γ is the ratio of the two Henry law constants for the two permeable materials, that is, $\gamma = \kappa_1 / \kappa_2$.

Given γ and the two diffusion coefficients one can estimate the parameter $\gamma D_1 / D_2$. From the known value of a/h , the ratio of hole radius to gas side slab thickness, and $y = b/h$, the ratio of the liquid side slab thickness to that of the gas side one, the quantity $W/4D_1 a c_0 \rho$ can be obtained from the curves.

If the value of $\gamma D_1 / D_2$ does not exactly match any of the plotted values, linear interpolation between two charts can be used. From the numerical value of $W/4D_1 a c_0 \rho$ thus obtained, one obtains the value of W . The value of ρ in $W/4D_1 a c_0 \rho$ refers to the density of the solvent, that is, the permeable material. It has been assumed that the density of the two layers is the same (eq. 2.1.8). If not, we replace D_1 by $\rho_1 D_1$ and D_2 by $\rho_2 D_2$ in the expression $1 + \gamma D_1 / D_2$ which appears in eq. (2.1.30) and replace ρ by ρ_2 in $W/4D_1 a c_0 \rho$.

2.2 Leakage Rate Through Two Layers of Permeable Material With an Infinite Slit in the Barrier

In the preceding section the problem of the leakage rate through a bladder structure composed of two laminates of permeable material separated by an impermeable barrier with one circular hole was solved. The solution obtained was rigorous provided the radius of the hole is less than the thickness of either laminate. The only other simple geometry is obtained when the opening is an infinite slit. Such an opening corresponds to the real case of a rectangular opening which is very narrow so that the effects of the ends can be neglected.

It has not been possible to find a rigorous solution to this problem in the manner used for circular openings in section 2.1, although several attempts were made. An approximate solution can be constructed however by assuming a form for the leakage current across the slit opening and equating the average concentration values on each side of the slit proportioned by the ratio of the solubilities. A good assumption for the form of the leakage current is that for leakage through a slit into a semi-infinite medium. By comparing the results of such a calculation with those obtained using the digital computer, we can assess the validity of the assumption. The analytical calculations have advantages over those obtained using the digital program since the results can be tabulated in terms of dimensionless parameters as for a circular hole and will be available without the expense and effort of a computer run for any given case. Further, the assumptions stated above are quite reasonable so that the results are not expected to differ significantly from those of a more rigorous solution.

A cross section of the structure is shown in figure (2.3). The

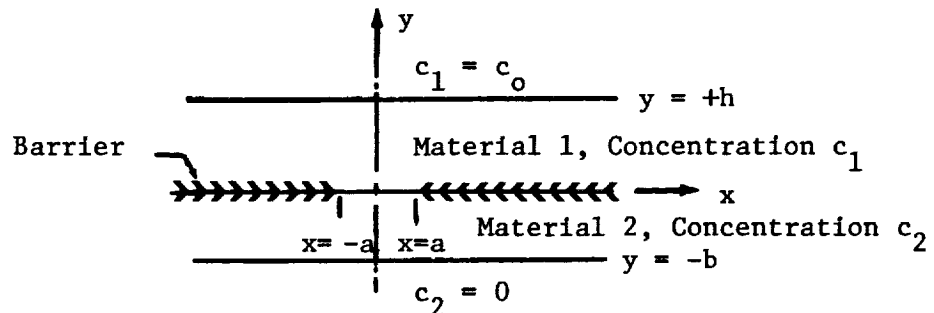


Figure 2.3

width of the slit is $2a$. In material 1, for $y > 0$, the concentration of the solute c_1 satisfies Laplace's equation in two dimensions

$$\frac{\partial^2 c_1}{\partial x^2} + \frac{\partial^2 c_1}{\partial y^2} = 0 \quad (2.2.1)$$

and takes on the boundary condition $c_1 = c_0$ at $y = +h$ for all x . Specification of the flow through the slit leads to a complete solution for $y > 0$. Along $y = 0$ we put

$$\begin{aligned} \rho_1 D_1 \frac{\partial c_1(x, 0)}{\partial y} &= w(x) , & |x| < a \\ &= 0 & |x| > a \end{aligned} \quad (2.2.2)$$

As stated above, the form of $w(x)$ for flow into or out of a semi-infinite medium through a slit of width $2a$ is $w(x) \propto 1/\sqrt{a^2 - x^2}$. We determine the proportionality constant so that the integral of $w(x)$ over the width of the slit is equal to the total steady state flow rate W (gms/sec per unit depth of slit). Since

$$\int_{-a}^{+a} w(x) dx = \int_{-a}^{+a} \frac{dx}{\sqrt{a^2 - x^2}} = \pi$$

this is accomplished by putting

$$w(x) = \frac{W}{\pi} \frac{1}{\sqrt{a^2 - x^2}} \quad (2.2.3)$$

The second boundary condition then reads

$$\begin{aligned} \rho_1 D_1 \frac{\partial c_1(x, 0)}{\partial y} &= \frac{W}{\pi} \frac{1}{\sqrt{a^2 - x^2}} & |x| < a \\ &= 0 & |x| > a \end{aligned} \quad (2.2.4)$$

As in section 2.1, replace c_1 by $c_0 - \psi(x,y)$. The conditions satisfied by $\psi(x,y)$ are

$$\frac{\partial^2 \psi}{\partial x^2} + \frac{\partial^2 \psi}{\partial y^2} = 0 \quad (2.2.5)$$

$$\psi(x,h) = 0 \quad (2.2.6)$$

$$-\rho_1 D_1 \frac{\partial \psi(x,0)}{\partial y} = \frac{W}{\pi} \frac{1}{\sqrt{a^2 - x^2}} \quad \begin{array}{l} |x| < a \\ |x| > a \end{array} \quad (2.2.7)$$

Since the problem is completely symmetrical about $x = 0$, the Fourier cosine transform can be employed. This is defined as

$$c_1(k,y) = \int_0^\infty c_1(x,y) \cos kx \, dx$$

with inverse

$$c_1(x,y) = \frac{2}{\pi} \int_0^\infty c_1(k,y) \cos kx \, dk$$

The cosine transform of $\psi(x,y)$ satisfies

$$\frac{d^2 \psi(k,y)}{dy^2} - k^2 \psi(k,y) = 0 \quad (2.2.8)$$

with solution vanishing on $y = h$,

$$\psi(k,y) = A_1(k) \frac{\sinh k(h-y)}{\sinh kh} \quad (2.2.9)$$

Taking the cosine transform of eq. (2.2.7) gives

$$\rho_1 D_1 \int_0^{\infty} \frac{\partial \psi(x,0)}{\partial y} \cos kx \, dx = -\frac{W}{\pi} \int_0^a \frac{\cos kx \, dx}{\sqrt{a^2 - x^2}}$$

The left hand side is $\rho_1 D_1 \frac{d\psi(k,0)}{dy}$ while the value of the right side is $-\frac{W}{2} J_0(ka)$ where $J_0(ka)$ is the zero order Bessel Function⁽⁸⁾. Using eq. (2.2.9) we obtain

$$\rho_1 D_1 k A_1(k) \operatorname{ctnh} kh = \frac{W}{2} J_0(ka) \quad (2.2.10)$$

from which

$$\psi(k,y) = \frac{W}{2\rho_1 D_1} \frac{\tanh kh}{k} J_0(ka) \frac{\sinh k(h-y)}{\sinh kh} \quad (2.2.11)$$

Taking the inverse transform gives $c_1(x,y)$.

$$c_1(x,y) = c_0 - \frac{W}{\rho_1 D_1 \pi} \int_0^{\infty} \tanh kh \frac{\sinh k(h-y)}{\sinh kh} J_0(ka) \cos kx \frac{dk}{k} \quad (2.2.12)$$

The value of W cannot be determined from this result. It must be calculated by obtaining a similar result for $y < 0$ and then requiring that the concentrations be proportional within the slit opening.

The solution for $c_2(k,y)$ which vanishes at $y = -b$ is

$$c_2(k,y) = A_2(k) \frac{\sinh k(b+y)}{\sinh kb} \quad (2.2.13)$$

Again the condition given by eq. (2.2.4) must be satisfied which gives

$$A_2(k) = \frac{W}{2\rho_2 D_2} \frac{\tanh kb}{k} J_0(ka) \quad (2.2.14)$$

and upon using the value of $A_1(k)$ and applying the inversion theorem we obtain

$$c_2(x,y) = \frac{W}{\rho_2 D_2 \pi} \int_0^{\infty} \tanh kb \frac{\sinh k(b+y)}{\sinh kb} J_0(ka) \cos kx \frac{dk}{k} \quad (2.2.15)$$

The flow rate W is now determined by requiring that

$$c_1(x, 0) = \gamma c_2(x, 0) \quad 0 \leq x \leq a \quad (2.2.16)$$

as in section 2.1, where γ is the ratio of the permeabilities of the two materials. From eqs. (2.2.12) and (2.2.15) we obtain

$$\begin{aligned} c_o &= \frac{W}{\pi \rho_1 D_1} \int_0^\infty \tanh kh J_o(ka) \cos kx \frac{dk}{k} \\ &= \gamma \frac{W}{\pi \rho_2 D_2} \int_0^\infty \tanh kh J_o(ka) \cos kx \frac{dk}{k} \quad 0 \leq x \leq a \end{aligned} \quad (2.2.17)$$

Clearly this will lead to a unique determination of W only if the integrals in eqs. (2.2.17) are independent of x in the interval $0 \leq x \leq a$. That this is not the case can be determined from the value of the integrals for small h and b . In that case $\tanh kh$ can be replaced in the integral by kh and the value of the resulting integral is $h/\sqrt{a^2 - x^2}$ for $0 \leq x \leq a$. The only way out of this difficulty is to average the equation over the slit opening by integrating out x . This gives

$$\begin{aligned} c_o &= \frac{W}{\pi a \rho_1 D_1} \int_0^\infty \tanh kh J_o(ka) \sin ka \frac{dk}{k^2} \\ &= \gamma \frac{W}{\pi a \rho_2 D_2} \int_0^\infty \tanh kh J_o(ka) \frac{dk}{k^2} \end{aligned} \quad (2.2.18)$$

which is independent of x . Solving for W gives

$$W = \frac{\pi a \rho_1 D_1 c_o}{\int_0^\infty \left(\tanh kh + \gamma \frac{\rho_1 D_1}{\rho_2 D_2} \tanh kh \right) J_o(ka) \frac{\sin ka}{k^2} dk} \quad (2.2.19)$$

The integrals are evaluated in Part 1, Appendix B by the Theory of Residues. The integrals are of the same type and depend only on either h and a or b and a . Using the result obtained in Appendix B, we find

$$W = \frac{2a\rho_1 D_1 c_o}{h \left(1 - \frac{2}{\pi} G\left(\frac{a}{h}\right)\right) + \frac{\gamma\rho_1 D_1}{\rho_2 D_2} b \left(1 - \frac{2}{\pi} G\left(\frac{a}{b}\right)\right)} \quad (2.2.20)$$

as the leakage rate in mass per unit time per unit length through a bladder composed of two laminates of thickness h and b respectively with a slit of width $2a$ in the barrier. The function G is given by

$$G(\alpha) = \sum_{n=0}^{\infty} \frac{I_0 \left[\left(n + \frac{1}{2}\right) \pi \alpha \right]}{\left(n + \frac{1}{2}\right)^2} e^{-\left(n + \frac{1}{2}\right) \pi \alpha} \quad (2.2.21)$$

when I_0 denotes the zero order modified Bessel function.

The quantity $(2a\rho_1 D_1 c_o) / [h + (\gamma\rho_1 D_1 / \rho_2 D_2)b]$ is the leakage rate through a two laminate bladder of width $2a$ and unit depth in the absence of a barrier. In order for the expression (2.3.20) for the leakage rate to give the correct value for $a \gg h$; $a \gg b$ it is necessary that G vanish for large values of the argument a/h ; a/b . This is indeed the case (See Appendix B).

Figure 2.4 shows a typical curve of $W/\rho_1 D_1 c_o$ plotted as a function of the ratios a/h and $y = b/h$. A more complete collection of such curves will be found in reference 9. Note that for a given value of $\gamma\rho_1 D_1 / \rho_2 D_2$ and y the curves become linear in a , the slit half width, when a/h is of the order of 0.5. This indicates that when the total width of the slit, $2a$, is of the order of the laminate thickness the effect of slit edge effects are negligible and the leakage rate can be calculated using the formula quoted above for leakage through a strip composed of two permeable slabs without a barrier, the width of the strip, of course, being $2a$. Since the results were obtained by an approximate method we have compared them with numerical calculations using the Diffusion Analyzer Program, DAP. Figure 2.5 gives a comparison of the two results. It can be seen that the approximate analysis is quite adequate.

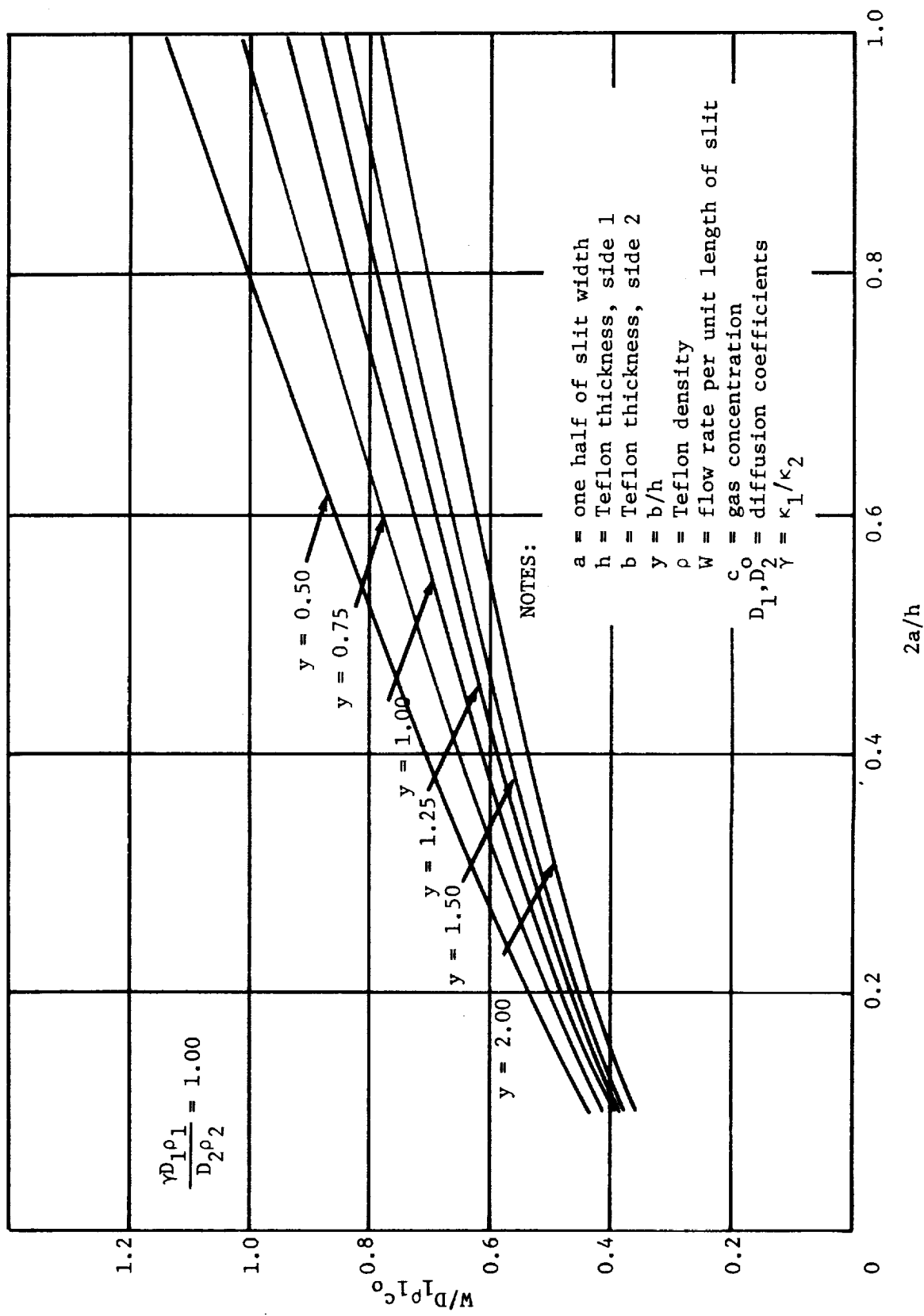


Figure 2.4 Diffusion Rates Through Laminated Bladder with Infinite Slit in Barrier

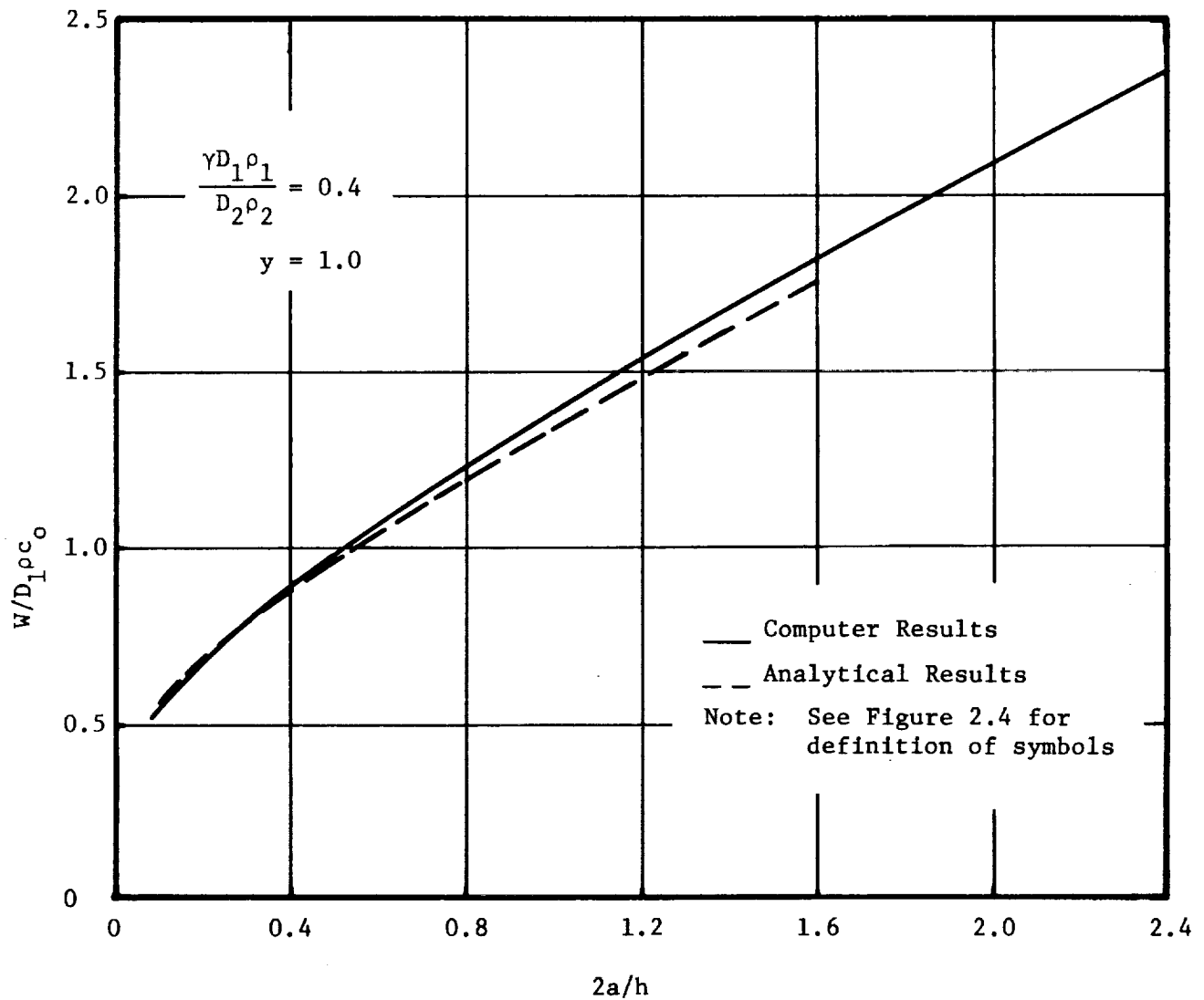


Figure 2.5 Comparison of Computer Results with Analytical Results for N_2 Flow Through Laminated Bladder with Infinite Slit in Barrier

2.3 Effective Area of Influence of Holes

Calculations of the leakage rate through a single hole in the barrier can be used for multiple holes provided these holes are sufficiently far apart. The calculation of section 2.1 can be used to determine the distance by which circular holes must be separated in order that leakage through two holes can be considered independent.

Referring to section (2.1), the concentration in the upper material (material 1) is given by

$$c_1(r,x) = c_o - \psi(r,x) \quad (2.3.1)$$

and from eq. (2.1.14) ψ is given by

$$\psi(r,x) = \int_0^\infty k A_1(k) \frac{\sinh k(h-x)}{\sinh kh} J_0(kr) dk \quad (2.3.2)$$

when the value of $A_1(k)$ is known from reference 6. If there were no hole in the barrier the concentration throughout material 1 would equal c_o . Therefore the radius at which $\psi(r,o)$ effectively vanishes is a good measure of the area effected by the hole. Inserting the value of $A_1(k)$ from reference 6 we have

$$\begin{aligned} \psi(r,o) = \int_0^\infty k A_1(k) J_0(kh) dk &= a_o a^{1/2} \int_0^\infty \frac{\tanh kh}{k^{1/2}} J_{1/2}(ka) J_0(kr) dk \\ &+ a_1 a^{1/2} \int_0^\infty \frac{\tanh kh}{k^{1/2}} J_{5/2}(ka) J_0(kr) dk \end{aligned} \quad (2.3.3)$$

Since a_1 is much smaller than a_o and also the second integral is smaller than the first, we can write

$$\psi(r,o) = a_o a^{1/2} \int_0^\infty \frac{\tanh kh}{k^{1/2}} J_{1/2}(ka) J_0(kr) dk \quad (2.3.4)$$

closely. Since $J_{1/2}(ka) = \sqrt{\frac{2}{\pi}} \frac{\sin ka}{(ka)^{1/2}}$, eq. (2.3.4) is equivalent to

$$\psi(r,0) = \sqrt{\frac{2}{\pi}} a_0 \int_0^\infty \frac{\tanh kh}{k} \sin ka J_0(kr) dk \quad (2.3.5)$$

Putting $ka = u$ reduces eq. (2.3.5) to

$$\psi(r,0) = \sqrt{\frac{2}{\pi}} a_0 \int_0^\infty \tanh \beta u \sin u J_0(\gamma u) du \quad (2.3.6)$$

where $\beta = h/a$ and $\gamma = r/a$. Finally, using the expansion

$$\tanh \beta u = 1 + 2 \sum_{s=1}^{\infty} (-1)^s e^{-2s\beta u}$$

gives

$$\psi(r,0) = \sqrt{\frac{2}{\pi}} a_0 \int_0^\infty \left(1 + 2 \sum_{s=1}^{\infty} (-1)^s e^{-2s\beta u} \right) \sin u J_0(\gamma u) \frac{du}{u} \quad (2.3.7)$$

Integrating term by term after interchanging the order of integration and summation gives

$$\begin{aligned} \psi(r,0) &= \sqrt{\frac{2}{\pi}} a_0 \int_0^\infty \sin u J_0(\gamma u) \frac{du}{u} \\ &+ \sqrt{\frac{2}{\pi}} a_0 \sum_{s=1}^{\infty} (-1)^s \int_0^\infty e^{-2s\beta u} \sin u J_0(\gamma u) \frac{du}{u} \end{aligned} \quad (2.3.8)$$

We are interested in $\gamma > 1$. In this case the value of the first term is (8)

$$\sqrt{\frac{2}{\pi}} a_0 \sin^{-1}\left(\frac{a}{r}\right) = \sqrt{\frac{2}{\pi}} a_0 \left[\frac{a}{r} + \frac{1}{6} \frac{a^3}{r^3} + \frac{3}{40} \frac{a^5}{r^5} + \dots \right]$$

The second integral is also known.

$$\int_0^\infty e^{-2s\beta u} \frac{\sin u}{u} J_0(\gamma u) du = \sin^{-1} \left[\frac{2}{\sqrt{4s^2\beta^2 + (1 + \frac{r}{a})^2} + \sqrt{4s^2\beta^2 + (1 - \frac{r}{a})^2}} \right]$$

We thus find

$$\psi(r,0) = \sqrt{\frac{2}{\pi}} a_0 \left[\frac{a}{r} + \frac{1}{6} \frac{a^3}{r^3} + \frac{3}{40} \frac{a^5}{r^5} + \dots \right]$$

$$\sqrt{\frac{2}{\pi}} a_0 \sum_{s=1}^{\infty} (-1)^s \sin^{-1} \left[\frac{2}{\sqrt{4s^2\beta^2 + (1 + \frac{r}{a})^2} + \sqrt{4s^2\beta^2 + (1 - \frac{r}{a})^2}} \right]$$

(2.3.9)

The leading term in a_0 is independent of hole radius and ratio of slab thicknesses to hole radius. Therefore we calculate the ratio $\psi(r,0)/a_0$ as a function of a/r for various values of β . Figure 2.5 shows a plot of $\psi(r,0)/a_0$ as a function of a/r from eq. (2.3.9). It can be seen that the value of this quantity at $a/r = 5.0$ is about 10% of its value at $a/r = 1.0$, the hole edge. This ratio is not strongly dependent on the value β . Therefore, we conclude that 10-20 hole radii should be about the maximum extent over which the effect of a hole is felt. The same conclusion is, of course, valid for the second material.

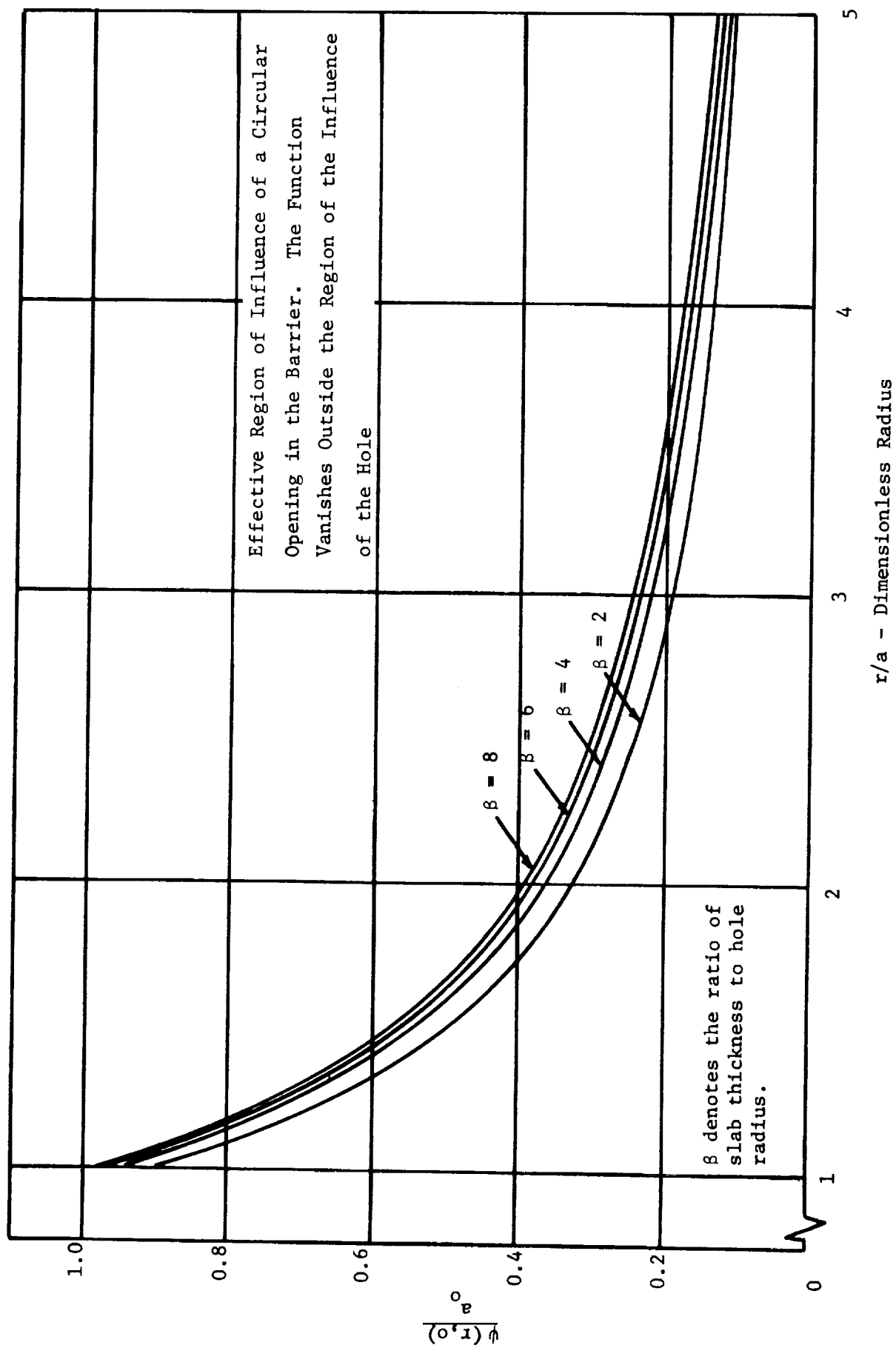


Figure 2.6

2.4 Leakage Through Periodic Slits

There is one other case which can be treated analytically in an approximate manner and which is of interest for determining the effect of adjacent holes on the leakage through each. This is the case of a laminated bladder structure constructed of laminates of permeable material and a barrier with periodic slits. A cross section of such a structure is shown in figure (2.7). The concentration on the barrier side is held at c_0 while that on the opposite side is zero. Each of the slits is of equal width, $2a$, and the intervening barrier is of width $2(d-a)$.

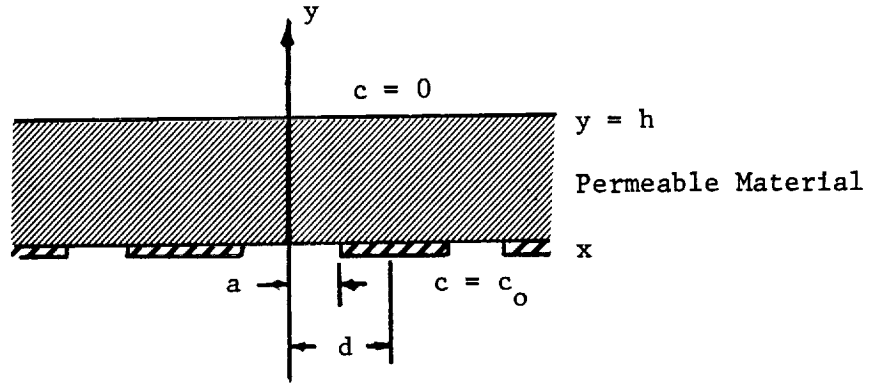


Figure 2.7

The concentration obeys Laplace's Equation in two dimensions (x,y) .

$$\frac{\partial^2 c}{\partial x^2} + \frac{\partial^2 c}{\partial y^2} = 0 \quad (2.4.1)$$

Since the concentration must be a periodic function with period $2d$ we expand $c(x,y)$ as follows:

$$c(x,y) = \sum_{n=0}^{\infty} f_n(y) \cos \frac{n\pi x}{d} \quad (2.4.2)$$

where $f_n(y)$ is an arbitrary function of y . Substitution of eq. (2.4.2) in (2.4.1) and use of the linear independence of the set $\cos \frac{n\pi x}{d}$ gives as the equation of the f_n

$$\frac{d^2 f_n}{dy^2} - \left(\frac{n\pi}{d}\right)^2 f_n(y) = 0 \quad (2.4.3)$$

with solution vanishing on $y = h$ of

$$f_n(y) = A_n \frac{\sinh \frac{n\pi}{d}(h-y)}{\sinh \frac{n\pi h}{d}} \quad (2.4.4)$$

where the A_n are arbitrary constants. Hence

$$c(x,y) = \sum_{n=0}^{\infty} A_n \frac{\sinh \frac{n\pi}{d}(h-y)}{\sinh \frac{n\pi h}{d}} \cos \frac{n\pi x}{d} \quad (2.4.5)$$

The current flow is

$$-\rho D \frac{\partial c(x,0)}{\partial y} = \rho D \sum_{n=0}^{\infty} \frac{n\pi}{d} A_n \frac{\cosh \frac{n\pi h}{d}}{\sinh \frac{n\pi h}{d}} \cos \frac{n\pi x}{d} \quad (2.4.6)$$

The flow rate in the interval $0 \leq x \leq d$ can be expanded in a Fourier cosine series. If W is the total leakage rate through the slit $-a < x < +a$ and if we assume the flow is uniform then $W/2a$ is the local current (per unit depth of bladder). The current vanishes, of course, for $a < x < d$.

$$\frac{W}{2a} = \sum_{n=0}^{\infty} B_n \cos \frac{n\pi x}{d} \quad (2.4.7)$$

where

$$B_0 = \frac{1}{a} \int_0^d \frac{W}{2a} dx = \frac{1}{d} \frac{W}{2a} a = \frac{W}{2d}$$

$$B_n = \frac{2}{d} \int_0^d \frac{W}{2a} \cos \frac{n\pi x}{d} dx = \frac{W}{\pi a} \frac{1}{n} \sin \frac{n\pi a}{d}$$

Therefore

$$\frac{W}{2a} = \frac{W}{2d} + \frac{W}{\pi a} \sum_{n=1}^{\infty} \frac{1}{n} \sin \left(\frac{n\pi a}{d} \right) \cos \left(\frac{n\pi x}{d} \right) \quad (2.4.8)$$

Equating the two expressions for the current gives

$$\begin{aligned} \rho D \left\{ \frac{A_0}{h} + \frac{\pi}{d} \sum_{n=1}^{\infty} n A_n \operatorname{ctnh} \left(\frac{n\pi h}{d} \right) \cos \left(\frac{n\pi x}{d} \right) \right\} \\ = \frac{W}{2d} + \frac{W}{\pi a} \sum_{n=1}^{\infty} \frac{1}{n} \sin \left(\frac{n\pi a}{d} \right) \cos \left(\frac{n\pi x}{d} \right) \end{aligned} \quad (2.4.9)$$

Thus

$$A_0 = \frac{W}{2\rho D} \frac{h}{d} ; \quad A_n = \frac{W}{\pi^2 \rho D} \frac{d}{a} \frac{\sin \left(\frac{n\pi a}{d} \right) \tanh \left(\frac{n\pi h}{d} \right)}{n^2}$$

giving at $y = 0$

$$c(x, 0) = \frac{W}{2\rho D} \frac{h}{d} + \frac{W}{\pi^2 \rho D} \frac{d}{a} \sum_{n=1}^{\infty} \frac{\sin \left(\frac{n\pi a}{d} \right) \tanh \left(\frac{n\pi h}{d} \right)}{n^2} \cos \frac{n\pi x}{d} \quad (2.4.9)$$

We now equate the average value of $c(x, 0)$ over $0 < x < a$ to c_0 , the concentration there. This gives

$$c_0 = \frac{W}{2\rho D} \frac{h}{d} + \frac{W}{\pi^3 \rho D} \frac{d^2}{a^2} \sum_{n=1}^{\infty} \frac{\sin \frac{n\pi a}{d} \tanh \frac{n\pi h}{d}}{n^3} \sin \frac{n\pi a}{d} \quad (2.4.11)$$

Solving for W we obtain

$$W = \frac{2\rho D c_0}{\left[\frac{h}{d} + \frac{2}{\pi^3} \frac{d^2}{a^2} \sum_{n=1}^{\infty} \frac{(\sin \frac{n\pi a}{d})^2 \tanh \left(\frac{n\pi h}{d} \right)}{n^3} \right]} \quad (2.4.12)$$

Since there are $1/2d$ openings per unit length, the leakage rate per unit area of the bladder if we assume a unit length for the depth is

$$W' = \frac{W}{2d} = \frac{\rho D c_0}{\left[h + \frac{2}{\pi^3} \frac{d^3}{a^2} \sum_{n=1}^{\infty} \frac{\sin \left(\frac{n\pi a}{d} \right)^2 \tanh \left(\frac{n\pi h}{d} \right)}{n^3} \right]} \quad (2.4.13)$$

A plot of $W'/\rho Dc_o$ as a function of a/d is shown in figure 2.8. As shown a/d is equal to the percent open area. For these calculations h was fixed at 5 mils and a at 1 mil and d was varied. This is unimportant, however, since $W'/\rho Dc_o$ depends only on the ratio a/d (as well as h/d , h and d). From the plot we draw the following conclusions.

- o For small percent open area the leakage rate increases linearly with a/d and very rapidly. At 15% open area the barrier permits about 60% of the leakage rate without any barrier at all. Thus a barrier which has more than a few percent open area will not be effective. To be really effective a barrier must be about 99% intact.
- o For open areas greater than about 15% the approximately linear dependence of the leakage rate on slit width no longer holds. This is apparently the region in which adjoining slits begin to significantly influence each other since the leakage rate for one slit is proportional to the slit width for large widths. This agrees in order of magnitude with our previous results for circular openings where it was concluded that about 10 hole radii separation was sufficient for non-interference.

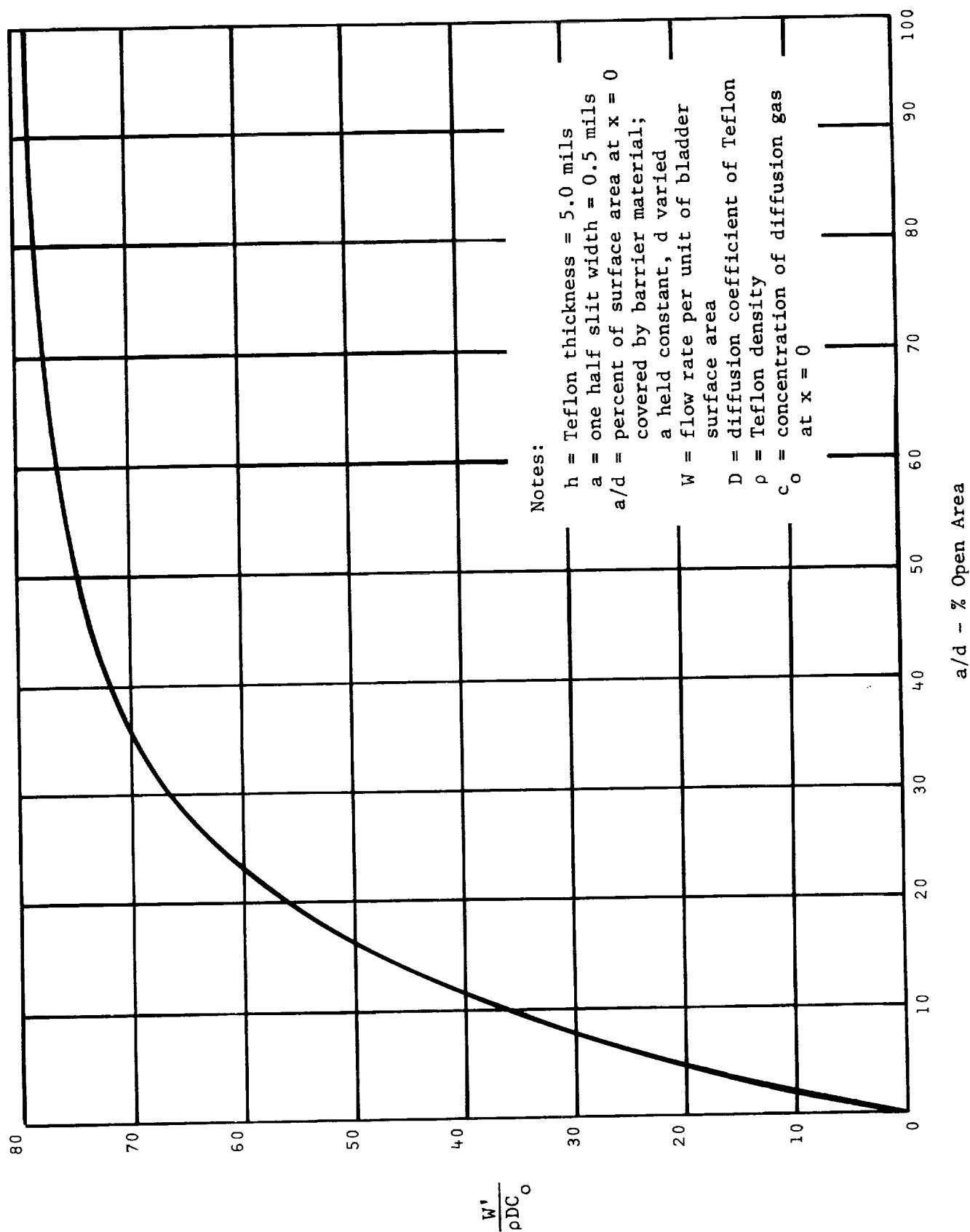


Figure 2.8 Leakage rate for Barrier with Periodic Slit Openings - A Specific Case.

2.5 Effect of Hole Shape on Leakage Rate

Pin holes as well as cracks which appear in the barrier of a laminated bladder structure will not, generally speaking, possess the geometrically regular shapes for which an analysis is possible. It is necessary, therefore, to determine as well as is possible the effect that hole shape itself will have on the leakage rate. To do this we compare the leakage rate through holes of different shape but having the same area. It seems reasonable to expect that the leakage rate will be about the same for holes having roughly similar shape but will diverge for holes which are very dissimilar, for example, a thin crack compared with a circular opening. The results obtained bear out this assertion.

First a comparison of some results obtained using computer program DAP⁽⁹⁾ comparing circular and square holes are given below

Table 2.1

| Hole Size Side or Diameter | Leakage Rate $\frac{\text{gms N}_2}{\text{sec(mil)}^2}$ | |
|-----------------------------------|---|-----------------------|
| | Square Hole | Circular Hole |
| 2 mils | 1.0×10^{-12} | 1.1×10^{-12} |
| 8 mils | 3.7×10^{-13} | 3.9×10^{-13} |

It can be seen that the leakage rate through a square hole and a circular hole of equal area are close enough to each other so that for practical purposes they may be considered the same. The above calculations were obtained for a bladder consisting of two layers of Teflon with Nitrogen gas diffusing. The results, of course, depend only on the geometry and not on the particular solute chosen.

A further comparison can be made using the analytical results of sections (2.1) and (2.2) for circular holes and rectangular slits. A value is chosen for the hole radius, a_h and the leakage rate obtained for typical conditions using the curves for circular holes. A slit

is chosen of width a_s and length ℓ which has the same area as the hole and the leakage rate through this structure obtained from the appropriate curves (Section 2.2). In order for the slit results to be applied to a rectangle it is necessary to choose $\ell \gg a_s$. The results are shown in figure (2.9). The solid line gives the leakage rate through the circular hole and the symbols denote the leakage rate through rectangular slits having length to width ratios of 2, 5 and 10. The values for $\ell = 2a_s$ are somewhat low since these rectangles are not long enough to be considered as infinite slits for which the analysis is valid. This is probably also true of the $\ell = 5a_s$ rectangles but less so. The leakage rate for the $\ell = 10a_s$ case should be accurate to within a few percent.

Figure (2.9) not only gives a comparison between rectangles of various shapes and circles of equal area but also between rectangles of equal area and different ratios of length to width. It appears from the figure that there is only a weak shape dependence for holes up to about 2 mils in radius and rectangles of up to about the same width. For larger holes the longer rectangles, $\ell = 10a_s$, appear to be diverging rapidly in leak rate from the value for circular holes. It appears, then that for holes (~ 1 mil radius) the shape could be changed from hole to square and to a long rectangle ($\ell = 10a_s$) without changing the leakage rate appreciably so long as the area remains fixed. For larger holes there would be a greater variation in the leak rate. However, even for the 3 mil radius hole the change to a rectangle having $\ell = 10a_s$ would only change the leak rate by about 20% (increase).

COMPARISON OF LEAKAGE RATE FOR CIRCULAR HOLES AND RECTANGULAR SLITS OF EQUAL AREA

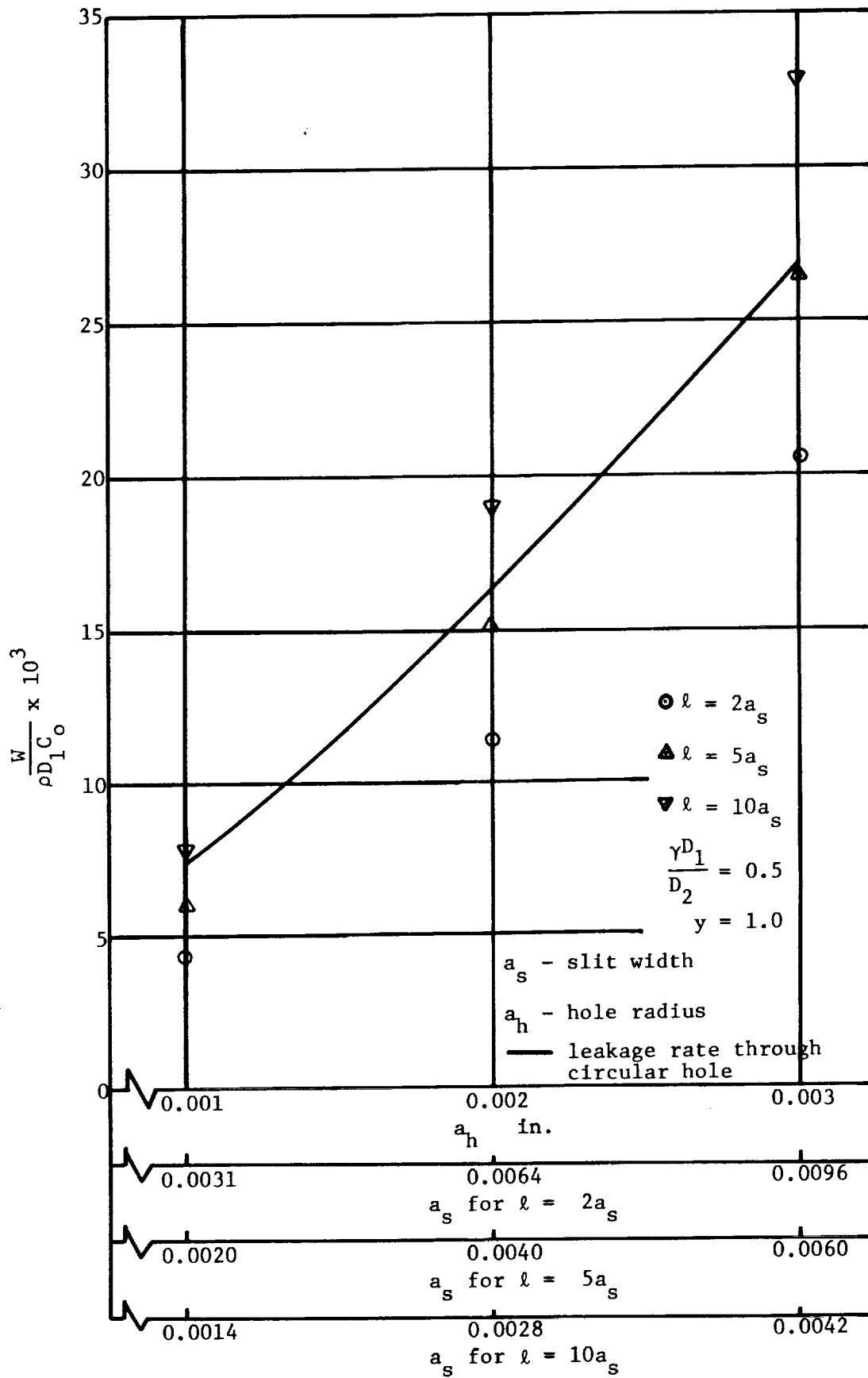


Figure 2.9

3.0 STEADY STATE LEAKAGE THROUGH HOLES IN METAL FOIL BARRIERS

The leakage rate through a laminated bladder structure with a circular hole in the barrier was calculated in section 2.1. In this section we calculate the rate of leakage of pressurant gas into liquid propellant through a circular opening in an uncoated barrier, that is, a barrier consisting only of metal foil. The leakage rate through such a structure has intrinsic interest since this is the simplest type of bladder. The results also afford the opportunity to evaluate the effectiveness of the Teflon coating as an inhibitor of leakage.

3.1 Leakage Through a Circular Hole in a Metal Foil Separating Pressurant Gas From Liquid Propellant

A finite body of liquid propellant is separated from the pressurant gas volume by an impermeable barrier containing one small circular hole of radius a . The total pressure is the same throughout the pressurant gas-liquid propellant container so that there is no net differential pressure across the barrier. Assuming that the hole is formed after the pressurant and propellant are in place, after formation the pressurant gas will be dissolved in the liquid within the radius of the hole and will subsequently diffuse into the body of the liquid. Simultaneously propellant is vaporized into the pressurant gas there and subsequently the vapor diffuses into the body of the pressurant gas. Equilibrium occurs when the total body of liquid is uniformly saturated with dissolved pressurant gas and the pressurant gas everywhere contains propellant vapor with a partial pressure corresponding to the vapor pressure of the liquid at the system temperature.

If the hole in the barrier is small and there are large volumes of gas and liquid present (relative to the dimensions of the hole), it should be possible to obtain a reasonable estimate of the leakage rate by considering the system as infinite with mass flow rate by diffusion between two semi-infinite media connected by a small opening. It will be shown subsequently (Section 4.3) that the mass flow rate obtained in this manner is a good approximation to the actual leakage rate between two finite volumes for most of the time span during which mass flow takes place.

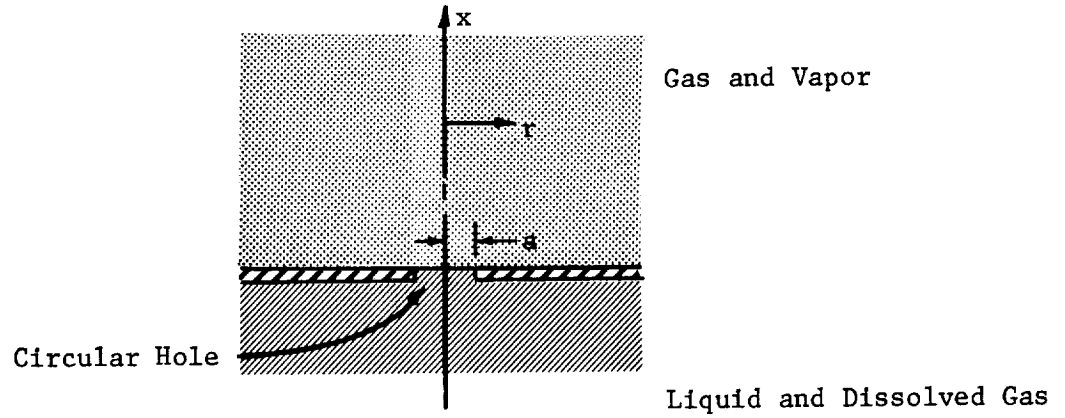


Figure 3.1

Figure 3.1 shows the geometry of the problem to be considered. Considering the vapor-pressurant gas mixture as a perfect gas the partial pressure of the pressurant gas in the gas phase ($x > 0$) obeys the equation (at uniform temperature)

$$\frac{\partial p_1}{\partial t} = D_g \nabla^2 p_1 \quad x > 0 \quad (3.1.1)$$

Within the liquid, the dissolved pressurant gas will constitute only a small fraction of the mass of the mixture. Thus if c_1 is the concentration of pressurant gas in the liquid propellant, $c_1 = \rho_g / (\rho_\ell + \rho_g) = \rho_g / \rho$, the mass fraction c_1 obeys the equation

$$\frac{\partial c_1}{\partial t} = D_\ell \nabla^2 c_1 \quad x < 0 \quad (3.1.2)$$

We have designated by D_g the diffusion coefficient of pressurant gas through the gas-vapor mixture and D_ℓ denotes that for the diffusion of dissolved gas through liquid. The quantity ρ_g refers to the mass of dissolved gas per cm^3 in the gas liquid mixture, ρ_ℓ the mass of liquid per cm^3 there and $\rho = \rho_\ell + \rho_g$ is the mixture density.

The equations (3.1.1) and (3.1.2) must be solved subject to the following boundary conditions. There must be no leakage of gas across the impermeable boundary for $r > a$. Thus for $r > a$ and $x = 0$, since the mass flux vectors are proportional to the gradients of p_1 and c_1 ,

$$\frac{\partial p_1}{\partial x} = \frac{\partial c_1}{\partial x} = 0 \quad (3.1.3)$$

For $r < a$ (and $x = 0$) the mass flux must be continuous. In the liquid the mass flux vector is $-\rho D_\ell \nabla c_1$ and its x component is $-\rho D_\ell (\partial c_1 / \partial x) \hat{i}$ where \hat{i} is a unit vector in direction x . In the gas phase the mass flux vector is $-m_1 D_g \nabla n_1$, with x component, $-m_1 D_g (\partial n_1 / \partial x) \hat{i}$. Here, m_1 is the mass of the pressurant gas molecule and n_1 is the number of such molecules per unit volume. The number of molecules per unit volume is related to the partial pressure (for a perfect gas mixture) by

$$n_1 = \frac{A}{RT} p_1$$

when A is Avogadro's number, R is the gas constant in appropriate units and T is the absolute temperature. The mass flux in terms of the partial pressure is then

$$-m_1 D_g \frac{A}{RT} \frac{\partial p_1}{\partial x} \hat{i} = -\frac{M_1 D_g}{RT} \frac{\partial p_1}{\partial x} \hat{i} \quad (3.1.4)$$

where $M_1 = m_1 A$ is the molecular weight of the pressurant gas. Thus conservation of mass requires

$$\rho D_\ell \frac{\partial c_1}{\partial x} = \frac{M_1 D_g}{RT} \frac{\partial p_1}{\partial x} \quad (3.1.5)$$

for $x = 0$, and all r since both $\partial p_1 / \partial x$ and $\partial c_1 / \partial x$ vanish for $r > a$.

Finally for $r < a$ and $x = 0$, we assume local thermodynamic equilibrium between the pressurant gas dissolved in the propellant and the pressurant gas dissolved in the gas phase. This gives the result, valid for dilute solutions of pressurant in propellant,

$$c_1 = \kappa p_1 \quad (3.1.6)$$

when κ depends only on the temperature. Here κ is, of course, the Henry's Law Solubility for pressurant gas in liquid propellant.

In a cylindrical coordinate system, and for the steady state, eqs. (3.1.1) and (3.1.2) take the form

$$\frac{\partial^2 p_1}{\partial r^2} + \frac{1}{r} \frac{\partial p_1}{\partial r} + \frac{\partial^2 p_1}{\partial x^2} = 0 \quad x > 0 \quad (3.1.7)$$

$$\frac{\partial^2 c_1}{\partial r^2} + \frac{1}{r} \frac{\partial c_1}{\partial r} + \frac{\partial^2 c_1}{\partial x^2} = 0 \quad x < 0 \quad (3.1.8)$$

A solution to these equations subject to the boundary conditions enumerated above, eqs. (3.1.5) and (3.1.6) must be found in order to calculate the steady state leak rate through the opening. The justification for obtaining a steady state solution is our surmise that the transient in the neighborhood of the opening should be short-lived so that the leakage rate will be virtually equal to the steady-state rate over most of the time span of interest. It will be shown later that the transient is indeed short compared to times of interest to a typical space mission.

For large values of $\sqrt{r^2 + x^2}$ the pressure p_1 must go to the total system pressure, p_o , say, since there the gas will contain no vapor. So we put $\psi = p_o - p_1$ for $x > a$ and

$$\frac{\partial^2 \psi}{\partial r^2} + \frac{1}{r} \frac{\partial \psi}{\partial r} + \frac{\partial^2 \psi}{\partial x^2} = 0 \quad (3.1.9)$$

The function ψ tends to zero for large values of r or x . Taking the Hankel Transform of order zero of eq. (3.1.9) with respect to the radial coordinate r , defined as

$$\psi(k, x) = \int_0^\infty r \psi(r, x) J_0(kr) dr \quad (3.1.10)$$

gives as the differential equation satisfied by (k, x)

$$\frac{d^2 \psi(k, x)}{dx^2} - k^2 \psi(k, x) = 0 \quad (3.1.11)$$

The solution to this equation which vanishes for large x is

$$\psi(k, x) = A_1(k) e^{-kx} \quad (3.1.12)$$

$A_1(k)$ being some function of k which must be found from the boundary conditions. From the inversion theorem for Hankel Transforms

$$\psi(r, x) = \int_0^\infty k A_1(k) e^{-kx} J_0(kr) dk \quad (3.1.13)$$

and therefore

$$p_1(r, x) = p_0 - \int_0^\infty k A_1(k) e^{-kx} J_0(kr) dk \quad x > 0 \quad (3.1.14)$$

The solution for $c_1(r, x)$ is the same except for the sign of the exponent

$$c_1(r, x) = \int_0^\infty k A_2(k) e^{kx} J_0(kr) dk \quad x < 0 \quad (3.1.15)$$

Applying the condition of conservation of mass flux at $x = 0$, eq. (3.1.5) leads to

$$\frac{M_1 D}{RT} \int_0^\infty k^2 A_1(k) J_0(kr) dk = \rho D_\ell \int_0^\infty k^2 A_2(k) J_0(kr) dk \quad (3.1.16)$$

which, since this must hold for all r , implies

$$A_2(k) = \frac{M_1 D}{RT} \frac{D}{\rho D_\ell} A_1(k) \quad (3.1.17)$$

The condition of local thermodynamic equilibrium, eq. (3.1.6) gives, after using eq. (3.1.17)

$$\kappa \left[p_0 - \int_0^\infty k A_1(k) J_0(kr) dk \right] = \frac{M_1 D}{RT} \frac{D}{\rho D_\ell} \int_0^\infty k A_1(k) J_0(kr) dk \quad (3.1.18)$$

which must hold for $r < a$. Finally for $r > a$, $\partial p_1 / \partial x = 0$ at $x = 0$, or

$$\int_0^{\infty} k^2 A_1(k) J_0(kr) dk = 0 \quad (3.1.19)$$

Hence we have the following set of dual integral equations for the unknown function $A_1(k)$.

$$\int_0^{\infty} k A_1(k) J_0(kr) dk = \frac{P_o}{1 + \frac{M_1 D_g}{RT \rho D_\ell} \frac{1}{\kappa}} \quad (r < a) \quad (3.1.20)$$

$$\int_0^{\infty} k^2 A_1(k) J_0(kr) dk = 0 \quad r > a \quad (3.1.21)$$

The solution to this set of equations is known⁽⁷⁾.

$$A_1(k) = \frac{2}{\pi} \left(\frac{P_o}{1 + \frac{M_1 D_g}{RT \rho D_\ell} \frac{1}{\kappa}} \frac{\sin ka}{k^2} \right) \quad (3.1.22)$$

Combining eqs. (3.1.22), (3.1.17) and (3.1.15) gives for the concentration of dissolved pressurant gas in liquid propellant,

$$c_1(r, x) = \frac{2}{\pi} \frac{M_1 D_g}{RT \rho D_\ell} \left(\frac{P_o}{1 + \frac{M_1 D_g}{RT \rho D_\ell} \frac{1}{\kappa}} \right) \int_0^{\infty} \frac{\sin ka}{k} e^{kx} J_0(kr) dk \quad (3.1.23)$$

From this result the leakage rate per unit area is

$$w(k) = \rho D_\ell \left. \frac{\partial c_2}{\partial x} \right|_{x=0} = \frac{2}{\pi} \frac{M_1 D_g}{RT} \left(\frac{P_o}{1 + \frac{M_1 D_g}{RT \rho D_\ell} \frac{1}{\kappa}} \right) \int_0^{\infty} \sin ka J_0(kr) dk \quad (3.1.24)$$

The integral vanishes for $r > a$ as it should. Its value for $r < a$ is $1/\sqrt{a^2 - r^2}$. Thus

$$w(r) = \frac{2}{\pi} \frac{M_1 D_g}{RT} \left(\frac{P_o}{1 + \frac{M_1 D_g}{RT \rho D_\ell} \frac{1}{\kappa}} \right) \frac{1}{\sqrt{a^2 - r^2}} \quad (3.1.25)$$

The total leakage rate is

$$W = 2\pi \int_0^a w(r) r dr \quad (3.1.26)$$

and is given by

$$W = 4a \frac{D_g M_1}{RT} \left(\frac{p_o}{1 + \frac{M_1 D_g}{RT \rho D_l \kappa}} \right) \quad (3.1.27)$$

The leakage rate thus depends directly on the total system pressure p_o , the radius of the hole, a , and the group of parameters $D_g M_1 / RT$. The retarding effect of the solubility in and diffusion of the gas through the liquid is contained in the group of parameters $(M_1 / RT) (D_g / \rho D_l) (1/\kappa)$, which can be recognized as the ratio of the gas to the liquid permeation rates. We estimate the value of this ratio for the typical case of Helium diffusing through N_2O_4 . For Helium at a temperature of 273°K, $M_1 / RT = 1.78 \times 10^{-4}$. According to the data of Chang and Gokcen(12), $\kappa \approx 4.3 \times 10^{-6} \text{ atm}^{-1}$. The density of N_2O_4 is about 1.45 gms/cm³. No data is available for the diffusivity of Helium in liquid N_2O_4 , but the value should not exceed $10^{-4} \text{ cm}^2/\text{sec}^{(1)}$. For gases through gases, the diffusivity is always of order 1.0. Using these numbers we find

$$\frac{M_1 D_g}{RT \rho D_l \kappa} \sim 10^6$$

We conclude that the leakage rate is controlled by the solubility and diffusivity of the gas through the liquid and for all practical purposes eq. (3.1.27) reduces to

$$W = 4a \rho \kappa p_o D_l \quad (3.1.28)$$

Equation (3.1.28) is the same result that one would get if the gas phase was entirely ignored and the problem was considered to be leakage through a hole into a half-space containing the liquid propellant, the pressurant gas within the radius of the hole being held at the value κp_o .

According to eq. (3.1.28) the leakage of pressurant gas into the liquid is directly proportional to the solubility of the gas in the liquid, the total system pressure and the diffusivity of the gas in the liquid as well as the radius of the hole. In the next section the leakage rate through such an opening will be compared with that obtained for leakage through a similar hole in the barrier of a Teflon laminated structure.

3.2 Effect of the Teflon Coating on Leakage

Assume that the hole in the barrier is 1 mil in radius and is circular. Take the total system pressure as 40 atmospheres. The value of D_g is estimated at 10^{-5} cm²/sec. According to Jost(1) all diffusion coefficients in liquids have a value in the neighborhood of this number. In the case of system N₂ gas diffusing through N₂O₄, the solubility, κ , is somewhat larger than for the system He-N₂O₄. For N₂ gas in N₂O₄, $\kappa = 1.8 \times 10^{-4}$ atms⁻¹ (1). The leakage rate obtained for the two systems from eq. (3.1.28) is shown below

| System | W gms/sec |
|--|-----------------------|
| He-N ₂ O ₄ | 2.5×10^{-11} |
| N ₂ - N ₂ O ₄ | 1.06×10^{-9} |

For purposes of comparison the leakage rate through a one mil radius hole in the barrier separating 5 mils of FEP on the gas side from 5 mils of TFE on the liquid side at the same total system pressure is shown below.

| Pressurant Gas | W gms/sec |
|----------------|------------------------|
| He | 3.0×10^{-11} |
| N ₂ | 1.67×10^{-11} |

Thus the Teflon coating reduces the leakage rate by about two orders of magnitude in the case of N₂ but does not significantly affect the leakage rate in He-N₂O₄ systems. The reason for this is that the diffusivity of He into Teflon is the same order of magnitude of He through N₂O₄. These conclusions as stated above are based on estimated values of the diffusion coefficients of both gases [He and N₂ through liquid N₂O₄] of about 10^{-5} cm²/sec and therefore must be regarded as tentative since at present there is no experimental data for the diffusivity of N₂ and H_e gases into liquid N₂O₄.

4.0 TRANSIENT LEAKAGE THROUGH BLADDER STRUCTURES

It was pointed out in section 1.1 that for a closed system, that is a gas reservoir separated by a permeable bladder from a liquid reservoir, the only steady state solution to the diffusion equation is the trivial one corresponding to an everywhere uniform concentration and no leakage. What must occur in reality is that after loading the system with pressurant and propellant, or, if after loading, a rupture in the diffusion barrier occurs there is a transfer of mass between the two compartments until the liquid is everywhere saturated with gas and conversely. This process does not take place at steady state but is accompanied by a constantly diminishing leak rate as each tank nears saturation since the driving force for the mass transfer steadily decreases.

However, if the leakage rate through the bladder is slow, that is, the holes in the barrier are small and if the pressurant and propellant reservoirs are relatively large, that is, so large that at the given leak rate the time required for saturation is long, it is possible to consider quasi-steady state solutions to the leakage problem. The steady state leakage rates calculated in sections (2.0) and (3.0) apply to this situation. This type of solution will give an accurate estimate of the leakage rate for periods of time over which the concentration of the solute at the bladder surface does not change appreciably. If the calculations are to be applicable to a real bladder situation it is clearly necessary that the transient time of the bladder structure itself be short compared to the time span over which the solute concentration in either the liquid or gas reservoirs changes appreciably. The latter time span must be large, of course, if the bladder is functioning properly, that is, preventing leakage. One of the main purposes of the transient calculations, therefore, is to determine if the relaxation time for the bladder is short compared to that for the system as a whole. If the ratio of the two times is sufficiently small the leakage rate through a bladder structure can be calculated from the steady state results since the integrated leakage over the bladder transient will be small compared to the steady state leakage integrated over periods of time of the order of a mission lifetime.

4.1 Approximate Calculation of the Transient Period For a Laminated Bladder with a Circular Hole in the Barrier

Consider a semi-infinite slab of material 1, extending from $x = 0$ to $x = h$ axially and to infinity radially. The plane $x = 0$ is covered by an impermeable sheet except for an opening of radius a which is exposed to the diffusing vapor. The concentration on the plane $x = h$ is held at zero. Initially, the concentration of the diffusing substance throughout the slab is zero. A cross section of the bladder is shown in the schematic.

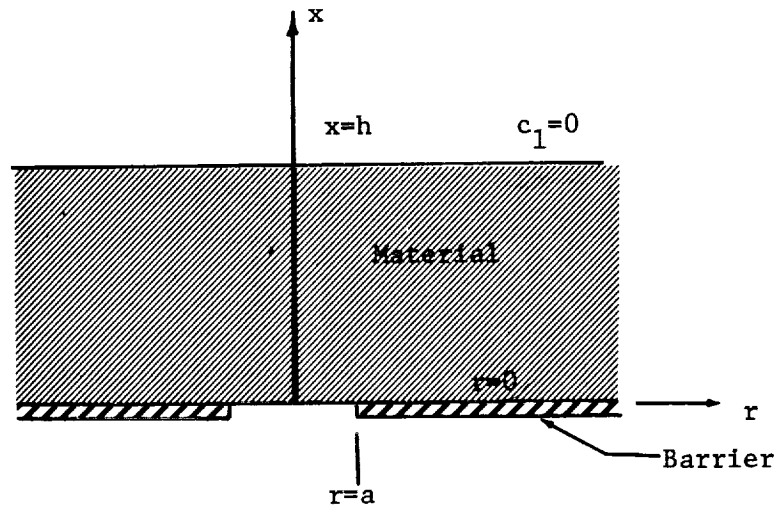


Figure 4.1

The basic difficulty with all problems of this type arises due to the mixed boundary condition which must be satisfied on the plane $x = 0$. Thus, one specifies the concentration for $r < a$ and the gradient of the concentration (zero) for $r > a$. If it were possible to specify either the concentration or the gradient over the whole plane $x = 0$ then the problem would be straightforward. This cannot be done exactly, of course. As an approximation, however, one can postulate that the flow rate across the opening ($r < a$, $x = 0$) experiences a very short transient before it takes on the final steady state value. The difference between the leakage rate, which is the flow across the plane $x = h$ at any given time and its steady state value is then due to the storage of diffusing material in material 1. This approach might be expected to give accurate results after the passage of a

period of time short compared to the relaxation time for the bladder as a whole because equilibrium should be reached very rapidly in the immediate vicinity of the hole.

To find the transient behavior of the leakage rate under these assumptions we solve

$$\nabla^2 c_1 = \frac{\partial^2 c_1}{\partial r^2} + \frac{1}{r} \frac{\partial c_1}{\partial r} + \frac{\partial^2 c_1}{\partial x^2} = \frac{1}{D_1} \frac{\partial c_1}{\partial t} \quad (4.1.1)$$

Subject to the boundary and initial conditions,

$$c_1(r, h, t) = 0 \quad (4.1.2a)$$

$$c_1(r, x, 0) = 0 \quad (4.1.2b)$$

$$-D_1 \frac{\partial c_1}{\partial x}(r, 0, t) = f(r, t) \quad (4.1.2c)$$

where $f(r, t)$ is zero for $r > a$, and is equal to the steady state flow rate divided by πa^2 for $r < a$. That is

$$f(r, t) = \frac{W_0}{\pi a^2} \quad r < a \quad (4.1.2d)$$

$$f(r, t) = 0 \quad r > a \quad (4.1.2e)$$

The Laplace Transform of Equation (4.1.1) then gives, using (4.1.2b)

$$\frac{s}{D_1} c_1(r, x, s) = \frac{\partial^2 c_1(r, x, s)}{\partial r^2} + \frac{1}{r} \frac{\partial c_1(r, x, s)}{\partial r} + \frac{\partial^2 c_1(r, x, s)}{\partial x^2} \quad (4.1.3)$$

where

$$c_1(r, x, s) = \int_0^\infty e^{-st} c_1(r, x, t) dt$$

Taking the zero order Hankel Transform of Equation (4.1.3) gives

$$\frac{d^2 c_1(k, x, s)}{dx^2} - (k^2 + \frac{s}{D_1}) c_1(k, x, s) = 0 \quad (4.1.4)$$

where

$$c_1(k, x, s) = \int_0^\infty r J_0(kr) c_1(r, x, s) dr$$

The solution to equation (4.1.4) which satisfies the condition (4.1.2a) is

$$c_1(k, x, s) = A_1(k, s) \frac{\sinh \sqrt{k^2 + \frac{s}{D_1}} (h-x)}{\sinh \sqrt{k^2 + \frac{s}{D_1}} h} \quad (4.1.5)$$

The Hankel-Laplace Transform of the conditions (4.1.2d) and (4.1.2e) determines $A_1(k, s)$, that is

$$\begin{aligned} -D_1 \frac{dc_1(k, 0, s)}{dx} &= \int_0^a r J_0(kr) dr \int_0^\infty e^{-st} \frac{W_0}{\pi a^2} dt \\ &= \frac{W_0}{\pi a^2} \frac{1}{s} \frac{a J_1(ka)}{k} \end{aligned} \quad (4.1.6)$$

We thus find

$$c_1(k, x, s) = \frac{W_0}{\pi a^2} \frac{a J_1(ka)}{D_1 k} \frac{1}{s} \frac{\sinh \sqrt{k^2 + \frac{s}{D_1}} (h-x)}{\sqrt{k^2 + \frac{s}{D_1}} \cosh \sqrt{k^2 + \frac{s}{D_1}} h} \quad (4.1.7)$$

The Hankel-Laplace transform of the flow rate through the plane $x = h$ is

$$W(k, x) = -D_1 \frac{dc_1(k, h, s)}{dx} = \frac{W_0}{\pi a^2} \frac{a J_1(ka)}{k} \frac{1}{s} \frac{1}{\cosh \sqrt{k^2 + \frac{s}{D_1}} h} \quad (4.1.8)$$

Performing the Hankel inversion gives

$$W(r, s) = \frac{W_0}{\pi a^2} \frac{a}{s} \int_0^\infty \frac{J_0(kr) J_1(ka)}{\cosh \sqrt{k^2 + \frac{s}{D_1}} h} dk \quad (4.1.9)$$

The total leakage rate, or rather its Laplace transform is given by

$$W(s) = 2\pi \int_0^\infty r dr W(r, s) = \frac{2W_0}{a^2} \frac{a}{s} \int_0^\infty r dr \int_0^\infty \frac{J_0(kr) J_1(ka) dk}{\cosh \sqrt{k^2 + \frac{s}{D_1}} h} \quad (4.1.10)$$

Interchanging the order of integration, and using the delta function character of the integral with respect to r , i.e.,

$$\int_0^{\infty} r J_0(kr) dr = \frac{\delta(k)}{k}$$

where $\delta(k)$ denotes the Dirac delta function, we get

$$W(s) = \frac{W_0}{s} \frac{1}{\cosh \sqrt{\frac{s}{D_1}} h} \quad (4.1.11)$$

Performing the Laplace inversion, which is straightforward in this case yields

$$W(t) = W_0 \left\{ 1 - \frac{4}{\pi} \sum_{n=0}^{\infty} (-)^n e^{-(2n+1)^2 \frac{\pi^2 D_1}{4h^2} t} \right\} \quad (4.1.12)$$

The leakage rate as a function of $D_1 t$ has been plotted in Figure (4.2). From the figure, it can be estimated, that for a 5 mil thick slab that the transient period will last about 700 seconds if D_1 is as large as 10^{-6} cm²/sec, while for D_1 as small as 10^{-9} this period will last 194 hours.

The value of the diffusion coefficient for pressurant gases through Teflon are about 10^{-7} cm²/sec (see the experimental section of this report). From figure (4.2) the transient time for a 5 mil thick Teflon laminated structure is about 3 hours or 10^4 seconds. For a bladder composed of two Teflon Laminates the time required would be about 4 times as long since the transient time depends on the square of the bladder thickness (eq. 4.1.12).

Although the above analysis is based on an approximate model, it is expected to give the accurate asymptotic solution because for long times the leakage rate across the opening must be the steady state leakage rate. This has been verified by running the problem on the digital computer using DAP. Figure (4.3) shows the analytical results for a 5 mil thick Teflon slab and a barrier with a one mil radius circular hole and the results obtained using the digital computer. It can be seen that the results are in fair agreement even over the early part of the transient and converge nicely for long times.

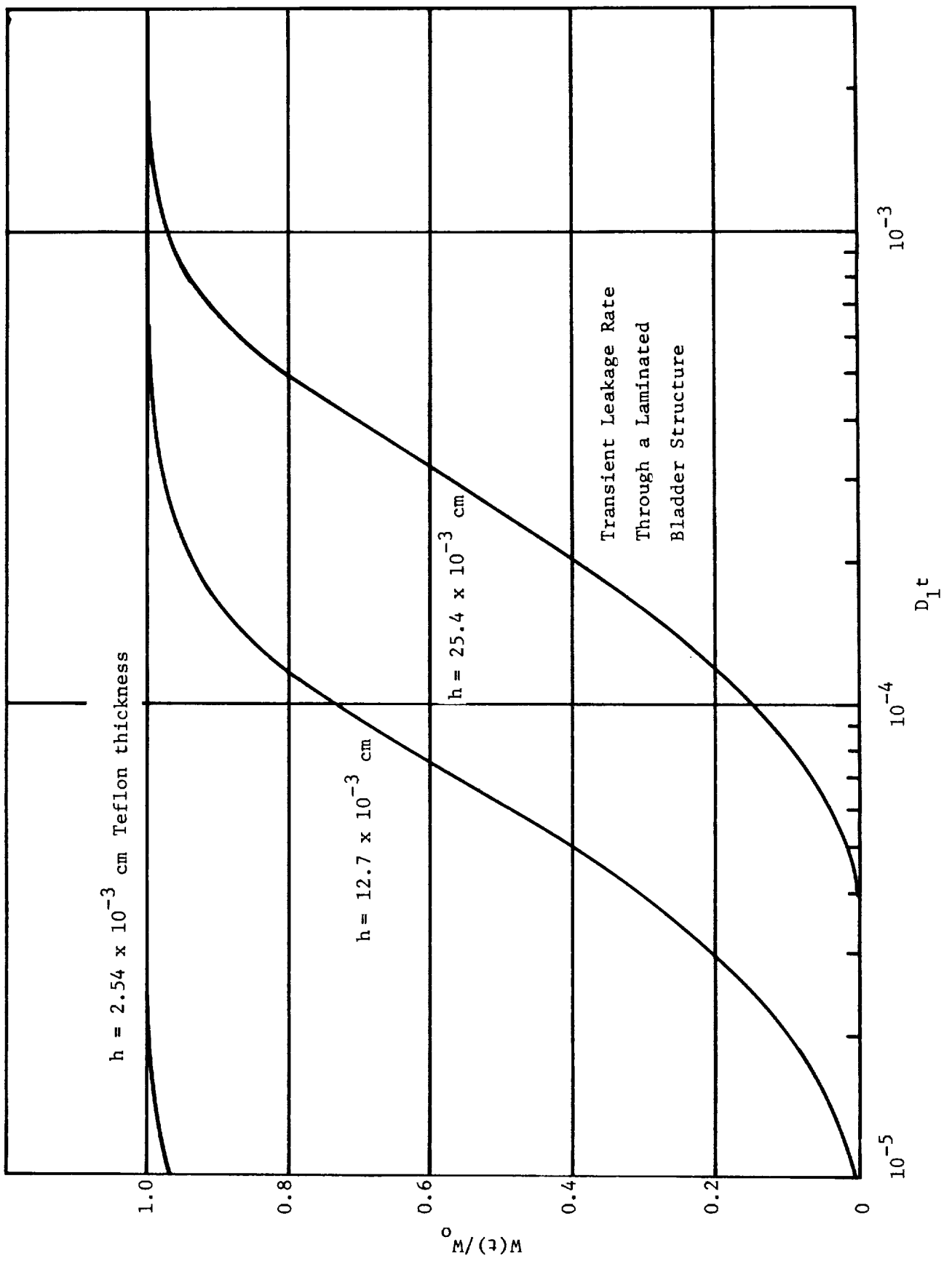


Figure 4.2

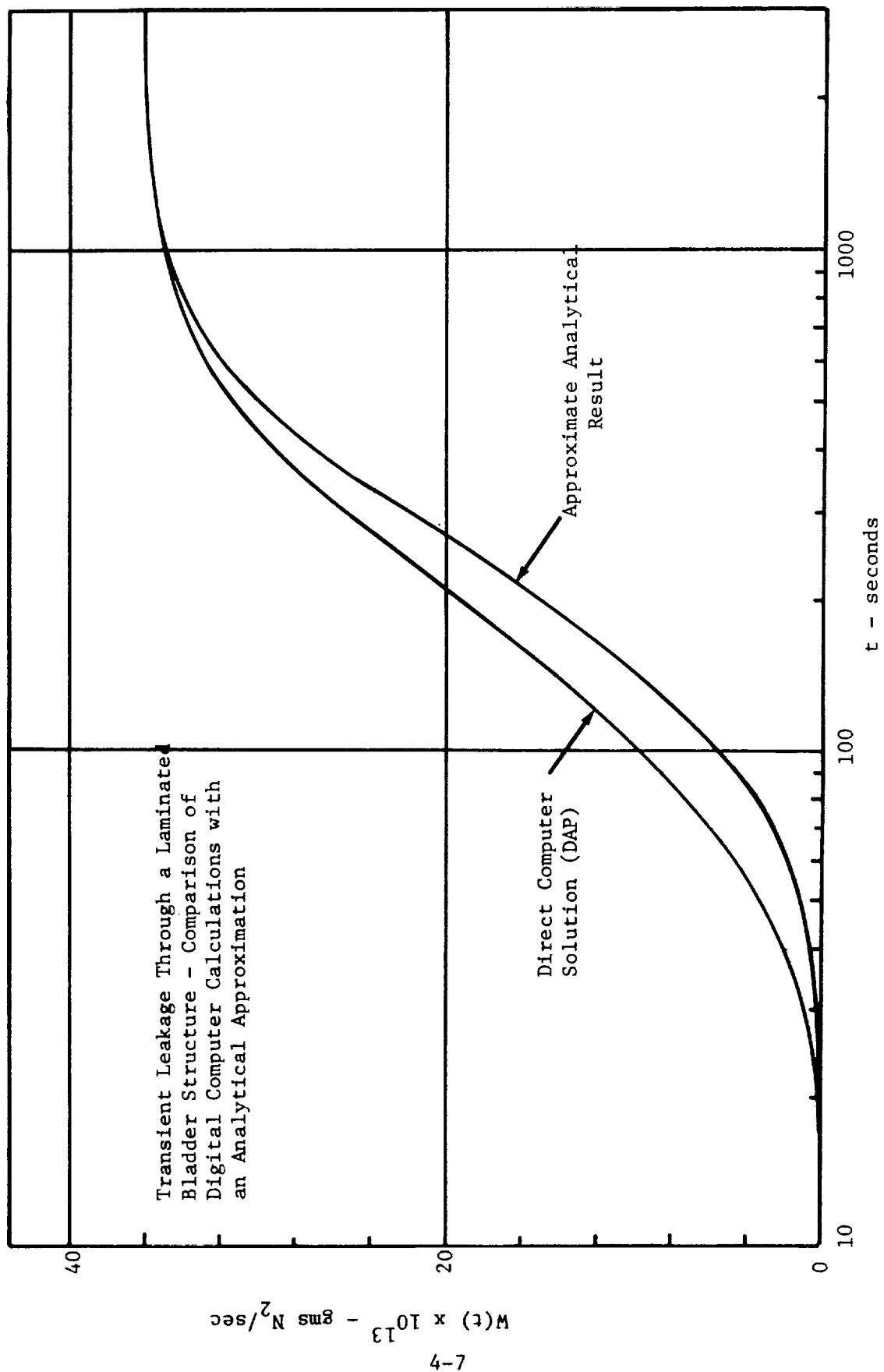


Figure 4.3

The following general conclusions can be drawn from the above results.

- o Transient times for a typical laminated bladder structure are of the order of a few hours. This is very short compared to the mission lifetime required for deep space exploration.
- o For a one mil radius hole in the barrier the steady state leakage rate for N_2 gas through two layers of Teflon each 5 mils thick (see section 3.2) is about 3.42×10^{-12} gms/sec. In a period of 10^5 seconds which should greatly exceed the transient time of the bladder structure, the accumulated steady state leakage rate would be 3.42×10^{-7} gms. The accumulated transient leakage rate would be less than this as can be seen from Figure 4.2. Such a low integrated leakage would scarcely affect the concentration of N_2 gas in the liquid propellant over a period of time of the order of 10^{12} seconds which is very long compared to the 10^4 second or so bladder transient time.

4.2 Further Remarks on the Transient Problem

Another instructive example for which an asymptotic (large values of the time) solution can be obtained is that of the transient diffusion of pressurant gas through a circular hole in a metallic foil bladder into an infinite body of liquid. This solution is developed in detail in reference 13. Here for the sake of brevity only the results will be given.

The initial conditions on the problem are that there is no gas dissolved in the liquid at time $t = 0$, and it is assumed that the concentration of the pressurant gas within the opening is held at the constant value c_o . This latter assumption is justified in section (3.1) and is due to the fact that diffusion through the gas phase is much more rapid than through the liquid. The leakage rate in gms/sec through a hole of radius a is then found to be

$$W(t) = 4apD_l c_o + a^3 \frac{\rho D_l c_o}{D_l t} + \frac{33}{48} a^5 \frac{\rho D_l c_o}{(D_l t)^2} + \dots \quad (4.2.1)$$

This formula is valid for sufficiently large values of the time and clearly goes to the steady state leakage rate

$$W_o = 4apD_l c_o \quad (4.2.2)$$

for large values of the time.

From eq. (4.2.1) the leading term in the time is small compared with the first when

$$\frac{a^2}{4D_l t} \ll 1$$

or when

$$4D_l t \gg a^2 \quad (4.2.3)$$

For a one mil hole, and an assumed value of D_l of 10^{-5} cm²/sec, the leading transient term in eq. (4.2.1) is 1% of the steady state term when $t = 16$ seconds. At this time the ratio of the next transient term to the steady state term is 1.35×10^{-4} , i.e., very small. Thus the transient is very short-lived for the hole sizes under discussion here.

Let us now compare this transient time with the time required to saturate a given quantity of propellant by leakage through a one mil radius hole at the steady state rate, eq. (4.2.2). At 40 atms the equilibrium concentration of He gas in N_2O_4 is about 1.74×10^{-4} (gms He)/(cm³ N_2O_4) according to the data of Chang and Gokcen. One ft³ of propellant contains 2825 cm³ and at saturation 0.492 gms of Helium. The steady state leakage rate from eq. (4.2.2) is 2.5×10^{-11} gms/sec. The time required to saturate 1 ft³ of propellant at the steady state leak rate would then be 1.96×10^{10} secs or 5.46×10^6 hrs. Actually it would require longer since the steady state leak rate above is greater than the actual leak towards the end of the time period required for saturation. Thus the transient period is extremely short compared to the time required for the transfer of any significant quantity of pressurant gas. Furthermore the leakage rate can be accurately calculated from eq. (4.2.2) for periods of time of the order of the time required for a deep space mission.

Finally it should be pointed out that the DAP program is now available for solving many transient problems involving two laminates of permeable material separated by a barrier with a hole in it. The hole shape may be circular, square, or rectangular. Running time for a typical transient problem, say leakage through two 5 mil layers of Teflon with a 1 mil circular hole in the barrier, will be from 10 to 20 minutes. The program is not particularly well suited for problems like the one discussed above where the transient time is very short, however. The computing time required is too long. For more detailed information on the program see reference 9.

5.0 INSPECTION TECHNIQUES FOR DETERMINING THE PRESENCE OF MICROSCOPIC HOLES IN METAL FOIL

Before the leakage rate through a given laminated bladder structure can be predicted, the size, shape, and distribution of holes in the barrier foil must be known to sufficient accuracy. Of these quantities the size and distribution are most important since as was shown in section (2.5) the leakage rate is only weakly dependent on the hole shape for not too gross differences in the shape. For small holes, however, the leakage rate is strongly dependent on the size of the hole in the sense that the leakage per unit open area is not constant. Thus the leakage rate through two circular holes will exceed that through one circular hole having an area equal to the sum of the areas of the smaller two holes. In addition, a certain minimum hole separation is necessary in order to be able to treat the holes individually. According to the results of section (2.3) this should be about 5 times the major open dimension of the hole. Thus an accurate estimate of the leakage rate through a bladder structure can only be made if a considerable amount of detailed information is available describing the holes in the barrier.

One of the most economical and well developed techniques for obtaining such information appears to be dye testing. This technique utilizes liquid dyes which are extremely good surface wetters along with subsidiary techniques for observing the hole. It appears that such techniques could be used for locating and photographing holes as small as 1 mil diameter in metal foil.

One such process is known as dy-chek and is a product of Turco Corporation. This test is carried out by first cleaning both surfaces of the foil carefully and then applying liquid dye-penetrant which is non-corrosive. After the dye-penetrant has dried an emulsifier is added followed by a developer. The presence of a hole is indicated by the appearance of dye coloring on the opposite side of the foil. An elaboration of this process is Zyglo, a product of the Magnaflux Corporation. It is similar to dy-chek except that the dye is fluorescent and can be viewed and photographed under black light. It should be possible to

obtain both the shape and size of the openings from enlargements of such photographs. After measurement of the holes in this manner the method could be checked by a gas leak rate test which would give the total open area available for gas leakage.

More exotic techniques can be imagined such as β particle attenuation, or optical methods using laser light. However these methods should not be attempted until the simpler and more economical methods suggested above have been exhausted.

6.0 SUMMARY OF ANALYTICAL RESULTS

In this section we summarize those general conclusions which can be drawn from the analytical study, compare the analytically predicted leak rate with experimentally measured values and point out those areas which need further attention.

6.1 Summary of Results

As a result of the work reported in sections one through five above, and elsewhere, several general conclusions concerning leakage and its calculation through laminated bladder structures consisting of two layers of permeable material separating a barrier with a hole can be stated. The most important of these for an understanding of the overall process are

- o The transient time for a typical bladder structure is small compared to the time required for a significant change in the concentration of the gas in the liquid propellant. This means that meaningful leakage rate calculations can be made by assuming the bladder structure is exposed to steady state conditions on each of its surfaces.
- o Concentration gradients in the gas phase can be ignored. This is shown in Appendix A. The reason is the gas offers essentially zero resistance to diffusion compared to the Teflon.
- o Concentration gradients in the liquid phase (propellant) can also be ignored to a first approximation. This conclusion, however, must remain tentative at present since there are no experimentally measured diffusion parameters available for the pressurant gases (N_2 , He) in the common earth storable propellants (N_2O_4 , N_2H_4).
- o As a consequence of the above results the upper bound for the leakage rate through a bladder structure can be calculated by specifying a constant concentration on the solute side, zero on the opposite side of the bladder. The solute here designates the diffusing component.

- o The shape of the hole in the bladder only weakly affects the leakage rate per unit area through the hole over a wide class of hole shapes. For example, a rectangular slot having a length 10 times its width will permit about the same leakage rate as a circular hole of the same area.
- o Openings in the barrier can be treated as independent provided they are separated by about 10 or more times the major dimension of the opening.
- o Provided the diffusion coefficients of the pressurant gases (N_2 , He) in liquid propellant (N_2O_4 , N_2H_4) are no smaller than about $10^{-5} \text{ cm}^2/\text{sec}$, the Teflon coating on the barrier foil reduces the leakage rate through the bladder structure significantly over what it would be for an uncoated bladder (plain foil with a hole).

✓ 6.2 Comparison of Calculated with the Experimentally Measured Leak Rate

To determine the validity of the analytical approach experiments were carried out to measure the leakage rate through a typical laminated bladder structure containing circular holes in the barrier. The sample bladder structure consists of a 10 mil layer of FEP separated from a 10 mil layer of TFE by a one mil thick aluminum foil. The foil was drilled with 100, 5 mil radius circular holes in a square pattern, approximately 125 mils on centers. The sample laminated bladder structure was obtained from the Dielectrix Corporation; the holes were previously drilled in the foil by National Jet Corporation.

The tests were carried out by initially evacuating both sides of the test assembly, then pressurizing one side with Helium gas, the other with N_2O_4 vapor. The two sides are separated by the laminated bladder structure. To eliminate the leakage during the transient period from the measured value of the leak rate, the gas and vapor were flowed through their respective sides of the assembly for several hours before the system was closed off. After close-off sufficient time was allowed to elapse to obtain a measurable quantity of the solute in the opposite chamber. The samples were analyzed using gas chromatography.

The experimental runs were carried out with the results shown in the table below. The leakage rate through the assembly was calculated ~~by~~ ^{from} the ~~method outlined in the design guide using the analytically generated curves for leakage through circular holes.~~ ^{curves of the preceding section} ~~the solubility and diffusivity of Helium and N₂O₄ vapor in Teflon (FEP and TFE)*~~ ^{experimentally determined values}

| Test | Temp. (°F) | Press. (Atm) | Duration (hrs) | W gms/sec (Exper.) | W gms/sec (Calc) |
|------|---------------|-----------------|-------------------|---|---|
| 1 | 187 | 9.6 | 2 | He→N ₂ O ₄ 2.72 x 10 ⁻⁹ N ₂ O ₄ →He (Not Measurable) | 4.20 x 10 ⁻⁹ |
| 2 | 200 | 10 | 64.5 | He→N ₂ O ₄ 15.5 x 10 ⁻⁹ N ₂ O ₄ →He 3.1 x 10 ⁻⁸ | 4.8 x 10 ⁻⁹ 4.35 x 10 ⁻⁸ |
| 3 | 150 | 4.9 | 44 | He→N ₂ O ₄ 17.35 x 10 ⁻⁹ N ₂ O ₄ →He 1.6 x 10 ⁻⁸ | 2.11 x 10 ⁻⁹ 1.7 x 10 ⁻⁸ |

All of the tests were carried out with the TFE on the N₂O₄ side.

It was subsequently found that Test 1 was invalid because the gas and vapor were not allowed to flow through the system for a sufficient length of time prior to closing the system off. The measured leakage rate is therefore an average value over a transient period and for this reason is low. The test was also of too short duration to allow the determination of the N₂O₄ rate.

For tests 2 and 3 the system was not only exposed to Helium and N₂O₄ for a sufficient length of time before close off but also the test was allowed to run for a period long compared to the estimated transient time for the laminated bladder structure. In this way valid determinations of the steady state leak rate were obtained.

~~The calculated values of the leak rate were obtained using the solubility and diffusivity data of tables 9-1, 9-4, and 9-7. The diffusivity data used was that obtained from unidirectional experiments.~~ The experimental leakage rate was obtained by measuring the total accumulated leakage and dividing by the elapsed time. From the results of tests 2 and 3 above, it can be seen that the predicted Helium leak rate is consistently lower than that measured while the predicted N₂O₄ rate

* The experiments were performed under contract NAS 7-505 for NASA, Western Operating Office. Reference 7 contains a summary of the data obtained.

is reasonably close to the measured value. However, there are several factors which must be considered before evaluating the accuracy of the predicted leak rate. The most important of these are the following.

(1) After completing the tests the laminated bladder structure was removed from the test assembly for examination. It was found that the TFE which was on the N_2O_4 side of the bladder was completely separated from the aluminum foil. The FEP bond remained intact however. In addition, there were cracks in the foil barrier at various places along the surface where the bladder met and was compressed by the flanges of the test assembly. Both these defects tend to increase the measured flow rate over what it would be for an unfaulted bladder structure. The theoretical calculations were based on the assumption that the bladder material was not separated from the foil barrier and that the only holes in the barrier were the drilled circular holes. Quantitatively the effect of the separation and rupture of the barrier on the leakage rate is difficult to account for precisely since the open area of the crack is not known, and the amount by which separation increases the leak rate is difficult to determine. Separation of one layer should not increase the leakage rate by more than 50% however, and a visual examination of the cracks indicate that the total open area was considerably less than that of the 100 drilled 5 mil radius holes. Thus one would expect the measured leakage rate through a bladder structure which did not experience separation and which had no cracks to be no less than about half the measured values reported above. In short the observed failures of the experimental sample could cause only a small change in the leakage rate, not order of magnitude changes.

(2) The permeation rate for Helium through Teflon in the presence of counterflowing N_2O_4 is higher than that for unidirectional flow of Helium alone. This result was observed experimentally by comparing the results of the unidirectional and the counterflow tests, and the results are recorded in ~~table 9-7~~. When these values of the permeation rate are used, the following calculated leakage rates are obtained for tests 2 and 3.

| <u>Test</u> | <u>W(gms/sec)</u> |
|-------------|-----------------------|
| 2 | 12.0×10^{-9} |
| 3 | 11.0×10^{-9} |

When these results are compared with the experimental leak rates given above, it can be seen that the experimental (as measured) and calculated leak rates are in fair agreement. When allowance is made for the observed defects in the bladder as discussed in (1) above, it appears that the calculated and experimental gas leak rates are in excellent agreement. Unfortunately, it is not possible to state this without reservation since no quantitative measure of the effect of the defects in the bladder structure is available.

(3) The experimentally determined effect of counterflow on the N_2O_4 leakage rate is to reduce it by about a factor of 10. ~~(See figure 9.5 which summarizes the experimental results.)~~ Thus when counter diffusion of Helium is taken into account the calculated leakage rates shown in the table for tests 2 and 3 would be reduced by about a factor of 10. Thus the agreement would not be nearly as good as is indicated by the table. On the other hand the experimental leakage rates are too high for the reasons discussed in (1) but not by as much as a factor of 10.

(4) The experimental data is itself uncertain perhaps to as much as a factor of 10. Further, there is considerable scatter between different samples of Teflon. Since the experimental data used to make the theoretical calculations was obtained from different Teflon from that used for the experimental leakage tests, there is some uncertainty involved.

When all the possible sources of error such as those discussed in (1)-(4) are taken into consideration, it seems reasonable to assert that the prediction of the leakage rates to within an order of magnitude is acceptable. Our experiments and analysis indicate that the unidirectional diffusion data is adequate for this purpose and that the leakage rates, calculated using this data is in satisfactory agreement with the experimentally measured leakage rates,



6.3 Suggestions for Further Study

The results obtained under this contract and reported above are all obtained by isolating the bladder structure from the rest of the system and calculating the leak rate as though it were in a fixed environment with respect to the diffusing components. It has been shown that so far as the gas space is concerned this is a very good assumption over long periods of time (times of the order of that required for deep space missions). However, the assumption of a vanishing concentration of the diffusing pressurant gas on the face of the bladder exposed to the liquid propellant is subject to question. True, if the ratio of the permeability of the gas through the liquid is much greater than that through the Teflon the mathematical problem can be treated as though the concentration in the Teflon vanishes at the surface exposed to the liquid (Part 1, Appendix A). We do not know that this condition is adequately satisfied since we do not know the permeation rate of pressurant gases through liquid propellants. Even if it is, the model depends on the bladder surface remaining in contact with the liquid, that is, no vapor phase is formed in the propellant space. But according to Raoult's law (14) the pressure in the liquid space will increase due to absorption of the pressurant gas in the liquid tending to force the bladder away from the liquid and forming a body of vapor in the liquid space. In fact, the formation of the vapor phase on the liquid side of the bladder has been observed.

The rate of formation of the vapor phase (we refer to the mixture of pressurant gas and propellant vapor as vapor phase) on the liquid side as a function of the degree of perforation of the diffusion barrier is a problem of considerable importance, since the presence of gas on the liquid side of the bladder can lead to engine malfunction if large quantities are present. Thus, the conditions under which a bubble forms and the rate of formation of the vapor phase for a given set of conditions should be studied. This can be carried out by extending the present study to include the liquid propellant and the pressurant gas adjacent to the bladder structure and making allowance in the calculations for the motion of the bladder. Further experimental work to determine the diffusion parameters of the pressurant gases through liquid propellant will be necessary in order to carry out this study.

7.0 EXPERIMENTAL EFFORT

The purpose of the experimental effort (Part II of the Bladder Permeation Program) was to support the development of an analytical model of bladder leakage by providing transport property data and identifying the mechanisms involved. In order to achieve the objective an experimental program was conducted to:

1. Measure the diffusion coefficient and solubility of gases and propellant vapors in bladder materials.
2. Assess the effects of two component counter diffusion.

The experimental program consisted of tests with a 10 mil sample of polytetrafluoroethylene (TFE), a 10 mil sample of tetrafluoroethylene-hexafluoropropylene copolymer (FEP) and a composite sample consisting of 1 mil of aluminum foil with 10 mils of TFE bonded to one face and 10 mils of FEP bonded to the other face. The gases and vapors of interest to the program were helium, nitrogen, nitrogen tetroxide and hydrazine. The teflon specimens were purchased from Dilectrix Corporation and were fabricated by the spray method normally used for fabricating bladders. The propellants were from lots analyzed to meet MIL-specifications and the pressurant gases were industrial cylinder gases.

For simple geometries, the permeation constant is directly proportional to the leakage rate. The mathematics involved and the mechanism are widely reported and discussed, for example, References 15 and 16. However, for the analysis of bladder leakage which involves flow through holes in an otherwise impermeable barrier, the transport property data required are solubility data in terms of a Henry's law constant and the diffusion coefficient. These data are seldom reported in the literature and, in fact, an extensive literature survey was reported in Quarterly Progress Report No. 2* which located only permeation constants.

*Report No. 07282-6006-R000 dated 4 January 1967.

The articles included in the survey pertinent to the present study are References 17, 18 and 19 which give helium and nitrogen permeation constants in TEP and FEP. A continuing search for data, particularly for nitrogen tetroxide and hydrazine, yielded only four additional reports (References 20 to 23) all of which report permeation data for nitrogen tetroxide. Diffusion coefficients were not located for any of the systems of interest and only one source gave data which involves solubility in any of the systems of interest. Reference 23 reported that at $75 \pm 5^{\circ}\text{F}$ after 183 days immersion in liquid nitrogen tetroxide, TFE increased 3.8% in volume and 2.6% in weight. This gives a solubility of 56 mg of nitrogen tetroxide per cm^3 of TFE compared to 22 mg/cm^3 which could be predicted from extrapolating the low pressure tests discussed in Section 8.0. The comparison of the available permeation data with results of this study is given in Section 9.4.

From an examination of the apparatus and results reported in the literature two types of experiments were selected to provide the required data. The first was an adsorption test to provide solubility data and the second was a permeation test to provide permeabilities and diffusion coefficients. These tests are discussed in Section 8.0 and the results obtained from the test program are given and discussed in Section 9.0.

8.0 TECHNICAL DISCUSSION

The experimental program provided the measured values of the Henry's Law solubility constant, the diffusion coefficient and the permeability constant through the reduction of data from two types of experiments. The solubility of gases or vapors in a solid of known volume was measured by introducing a known quantity of each in a closed bomb and allowing time for equilibrium to be reached. From the equilibrium values the solubility was calculated. In those tests where the transient decay was sufficiently long, the diffusion coefficient also was calculated. The permeability constant for unidirectional gaseous diffusion through a membrane was measured by an apparatus in which a membrane was subjected initially to a small differential pressure. The differential pressure decreases in the closed system as a function of time due to permeation of gas from the high pressure to the low pressure side. From an evaluation of the differential pressure-time data, the permeability constant was calculated.

The following sections describe the tests which were conducted as a part of this study. Section 8.1 describes the experiments using the adsorption apparatus and Section 8.2 describes the unidirectional permeation and counter flow tests using the permeation cell.

8.1 Adsorption Tests

In principle, the adsorption tests for gas solubility in solids is a relatively uncomplicated test that provides a maximum of information. In actual practice, it is capable of producing good results but requires careful calibration and attention to detail. The schematic diagram of the adsorption apparatus used in this program is given in Figure 8.1. The supply tank fill system, the evacuation connections and the associated valving were omitted in order to provide a clear understanding of the basic apparatus.

There are three key volumes which must be known accurately. These are: 1) the volume included between the two valves which includes the transducer, 2) the volume of the empty adsorption bomb and all fittings

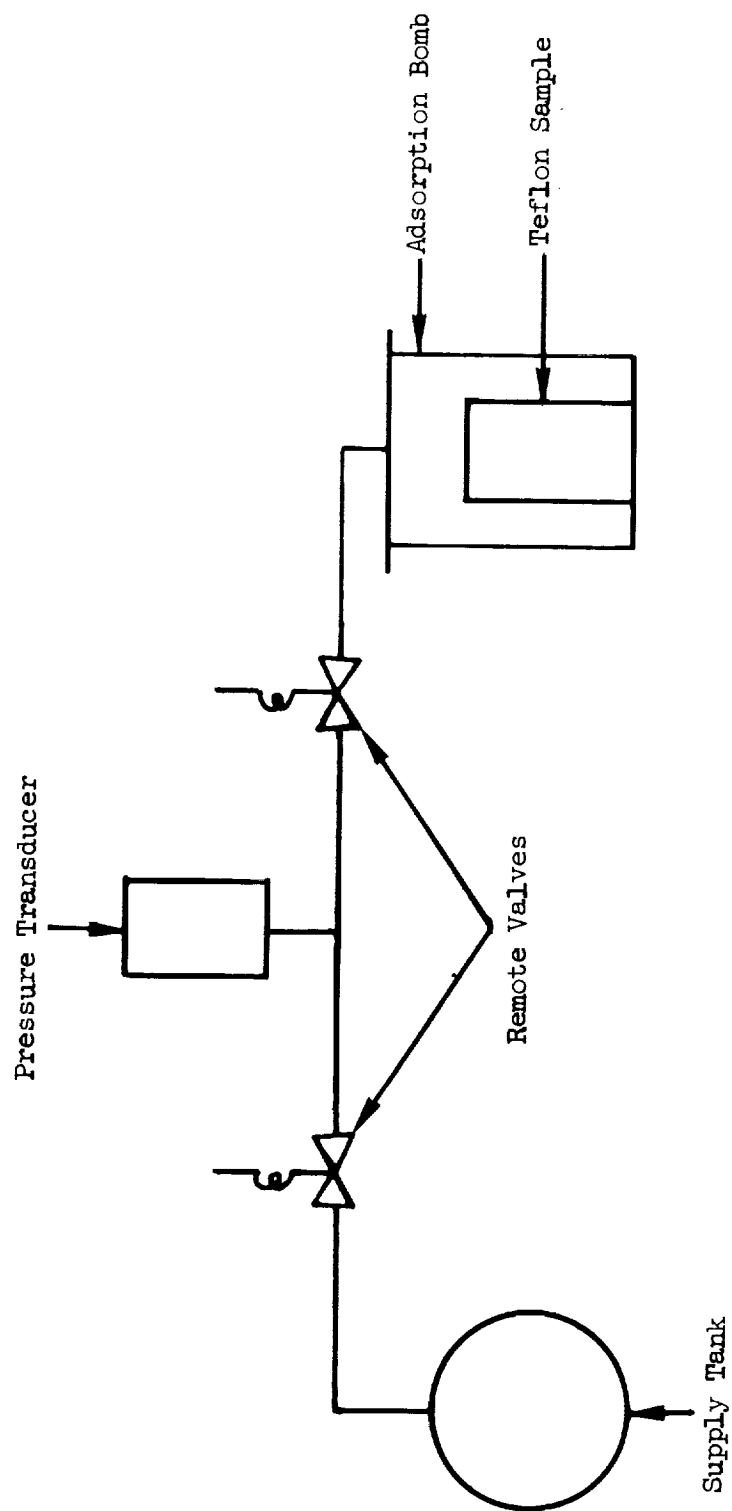


Figure 8.1 Adsorption Apparatus

and connections, and 3) the volume of the Teflon sample. In addition, the complete apparatus must be carefully temperature controlled for, in effect, it functions as a gas thermometer.

The procedure which was followed during a test is the following:

1. The sample volume and transducer section were swept with the gas or vapor and evacuated for a length of time sufficient to assure desorption of all gases. (Typically one to sixteen hours.)
2. A sample of gas or vapor was introduced into the calibrated volume between the two valves and its pressure was allowed to stabilize.
3. The valve between the transducer and the sample was opened and the pressure in the system was periodically read on a potentiometer until no further decrease was observed.
4. This valve was closed and a second sample of gas or vapor was admitted to the calibrated volume as in step 2.
5. This second sample was added to the first as in step 3 and the procedure of steps 2 and 3 continued until the desired total pressure was attained. (Usually a total of four or five times.)

The data were reduced in a direct manner when a permanent gas (nitrogen or helium) was used but by a more complicated technique when nitrogen tetroxide was used. For permanent gases, the mass (or standard volume) of gas in the system at any time was calculated from the pressure volume relationships. The difference between the quantity added and the quantity indicated at any time is the quantity adsorbed in the Teflon sample.

$$\frac{CC(STP)_{gas}}{CC_{Teflon}} = \frac{273.15}{V_{Tef} T} \left[P_{TR} V_{TR} + P_O (V_B - V_{TEF}) - P_{EQ} (V_{TR} + V_B - V_{Tef}) \right] \quad (8.1.1)$$

where

T = temperature, $^{\circ}\text{K}$

V_{Tef} = volume of the teflon sample, cm^3

V_{B} = volume of adsorption bomb, cm^3

V_{TR} = volume of transducer section, cm^3

P_{TR} = pressure in transducer section prior to addition to the bomb, atm

P_{O} = equilibrium pressure in the bomb prior to the addition, atm

P_{EQ} = equilibrium pressure in the bomb after the addition, atm

When the nitrogen tetroxide adsorption data was reduced it was necessary to account for the dissociation reaction



which is a function of temperature and pressure. A second factor related to the fact that it was a condensable vapor. Liquid nitrogen tetroxide was held in the supply tank at the same temperature as the complete apparatus. When a vapor sample was drawn into the transducer section a variable quantity of liquid was entrained with the vapor. Thus, it was not possible from the initial transducer pressure-volume relationship to determine the quantity of nitrogen tetroxide added to the sample bomb. Since the adsorption of nitrogen tetroxide in Teflon is a slow process, it was possible to take a large number of pressure-time readings after the nitrogen tetroxide was introduced but before equilibrium was attained. From these measurements, it was possible to derive both the zero time pressure of the bomb (actually the gas density was used) and the diffusion coefficient of nitrogen tetroxide into the Teflon sheet. The equation which describes the gas density in the bomb as a function of time is:

$$\frac{\rho_{\text{O}} - \rho}{\rho_{\text{O}} - \rho_{\infty}} = 1 - 2\rho_{\infty} \sum_{n=1}^{\infty} \frac{\rho_{\text{O}}}{\rho_{\text{O}}^2 - \rho_{\text{O}}\rho_{\infty} + \rho_{\infty}^2 q_n} \exp - \frac{D q_n^2 t}{l^2} \quad (8.1.3)$$

where:

ρ = density of gas in the bomb at any time, mg/cm^3

ρ_0 = unknown zero time density, mg/cm^3

ρ_∞ = equilibrium density in the bomb, mg/cm^3

l = half thickness of the sheet, cm

D = unknown diffusion coefficient, cm^2/sec

t = time, sec

q_n = all non zero positive roots of the equation

$$\tan q_n = \frac{q_n \rho_\infty}{\rho_0 - \rho_\infty} \quad (8.1.4)$$

A generalized least squares method was applied to the pressure-time data for each test and the best estimate for ρ_0 and D were obtained.

Figures 8.2 and 8.3 show data for two nitrogen tetroxide/TFE runs at different temperatures. The solid curve in each Figure was calculated from the best ρ_0 and D while the circled points are the experimental data.

8.2 Permeation Tests

Two types of permeation tests were conducted during this study. The unidirectional tests were conducted by admitting the same gas or vapor to each side of a membrane but at approximately a 10 psi pressure difference. The counter diffusion tests were conducted with nitrogen or helium on one side and nitrogen tetroxide on the opposite side of the membrane at a near zero pressure differential. The method of operation and the method of data reduction differed for the two types of tests and thus are described separately.

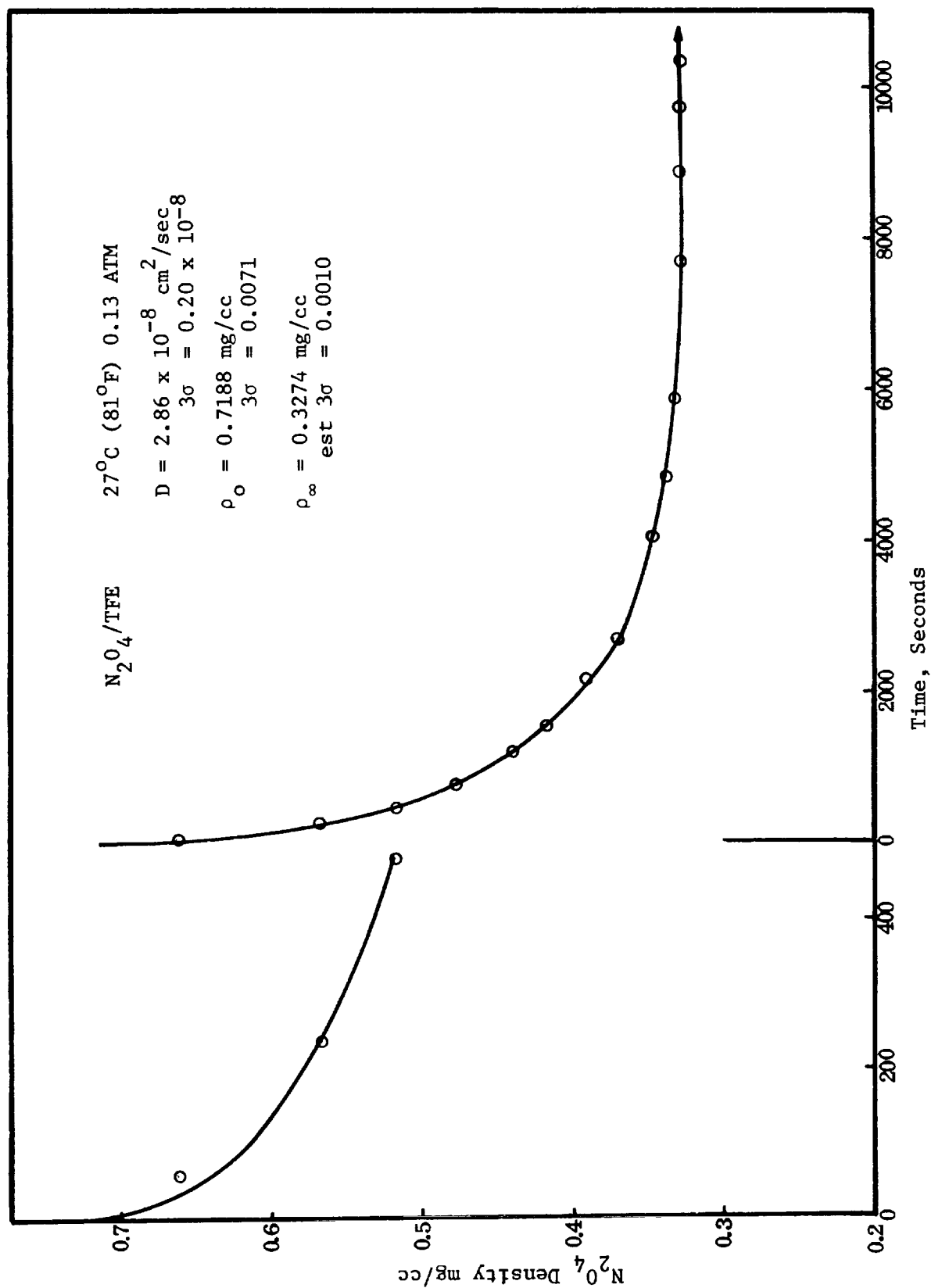


Figure 8.2 Adsorption of Nitrogen Tetroxide at $81^\circ F$

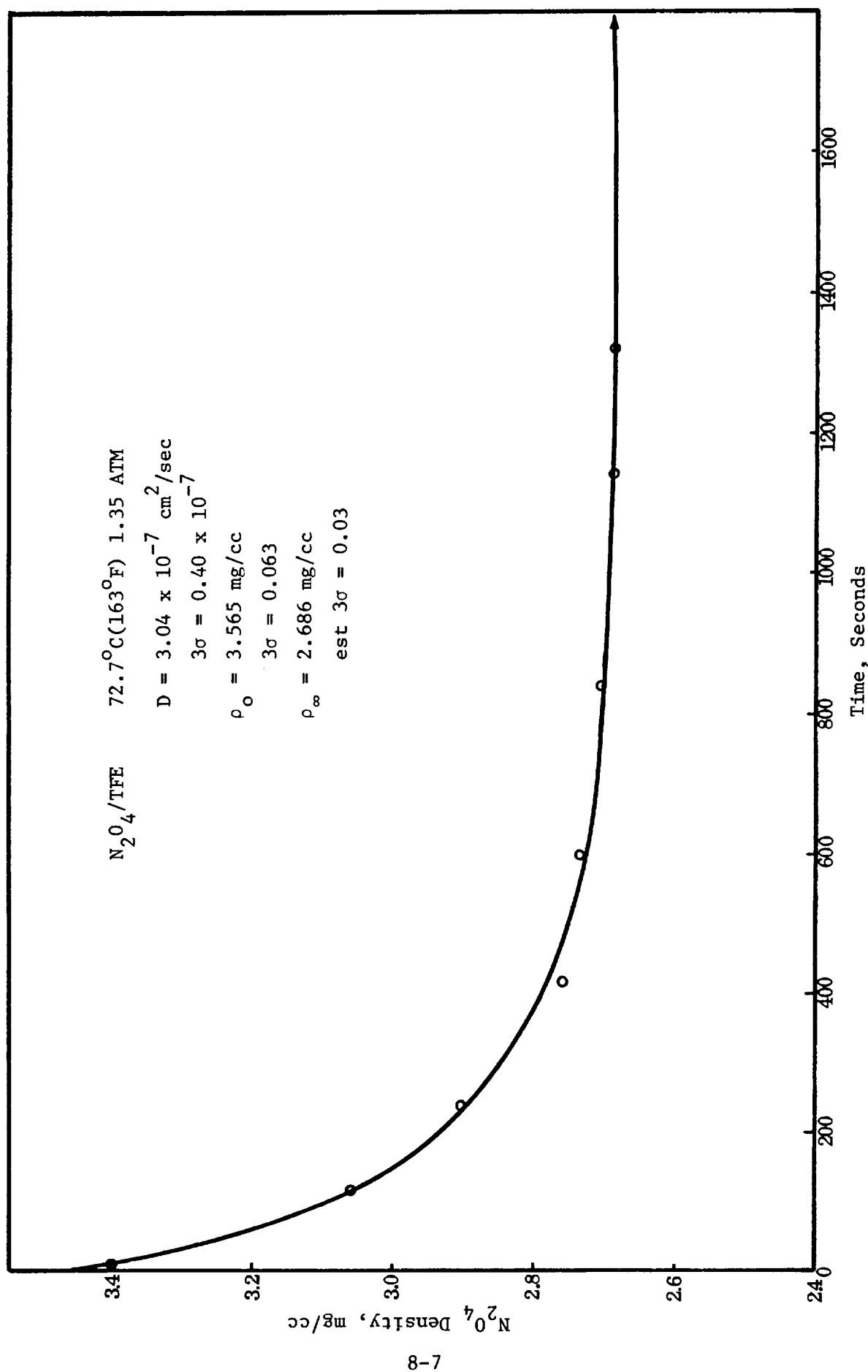


Figure 8.3 Adsorption of Nitrogen Tetroxide at 163°F

8.2.1 Unidirectional Permeation

The unidirectional permeation of a single gas, vapor or liquid through a membrane is widely measured and reported in the literature. Many designs of cells are described which produce scientific data, comparative data or go-no go results. The tests conducted as a part of this study were designed to provide scientific data and in particular the permeation constant defined by

$$Q = \frac{p A \Delta P}{l} t \quad (8.2.1)$$

where:

Q = quantity passed through the membrane in time (t), CC(STP) or g

p = the permeation constant, $\frac{\text{CC(STP) cm}}{\text{sec cm}^2 \text{ atm}}$ or $\frac{\text{g cm}}{\text{sec cm}^2 \text{ atm}}$

ΔP = pressure difference across the membrane, atm

l = membrane thickness, cm

A = active area, cm^2

t = time, sec

A diagram of the unidirectional permeation apparatus is given in Figure 8.4. The fill lines and vacuum lines and associated valving were omitted for clarity. The test procedure consisted of the following steps:

1. The bypass valve was opened and the cell and transducers were thoroughly degassed under vacuum.
2. The test gas or vapor was introduced to the cell until the desired total pressure of the test was reached. In most tests one side of the cell was initially at vacuum and this step was eliminated.
3. The bypass valve was closed and additional gas was introduced into the high pressure side (left side in the Figure) until the desired initial ΔP was established.

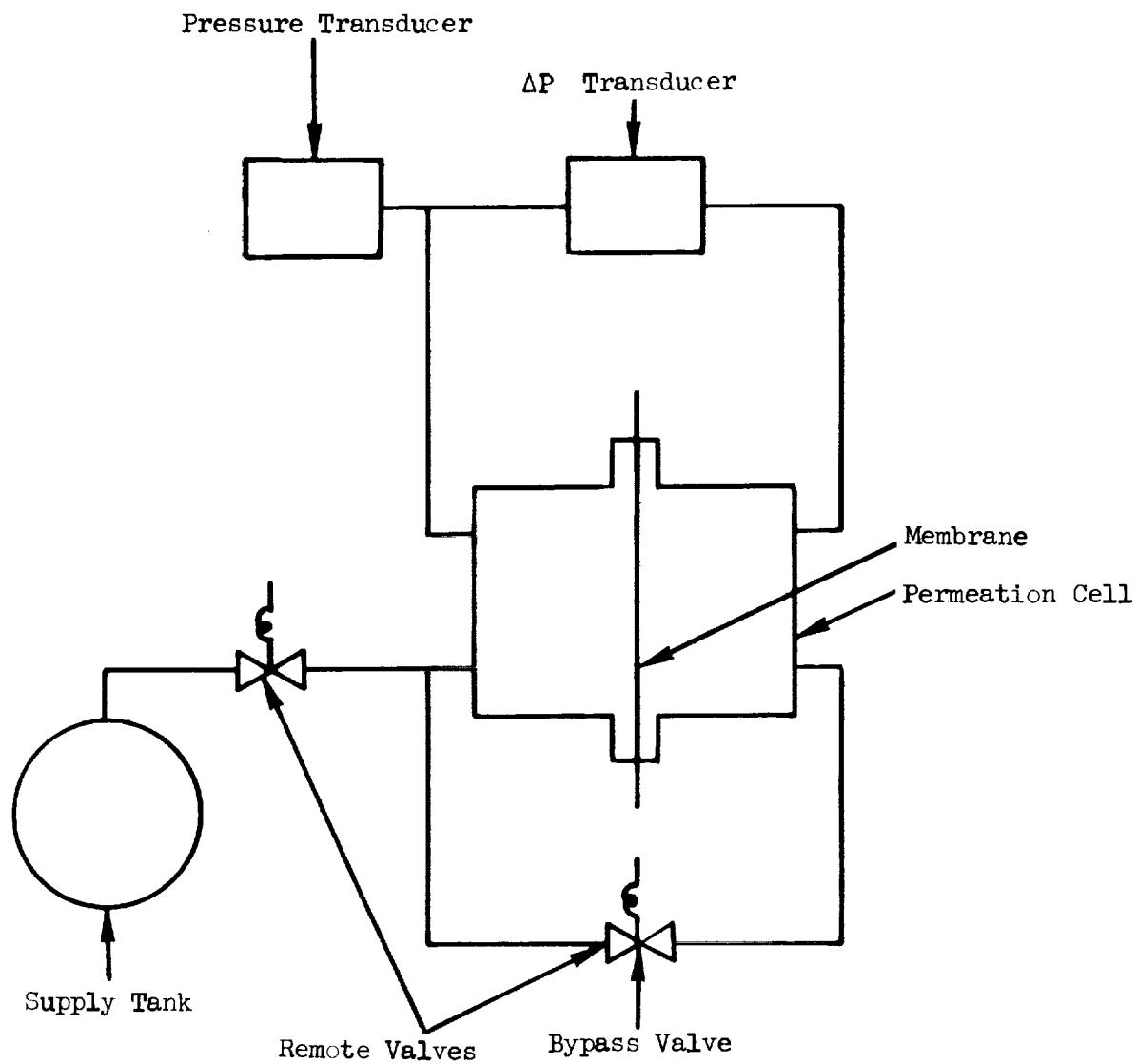


Figure 8.4 Unidirectional Permeation Apparatus

4. The supply gas valve was closed and both the absolute pressure and the differential pressure were recorded as a function of time. Normally the tests were terminated when the differential pressure was one-half to three-fourths of its initial value.

As in the case of the adsorption bomb tests described previously, the data reduction method for nitrogen tetroxide was different than the method for the permanent gases. When the change in differential pressure is small, it is possible to select an average ΔP and to obtain the permeation constant by an algebraic solution. However, when ΔP changes are large during the test and when a statistical treatment of the data is desired, the differential equation must be solved. For the permanent gases which obey the ideal gas law a closed form solution was obtained

$$\ln \Delta P = \ln \Delta P^0 - \frac{RTAt}{M\ell} \left(\frac{1}{V_H} + \frac{1}{V_L} \right) p \quad (8.2.2)$$

when:

ΔP = differential pressure at any time, atm

ΔP^0 = differential pressure at the start of the test, atm

R = gas constant, $82.054 \frac{\text{cm}^3 \text{ atm}}{\text{g mole } ^\circ\text{K}}$

M = gas molecular weight

T = temperature, $^\circ\text{K}$

A = active cross-sectional area, cm^2

ℓ = membrane thickness, cm

t = time, sec

V_H = volume on high pressure side, cm^3

V_L = volume on low pressure side, cm^3

p = permeability constant, $\frac{\text{g cm}}{\text{sec cm}^2 \text{ atm}}$

The best value of p is determined by a least square treatment of the ΔP vs t data derived during the test.

For nitrogen tetroxide in which dissociation is a function of temperature and pressure, a closed form solution was not found. The differential equation which defines the permeation is the following:

$$\frac{dm}{dt} = \frac{A}{l} C_1 \left\{ C_2 (m_H^0 - m) + \left[2 C_2 (m_H^0 - m) + 1 \right]^{1/2} - C_3 (m_L^0 + m) - \left[2 C_3 (m_L^0 + m) + 1 \right]^{1/2} \right\} \quad (8.2.3)$$

where:

$$C_1 = K_p / 8 \quad (8.2.4)$$

$$C_2 = \frac{4RT}{46.008 V_H K_p} \quad (8.2.5)$$

$$C_3 = \frac{4RT}{46.008 V_L K_p} \quad (8.2.6)$$

$$K_p = \text{the equilibrium constant of dissociation} \quad \frac{P_{NO_2}^2}{P_{N_2O_4}}$$

T = the absolute temperature, $^{\circ}K$

V_L = the volume of the low pressure side of the permeation cell cm^3

V_H = the volume of the high pressure side of the permeation cell cm^3

R = universal gas constant, $82.054 \frac{cm^3 \text{ atm}}{g \text{ mole } ^{\circ}K}$

m_L^0 = the zero time mass on the low pressure side of the membrane, g

m_H^0 = the zero time mass on the high pressure side of the membrane, g

Various values of p are assumed and the equation is numerically integrated. The value of p is selected which gives a least square error of pressure difference as a function of time calculated from the integrated values compared with the measured pressure differences.

8.2.2 Counter Diffusion

The simultaneous counter diffusion of two gases through a membrane with a partial pressure difference but no total pressure difference is useful in determining whether interactions occur which affect permeation rates. The experimental apparatus which was used for this testing is shown in Figure 8.5. Again some accessory lines and valves were omitted to provide clarity. The test involved a continuous flow of the two gases from the supply tanks, through the cell and into or through the sample bottles. By careful adjustments of the several valves, the flow rate, the cell pressure and differential pressure were adjusted. After sufficient time was allowed for equilibrium to be established, a sample of each gas was taken for analysis.

In all cases the partial pressure difference was equivalent to the absolute pressure of the cell and data reduction required only the algebraic solution of the standard permeation equation

$$Q = \frac{PA \Delta P}{l} t \quad (3.2.7)$$

where the terms were defined previously.

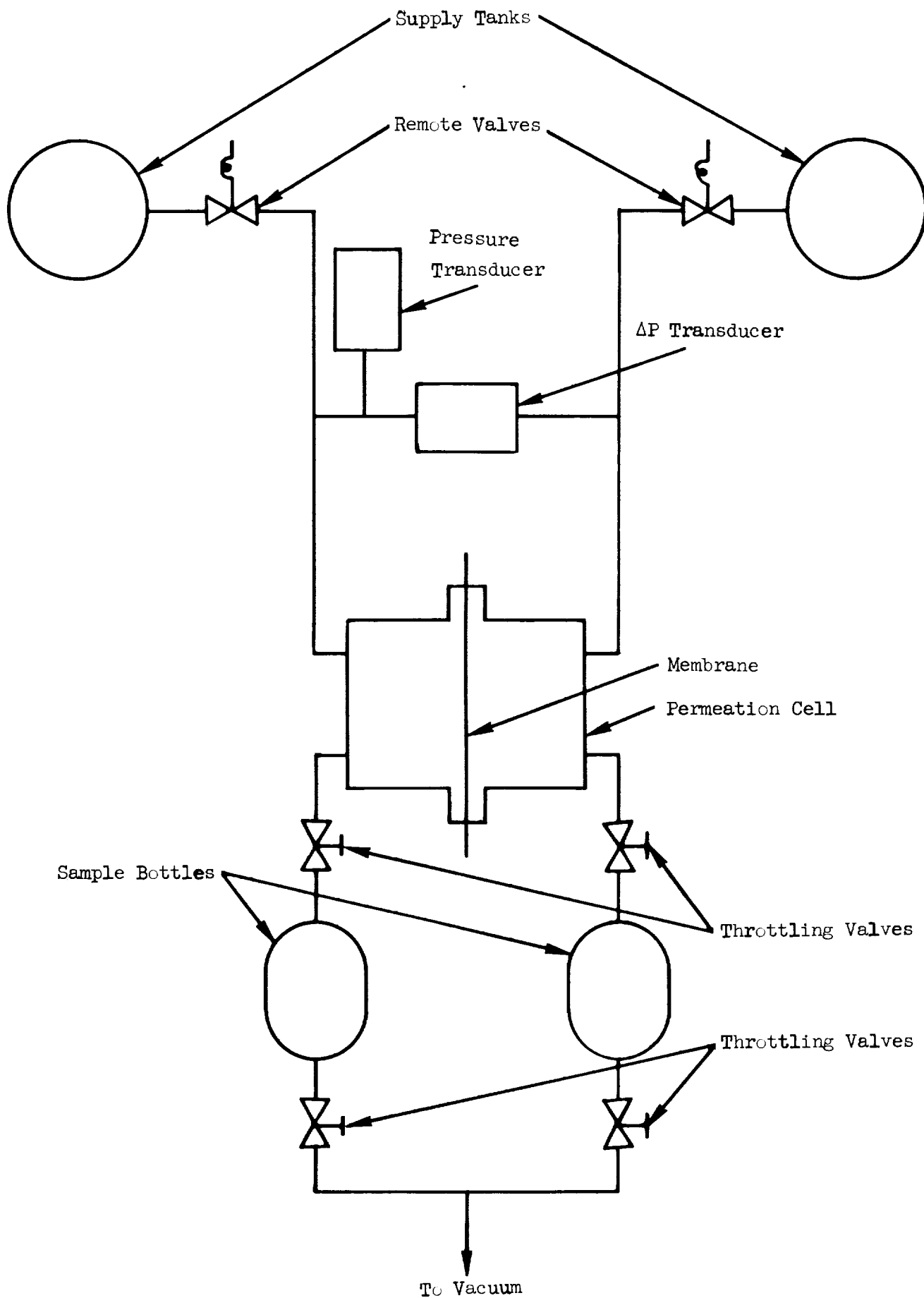


Figure 8.5 Counter Diffusion Apparatus

9.0 RESULTS

There are three basic classes of engineering data which were obtained during this study. These classes are: primary (calculated directly from the experimental measurement), secondary (calculated from the experimental data but requiring assumptions relative to mechanism) and derived (calculated from primary or secondary data). It is evident that solubility is primary data, since the quantity of a gas which dissolves in a unit volume of a material is directly measurable. However, the Henry's Law constant (S) which is defined by

$$q = SP \quad (9.0.1)$$

where:

q = the quantity dissolved per unit volume (usually

$$\frac{\text{CC(STP)}}{\text{cm}^3} \text{ or } \frac{\text{g}}{\text{cm}^3}$$

P = pressure, atm

S = proportionality constant

is secondary data which depends on the manner in which the solubilities follow the assumed law over the pressure range of interest. Similarly the diffusion coefficient computed from the transient adsorption data and the permeation constant obtained from the permeation cell tests represent secondary data. Examples of derived data include S, D or p calculated from the other two using the equation

$$p = DS \quad (9.0.2)$$

where:

p = permeability constant, $\frac{\text{CC(STP) cm}}{\text{sec cm}^2 \text{ atm}}$

D = diffusion coefficient, cm^2/sec

S = Henry Law constant $\frac{\text{CC(STP)}}{\text{atm cm}^3 \text{ of Teflon}}$

Thus, it should be noted that the engineering data required for the analysis of bladder leakage which was obtained as a result of the experimental effort is all of the secondary and derived types. In some cases the theory was found to be only marginally applicable and extrapolation of data outside of the range of measurement must be considered a dangerous practice.

9.1 Solubility Data

Henry's Law constants (S) were obtained from the bomb tests for nitrogen, helium and nitrogen tetroxide in polytetrafluoroethylene (TFE) and tetrafluoroethylene-hexafluoropropylene copolymer (FEP). Numerous attempts were made to obtain solubility data for hydrazine vapor but the gas phase decomposition was sufficiently rapid in the Cres steel (Types 316) apparatus to prevent meaningful data from being obtained.

For both nitrogen (N_2) and helium (He), S was found to be independent of pressure over the range of pressure investigated and could be fit to the usual Arrhenius type equation for temperature with an apparent accuracy of about $\pm 10\%$. Nitrogen tetroxide (NTO) data showed that S increased with increasing pressure but over the pressure range studied (i.e., about one-tenth to one-half the vapor pressure) an average value was selected which represented the data within about $\pm 25\%$.

Figure 9.1 shows an example of the nitrogen tetroxide solubility data. The Henry's law constants which best represent these data give the straight lines which cross the data. Clearly the curved lines represent the data more accurately.

The equations for these curves are:

$$\text{NTO/TFE} \quad q = 3.42 \times 10^{-3} p^{1.36} \text{ g/cm}^3 \quad (9.1.1)$$

$$\text{NTO/FEP} \quad q = 1.84 \times 10^{-3} p^{1.59} \text{ g/cm}^3 \quad (9.1.2)$$

These equations represent the experimental data within $\pm 2\%$. If S is defined as dq/dP , then

$$\text{NTO/TFE} \quad S = 4.65 \times 10^{-3} p^{0.36} \text{ g/atm cm}^3 \quad (9.1.3)$$

$$\text{NTO/FEP} \quad S = 2.93 \times 10^{-3} p^{0.59} \text{ g/atm cm}^3 \quad (9.1.4)$$

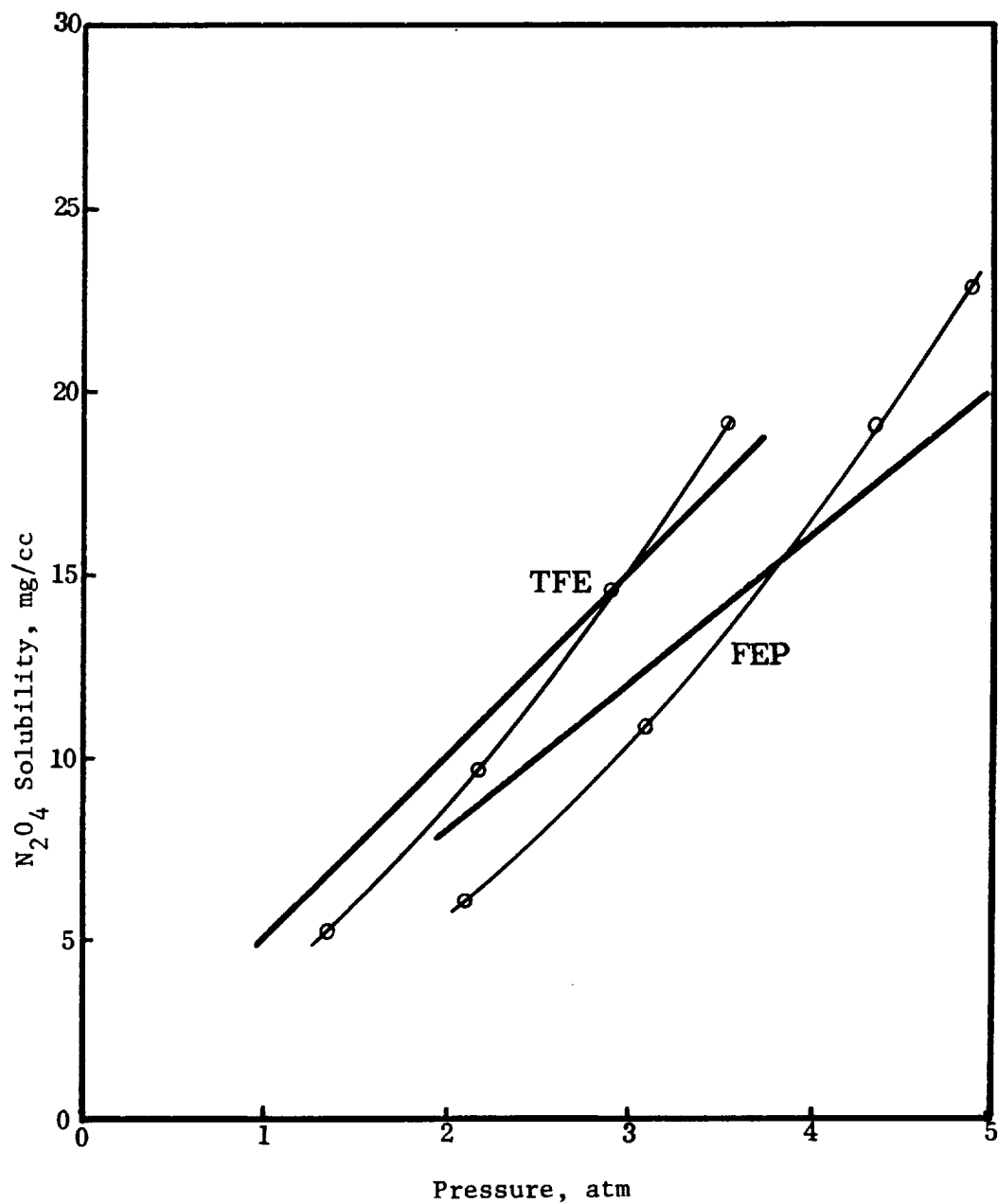


Figure 9.1 Nitrogen Tetroxide Solubility in Teflon
at $160 \pm 5^\circ F$

However, average values for S in the experimental range were used. These data were fit to an Arrhenius type equation to provide a good representation of the effect of temperature. The experimental data are summarized in Table 9 in the form of Arrhenius type plots which represent the experimental data to approximately the indicated accuracy.

Table 9-1
Henry's Law Solubility Constants

N₂/TFE (± 10%)

$$S = 6.6 \times 10^{-4} \exp \frac{1500}{T^{\circ}\text{K}} \text{ CC(STP)/atm cm}^3 \quad \begin{array}{l} 4-30 \text{ atm} \\ 25-100^{\circ}\text{C} \end{array}$$

N₂/FEP (±10%)

$$S = 4.2 \times 10^{-3} \exp \frac{900}{T^{\circ}\text{K}} \text{ CC(STP)/atm cm}^3 \quad \begin{array}{l} 8-30 \text{ atm} \\ 25-100^{\circ}\text{C} \end{array}$$

He/TFE (±10%)

$$S = 2.5 \times 10^{-4} \exp \frac{1400}{T^{\circ}\text{K}} \text{ CC(STP)/atm cm}^3 \quad \begin{array}{l} 6-30 \text{ atm} \\ 25-100^{\circ}\text{C} \end{array}$$

He/FEP (±10%)

$$S = 1.1 \times 10^{-3} \exp \frac{1100}{T^{\circ}\text{K}} \text{ CC(STP)/atm cm}^3 \quad \begin{array}{l} 8-25 \text{ atm} \\ 25-100^{\circ}\text{C} \end{array}$$

N₂O/TFE (±25%)

$$S = 3.4 \times 10^{-7} \exp \frac{3300}{T^{\circ}\text{K}} \text{ g/atm cm}^3 \quad \begin{array}{l} 0.1-0.5 \text{ v.p.} \\ 25-100^{\circ}\text{C} \end{array}$$

N₂O/FEP (±25%)

$$S = 1.2 \times 10^{-7} \exp \frac{3600}{T^{\circ}\text{K}} \text{ g/atm cm}^3 \quad \begin{array}{l} 0.1-0.5 \text{ v.p.} \\ 25-100^{\circ}\text{C} \end{array}$$

9.2 Diffusion Coefficients

Diffusion coefficients for gases and vapors in teflon were obtained both as secondary data and derived data. In this section only the secondary data, namely those obtained from the bomb tests, are discussed. Data were obtained for both nitrogen and nitrogen tetroxide with TFE and FEP. With helium the adsorption was so rapid, useful data points were not recorded and hydrazine vapor decomposed as discussed previously.

Data for nitrogen diffusion were derived point by point and Figure 9.2 shows the adsorption curve for one test and the calculated point by point diffusion coefficients for this test and also for a duplicate test. The data were generally within $\pm 20\%$ of the mean value for each temperature.

Data for nitrogen tetroxide diffusion required a computer solution due to the dissociation reaction. These data are given in Tables 9-2 and 9-3 for TFE and FEP respectively. There appears to be some pressure dependence for D , particularly in the NTO/TFE system, but the scatter is sufficient to limit this to an observation only. The high temperature tests generally contained an insufficient number of data points in each test to provide high confidence in any specific value of D . However, the 3σ deviations are given to indicate the conformity of the data from each run to the best value of the calculated diffusion coefficient.

The NTO/TFE data (except for the one point at 100°C) were fit to an Arrhenius equation which was then evaluated at the four test temperatures. The results given in Table 9-2 show that most data points are within $\pm 50\%$ and the worst is about a factor of 3 from that best fit to the Arrhenius equation. The NTO/FEP data given in Tables 9-3 show less scatter. The lower scatter in the data is attributed to the lower value for D which permitted a larger number of data points to be taken during each test. For NTO/FEP the data generally is within $\pm 20\%$ and the worst point is less than a factor of 2 from the best fit to the Arrhenius equation.

The diffusion coefficient data obtained from the adsorption bomb test and the indicated accuracy are summarized in Table 9-4.

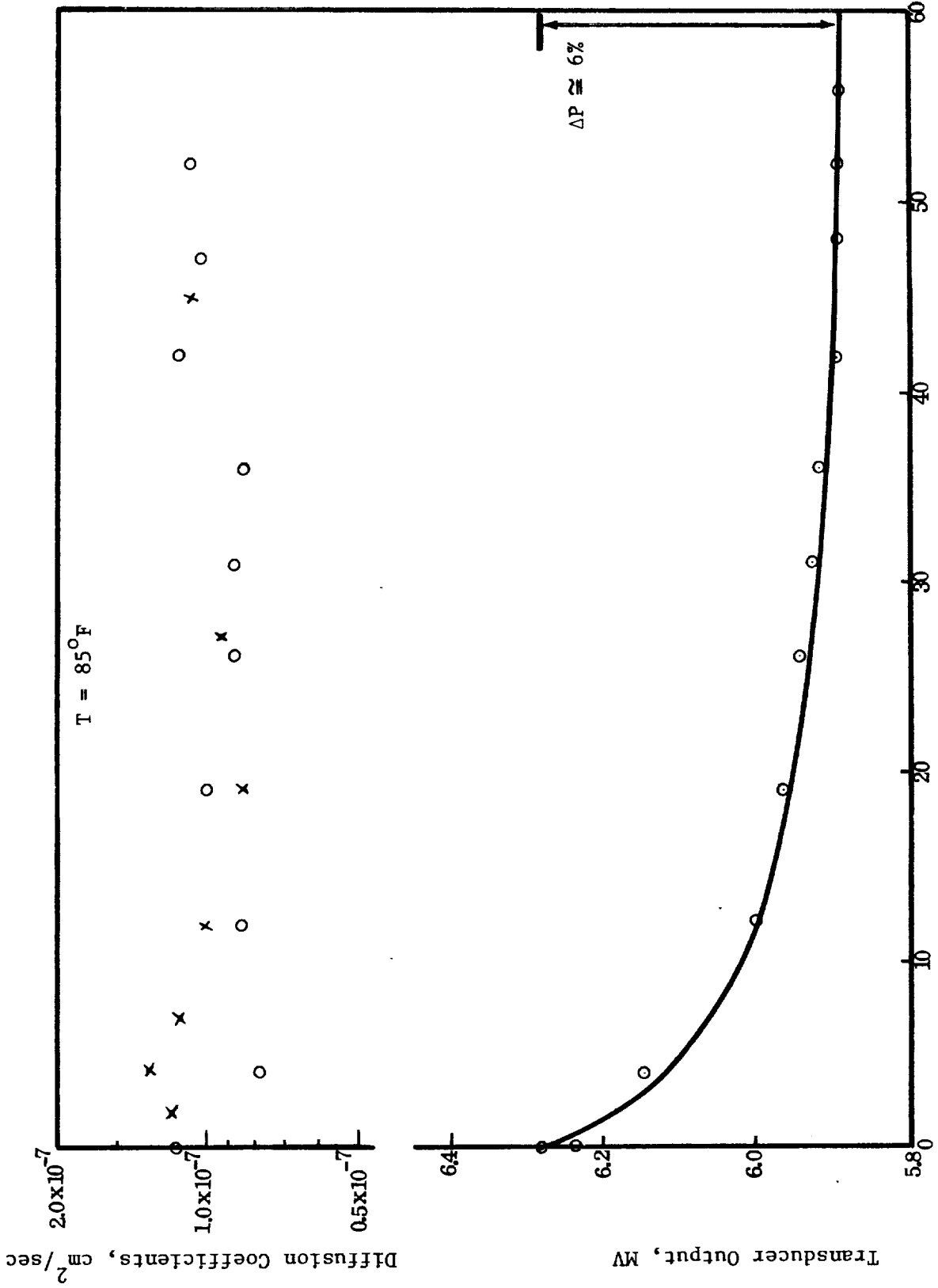


Figure 9.2 Adsorption of Nitrogen in FEP

Table 9-2

Experimental D for NTO/TFE

| <u>Temp. °C</u> | <u>P ave, atm</u> | <u>D x 10⁸, cm²/sec</u> | <u>Remarks</u> |
|-----------------|-------------------|---|----------------------------|
| 27 | .15 | 2.86 ± .20 | 15 data points |
| 27 | .25 | 4.77 ± .63 | 14 data points |
| 28 | .3 | 5.98 ± .63 | 12 data points |
| 73 | 1.4 | 30.4 ± 4.0 | 8 data points |
| 73 | 2.2 | 33.7 ± 6.4 | 5 data points |
| 73 | 2.9 | 38.8 ± 1.4 | 5 data points |
| 74 | 3.5 | 66.3 ± 4.4 | 5 data points |
| 96 | 5.8 | 156 ± 6 | 4 data points |
| 96 | 7.5 | 113 ± 11 | 4 data points |
| 96 | 8.7 | 137 ± 14 | 5 data points |
| 96 | 9.7 | 186 ± 3 | 4 data points |
| 96 | 8.0 | 87 | 2 data points |
| 100 | 3.3 | 77 ± 13 | 4 data points |
| 100 | 4.3 | 63 ± 5 | 4 data points |
| 100 | 5.1 | 152 ± 560 | 4 data points (deleted) |
| 100 | 5.8 | 34 ± 2 | 4 data points |

Calculated from Arrhenius Equation

| | | |
|-----|------------------------|----------------------|
| 27 | 4.5 x 10 ⁻⁸ | cm ² /sec |
| 73 | 38 x 10 ⁻⁸ | cm ² /sec |
| 96 | 90 x 10 ⁻⁸ | cm ² /sec |
| 100 | 100 x 10 ⁻⁸ | cm ² /sec |

Table 9-3
Experimental D for NT0/FEP

| <u>Temp. °C</u> | <u>P ave, atm</u> | <u>D x 10⁸, cm²/sec</u> | <u>Remarks</u> |
|-----------------|-------------------|---|---|
| 26 | 0.3 | 0.90 ± .14 | Uncertainty in final |
| 28 | 0.3 | 0.81 ± .13 | Temperature measure- ment, 9 data points |
| 29 | 0.2 | 0.97 ± .07 | 16 data points |
| 76 | 2.3 | 19.8 ± 2.4 | 5 data points |
| 77 | 4.4 | 19.9 ± 3.3 | 6 data points |
| 77 | 4.9 | 36.1 ± 1.1 | 5 data points |
| 78 | 3.2 | 17.9 ± 1.9 | 7 data points |
| 78 | 3.9 | 21.2 ± 2.5 | 5 data points |
| 92 | 2.3 | 40.3 ± 6.3 | 6 data points |
| 92 | 4.1 | 41.6 ± 4.2 | 5 data points |
| 93 | 5.8 | 53. ± 15 | 4 data points |
| 94 | 7.2 | 70. ± 10 | 3 data points |
| 95 | 8.4 | 54 ± 11 | 6 data points |

Calculated from Arrhenius Equation

28 0.8 x 10⁻⁸ cm²/sec

77 20 x 10⁻⁸ cm²/sec

93 50 x 10⁻⁸ cm²/sec

Table 9-4

Diffusion Coefficients

N₂/TFE (±20%)

$$D = 0.83 \exp - \frac{4500}{T^{\circ K}} \text{ cm}^2/\text{sec} \quad \begin{array}{l} 3 - 30 \text{ atm} \\ 25 - 100^{\circ}\text{C} \end{array}$$

N₂/FEP (±20%)

$$D = 5.5 \times 10^{-2} \exp - \frac{4000}{T^{\circ K}} \text{ cm}^2/\text{sec} \quad \begin{array}{l} 10 - 25 \text{ atm} \\ 25 - 100^{\circ}\text{C} \end{array}$$

NTO/TFE (±50%)

$$D = 0.40 \exp - \frac{4800}{T} \text{ cm}^2/\text{sec} \quad \begin{array}{l} 0.1 - 0.4 \text{ v.p.} \\ 25 - 100^{\circ}\text{C} \end{array}$$

NTO/FEP (±20%)

$$D = 56 \exp - \frac{6800}{T} \text{ cm}^2/\text{sec} \quad \begin{array}{l} 0.2 - 0.4 \text{ v.p.} \\ 25 - 100^{\circ}\text{C} \end{array}$$

9.3 Permeability Constants

Unidirectional permeation measurements were made with helium, nitrogen and nitrogen tetroxide through TFE and FEP membranes. The results of these measurements are given in Table 9-5. The helium data gave permeability constants that were independent of total pressure and differential pressure and were a function of temperature only. Except for two tests, nitrogen gave similar results.

The nitrogen tetroxide data presents a more complicated picture. The calculated permeability constants in both TFE and FEP show no clear dependence on temperature but are strongly influenced by the total pressure. The pressure dependence was computed by least squares and gave the following relationships:

$$\text{NTO/TFE} \quad p \times 10^{10} = 5 + 8 P \text{ atm} \frac{\text{g cm}}{\text{sec atm cm}^2} \quad \sigma = 23 \times 10^{-10}$$

$$\text{NTO/TFE} \quad p \times 10^{10} = 3.7 + 2.3 P \text{ atm} \frac{\text{g cm}}{\text{sec atm cm}^2} \quad \sigma = 1.8 \times 10^{-10}$$

Clearly in the case of NTO/TFE, the data have excessive scatter as indicated by the high value of σ and the equation cannot be used with any confidence. Additional testing at high pressure is required to define more accurately the pressure dependence.

Counter flow permeation measurements were made with helium and nitrogen tetroxide through TFE and FEP. These data are presented in Table 9-6 in the same format and order as the unidirectional data of Table 9-5. The permeability data for all systems including nitrogen tetroxide appear to have a tendency to increase with increasing temperature. There are a sufficient number of exceptions to limit this to an observation only.

The counter diffusion data generally shows that helium permeates more rapidly by a factor of 2 or 3, nitrogen tetroxide permeates more slowly at low pressure by a factor of 2 to 5 and nitrogen varies in both directions within a factor of about 2.

Table 9-5

Experimental Unidirectional Permeation

| Temp, °C | P ave, atm | ΔP , atm | $p, \frac{\text{CC(STP) cm}}{\text{sec cm}^2 \text{ atm}}$ |
|---------------------|------------|------------------|--|
| He/TFE | | | |
| 23 | 0.6 | 0.6 | $3.4 \pm 0.01 \times 10^{-7}$ |
| 23 | 3.3 | 0.6 | 3.4 ± 0.1 |
| 65 | 0.6 | 0.6 | 8.1 ± 0.4 |
| 74 | 18.3 | 0.6 | 7.9 ± 0.1 |
| 86 | 1.4 | 0.8 | 8.2 ± 0.6 |
| He/FEP | | | |
| 21 | 17.5 | 0.2 | $2.5 \pm 0.2 \times 10^{-7}$ |
| 39 | 0.3 | 0.2 | 2.8 ± 0.02 |
| 39 | 0.7 | 0.7 | 2.7 ± 0.2 |
| 60 | 18.9 | 0.7 | 4.3 ± 0.1 |
| 65 | 0.6 | 0.6 | 4.8 ± 0.5 |
| 90 | 0.8 | 0.8 | 9.8 ± 0.5 |
| N ₂ /TFE | | | |
| 29 | 4.7 | 0.7 | $1.5 \pm 0.2 \times 10^{-8}$ |
| 38 | 0.6 | 0.6 | 1.7 ± 0.7 |
| 69 | 0.6 | 0.6 | 6.1 ± 0.1 |
| 69 | 5.8 | 0.7 | 9.8 ± 0.7 |
| 77 | 19.3 | 0.7 | 8.5 ± 0.5 |
| 90 | 0.7 | 0.7 | 1.4 ± 0.1 |

Table 9-5 (cont.)

| Temp, °C | P ave, atm | ΔP, atm | $p, \frac{\text{CC(STP) cm}}{\text{sec cm}^2 \text{ atm}}$ |
|--|------------|---------|--|
| N₂/FEP | | | |
| 35 | 5.6 | 0.7 | $2.2 \pm 0.5 \times 10^{-8}$ |
| 37 | 0.3 | 0.2 | 0.8 ± 0.3 |
| 38 | 17.6 | 0.6 | 11.2 ± 0.3 |
| 39 | 5.1 | 0.7 | 1.7 ± 0.8 |
| 40 | 1.1 | 0.7 | 0.5 ± 0.1 |
| 62 | 0.7 | 0.7 | 3.2 ± 0.3 |
| 62 | 19.3 | 0.7 | 4.7 ± 0.4 |
| 85 | 17.8 | 0.7 | 7.1 ± 0.8 |
| 91 | 0.5 | 0.5 | 10.3 ± 0.2 |
| $p, \frac{\text{g cm}}{\text{sec cm}^2 \text{ atm}}$ | | | |
| NTO/TFE | | | |
| 26 | 0.6 | 0.6 | $5.1 \pm 0.5 \times 10^{-10}$ |
| 60 | 0.7 | 0.6 | 7.9 ± 0.5 |
| 61 | 4.9 | 0.5 | $84. \pm 1$ |
| 64 | 0.5 | 0.5 | 4.7 ± 0.1 |
| 85 | 0.6 | 0.6 | 6.2 ± 0.4 |
| 87 | 7.9 | 0.7 | $45. \pm 8$ |
| NTO/FEP | | | |
| 25 | 0.5 | 0.5 | $5.1 \pm 0.8 \times 10^{-10}$ |
| 64 | 5.2 | 0.6 | 18 ± 1.5 |
| 65 | 0.5 | 0.5 | 3.4 ± 0.6 |
| 84 | 0.5 | 0.5 | 4.9 ± 0.1 |
| 84 | 8.1 | 0.5 | 21 ± 0.3 |

Table 9-6

Experimental Counter Flow Permeation

| Temp, °C | P ave, atm | ΔP , atm | $p, \frac{\text{CC(STP)} \text{ cm}}{\text{sec cm}^2 \text{ atm}}$ |
|---------------------|------------|------------------|--|
| He/TFE | | | |
| 25 | 0.3 | 0.6 | 9.2×10^{-7} |
| 62 | 1.0 | 2.0 | 23. |
| 87 | 0.6 | 1.3 | 26. |
| 89 | 1.0 | 2.0 | 27. |
| He/FEP | | | |
| 25 | 0.3 | 0.7 | 8.7×10^{-7} |
| 30 | 0.3 | 0.7 | 1.3 |
| 88 | 0.3 | 0.7 | 8.9 |
| 88 | 0.6 | 1.3 | 7.6 |
| 88 | 1.0 | 2.1 | 16. |
| N ₂ /TFE | | | |
| 25 | 0.3 | 0.7 | 12×10^{-8} (questionable analysis) |
| 87 | 0.6 | 1.3 | 2.3 |
| 87 | 1.0 | 2.0 | 3.8 |
| N ₂ /FEP | | | |
| 88 | 1.0 | 2.0 | $13. \times 10^{-8}$ |

Table 9-6 (cont.)

| Temp, °C | P ave, atm | ΔP, atm | $p, \frac{\text{g cm}}{\text{sec cm}^2 \text{ atm}}$ |
|----------|------------|---------|--|
| NT0/TFE | | | |
| 25 | 0.4 | 0.8 | 0.29×10^{-10} |
| 25 | 0.3 | 0.7 | 0.42 |
| 62 | 1.0 | 2.1 | 2.4 |
| 87 | 0.6 | 1.3 | 0.96 |
| 87 | 1.0 | 2.0 | 1.25 |
| 87 | 0.6 | 1.3 | 1.67 |
| 89 | 1.0 | 2.0 | 3.1 |
| NT0/FEP | | | |
| 25 | 0.3 | 0.7 | 0.18×10^{-10} |
| 30 | 0.3 | 0.7 | < 0.1 |
| 88 | 0.3 | 0.7 | 0.78 |
| 88 | 0.7 | 1.3 | < 0.09 |
| 88 | 1.0 | 2.1 | 1.03 |
| 88 | 1.0 | 2.0 | 1.35 |

A review of all the experimental and analytical steps involved in making the permeability measurements showed no clear reason for the variability of the data. The least squares determination of the unidirectional permeation data for nitrogen tetroxide reported in Table 9-5 (see Section 8.2) showed that p is not constant but decreases during each run. The reported values are the best constant which fits the data over the pressure range for each test. It was estimated from the apparent pressure sensitivity that p would not vary by more than about 20% during any test. The effect on the tabulated data would probably be small since an average pressure, rather than the final, pressure was reported. Table 9-7 summarizes the permeability results and indicates the range of conditions over which the data were obtained.

Table 9-7
Permeation Constants

He/TFE

$$p_u = 0.88 \times 10^{-4} \exp - \frac{1650}{T^{\circ}\text{K}} \frac{\text{CC(STP)cm}}{\text{sec cm}^2 \text{ atm}} \quad \begin{array}{l} 0.5 - 18 \text{ atm} \\ 20 - 90^{\circ}\text{C} \end{array}$$

$$p_c = 9 \text{ to } 27 \times 10^{-7} \frac{\text{CC(STP)cm}}{\text{sec cm}^2 \text{ atm}} \quad \begin{array}{l} 0.3 - 1 \text{ atm} \\ 25 - 90^{\circ}\text{C} \end{array}$$

He/FEP

$$p_u = 1.5 \times 10^{-4} \exp - \frac{1950}{T^{\circ}\text{K}} \frac{\text{CC(STP)cm}}{\text{sec cm}^2 \text{ atm}} \quad \begin{array}{l} 0.3 - 19 \text{ atm} \\ 20 - 90^{\circ}\text{C} \end{array}$$

$$p_c = 1.3 \text{ to } 16 \times 10^{-7} \frac{\text{CC(STP)cm}}{\text{sec cm}^2 \text{ atm}} \quad \begin{array}{l} 0.3 - 1 \text{ atm} \\ 25 - 90^{\circ}\text{C} \end{array}$$

N₂/TFE

$$p_u = 2.0 \times 10^{-2} \exp - \frac{4300}{T} \frac{\text{CC(STP)cm}}{\text{sec cm}^2 \text{ atm}} \quad \begin{array}{l} 0.6 - 19 \text{ atm} \\ 30 - 90^{\circ}\text{C} \end{array}$$

$$p_c = \text{about } 3 \times 10^{-8} \frac{\text{CC(STP)cm}}{\text{sec cm}^2 \text{ atm}} \quad \begin{array}{l} 0.6 - 1 \text{ atm} \\ 85^{\circ}\text{C} \end{array}$$

N₂/FEP

$$p_u = 2.4 \times 10^{-2} \exp - \frac{4500}{T^{\circ}\text{K}} \frac{\text{CC(STP)cm}}{\text{sec cm}^2 \text{ atm}} \quad \begin{array}{l} 0.3 - 19 \text{ atm} \\ 35 - 90^{\circ}\text{C} \end{array}$$

$$p_c = \text{about } 13 \times 10^{-8} \frac{\text{CC(STP)cm}}{\text{sec cm}^2 \text{ atm}} \quad \begin{array}{l} 1 \text{ atm} \\ 90^{\circ}\text{C} \end{array}$$

NT0/TFE

$$p_u = \text{about } 6 \times 10^{-10} \frac{\text{g cm}}{\text{sec cm}^2 \text{ atm}} \quad \begin{array}{l} 0.6 \text{ atm} \\ 25 - 90^{\circ}\text{C} \end{array}$$

$$p_c = 0.3 \text{ to } 3 \times 10^{-10} \frac{\text{g cm}}{\text{sec cm}^2 \text{ atm}} \quad \begin{array}{l} 0.3 - 1 \text{ atm} \\ 25 - 90^{\circ}\text{C} \end{array}$$

Table 9-7 (Cont.)

NT0/FEP

$$p_u = \text{about } 5 \times 10^{-10} \frac{\text{g cm}}{\text{sec cm}^2 \text{ atm}}$$

0.5 atm
25 - 90°C

$$p_c = 0.2 \text{ to } 1.4 \times 10^{-10} \frac{\text{g cm}}{\text{sec cm}^2 \text{ atm}}$$

0.3 - 1 atm
25 - 90°C

p_u = permeability constant from unidirectional tests

p_c = permeability constant from counter flow tests

9.4 Summary of Results

The preceding sections presented the experimental results separately for each type of test conducted during the experimental program. In this section the complete data generated by the experimental program is inter-compared and then compared with the available literature. Since only permeability constants were found in the literature, it is most convenient to examine all data in terms of the permeability constant. This constant for many flow geometries is directly proportional to the leakage rate.

9.4.1 Helium Permeation

Helium permeation data are available from the experimental program for both counter diffusion and unidirectional permeation through TFE and FEP. Since diffusion coefficients for helium could not be measured during the adsorption tests, there is no permeation data derived from the SD product.

Stern et al (Reference 18) give an Arrhenius type equation for helium permeation in FEP which applies over the measured range of 0.1 to 4 atm and 25 to 100°C. Their equation reduces to the following:

$$p_{\text{He}} = 1.4 \times 10^{-3} \exp - \frac{2400}{T} \frac{\text{CC(STP)cm}}{\text{sec atm cm}^2}$$

In an earlier article, Stern et al (Reference 19) gave data for helium permeation in TFE in graphical form over the same temperature range. Graphical data from duPont was also reported by Redel (Reference 22) in the same temperature range.

The only other data found for helium permeation of Teflon is from Rocketdyne (Reference 21) where data is given for a mixed sheet of TFE and FEP and for TFE sheet containing aluminum flakes. This cannot be readily compared with data for pure materials.

All the available permeation data are summarized in Figure 9.3. The literature values are represented by the solid lines and the least square fits of the unidirectional permeation data are represented by the

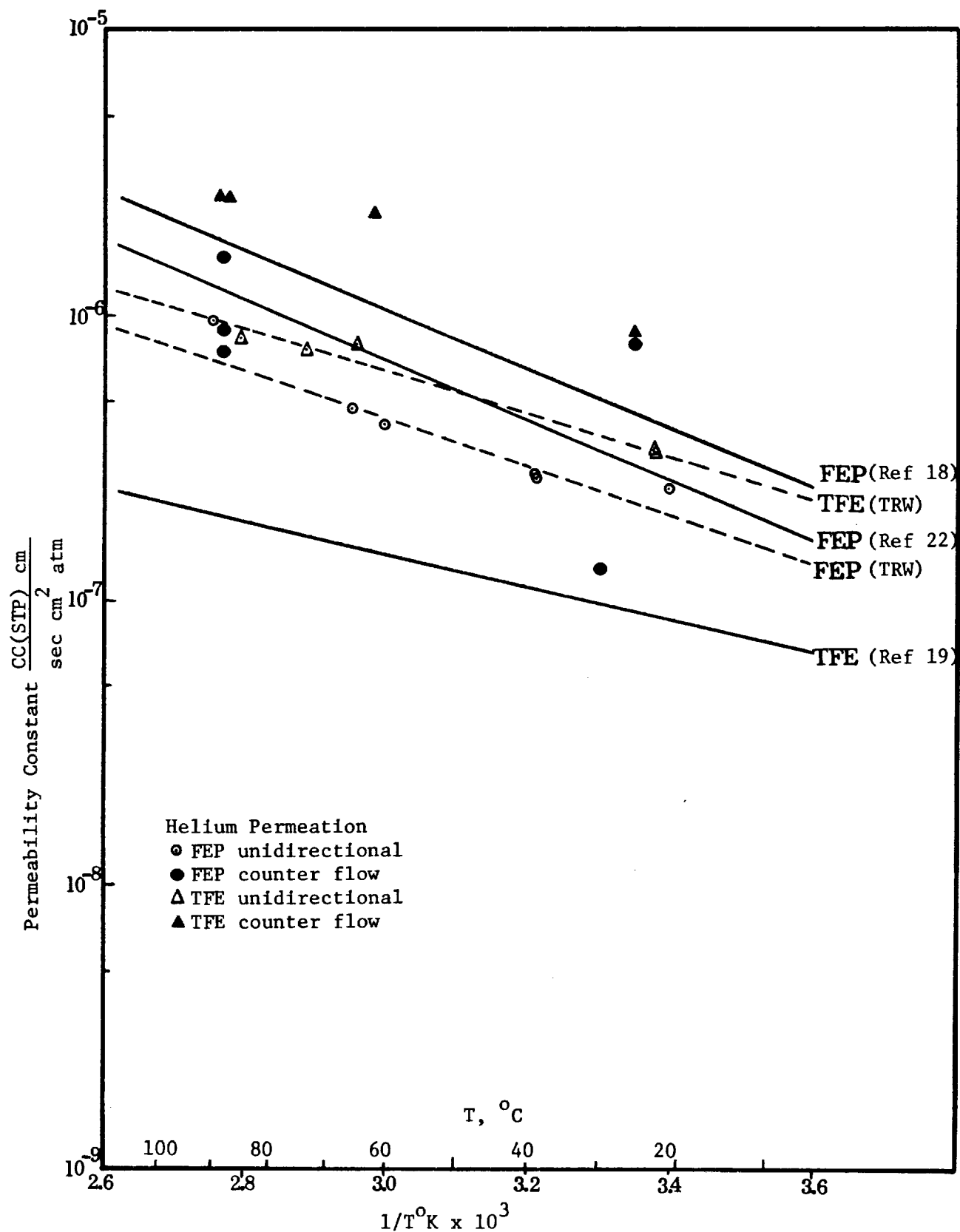


Figure 9.3 Experimental Permeation of Helium

dashed lines. The actual unidirectional data are shown as open circles and triangles and the counter flow data by the corresponding filled symbols. The literature data is in good agreement with the data obtained during this study.

9.4.2 Nitrogen Permeation

Nitrogen permeation data are available from the experimental program for both counter diffusion and unidirectional permeation through TFE and FEP. It also was possible to compute the S·D product for both TFE and FEP from the data measured in the adsorption bomb tests, namely:

$$N_2/\text{TFE} \quad S \cdot D = 5.5 \times 10^{-4} \exp - \frac{3000}{T} \frac{\text{CC(STP)cm}}{\text{sec atm cm}^2}$$

$$N_2/\text{FEP} \quad S \cdot D = 2.3 \times 10^{-4} \exp - \frac{3100}{T} \frac{\text{CC(STP)cm}}{\text{sec atm cm}^2}$$

Stern et al (Reference 18) give an Arrhenius type equation for nitrogen permeation in FEP which is applicable at pressures from 0.1 to 4 atm at temperatures from 60° to 100°C. Below 60°C it is applicable at low pressures and higher, at least as high as 4 atmospheres if sufficient time is allowed for equilibrium to be attained. At room temperature the times required for equilibrium appears to be of the order of a few hours. Their equation reduces to the following:

$$p = 3.2 \times 10^{-3} \exp - \frac{3600}{T} \frac{\text{CC(STP)cm}}{\text{sec atm cm}^2}$$

In an earlier article Stern et al (Reference 19) gave data for nitrogen permeation in TFE in graphical form over the range 25 to 90°C. No mention was made of pressure dependence at low temperature with TFE.

Lebovits (Reference 17) gave a value of 1.6×10^{-8} CC(STP)cm/sec atm cm² for the permeation constant of nitrogen through FEP at 20 to 30°C and Rocketdyne reported a value of 4.6×10^{-9} CC(STP)cm/sec atm cm² at 21 to 24°C. Graphical data from duPont for nitrogen permeation of FEP over the temperature range of 0 to 100°C was reported by Redel (Reference 22).

These data are summarized in Figure 9-4. The literature data are represented by solid lines, the least square fits of the unidirectional permeation data obtained during this study are represented by dashed lines and the SD products are shown by dotted lines. The unidirectional and counter flow data points are shown in the figure as open and filled symbols respectively. The literature data and those data obtained during this study are in good agreement. In view of the discussion of Stern (Reference 18) of the long times required for N_2/FEP to reach equilibrium at pressure as high as 4 atmospheres and at temperatures below $60^\circ C$, the unidirectional data at 35 to $40^\circ C$ should be noted. These data range from 5×10^{-9} to 1.1×10^{-7} CC(STP)cm/sec atm cm^2 for average pressures ranging from 0.3 to 18 atmospheres. The highest value taken at 18 atm was not included in the curve fit which is believed to represent the equilibrium values. Considering the probable precision of the experiments, it is likely that this point represents a nonequilibrium value of the permeability constant.

9.4.3 Nitrogen Tetroxide Permeation

Nitrogen tetroxide permeation data were obtained in the experimental program for both unidirectional and counter flow through TFE and FEP. Since the adsorption tests provided both solubilities and diffusion coefficients, it was also possible to obtain the corresponding SD product namely:

$$NTO/TFE \quad S \cdot D = 1.4 \times 10^{-7} \exp - \frac{1500}{T} \frac{g \text{ cm}}{\text{sec atm cm}^2}$$

$$NTO/TFE \quad S \cdot D = 6.7 \times 10^{-6} \exp - \frac{3200}{T} \frac{g \text{ cm}}{\text{sec atm cm}^2}$$

The literature also provided some permeation data but these data were available at only one or two temperatures and in a form which requires assuming the differential pressure to derive the permeability constant. JPL (Reference 20) reported the results of a test at $20^\circ C$ through a 10 mil teflon film (assumed to be TFE) which showed an equilibrium leakage rate of 5.6×10^{-4} g/ hr in^2 . From the nature of the experiment, it was possible to estimate an equilibrium permeability constant of 6.5×10^{-10} g cm/sec atm cm^2 .

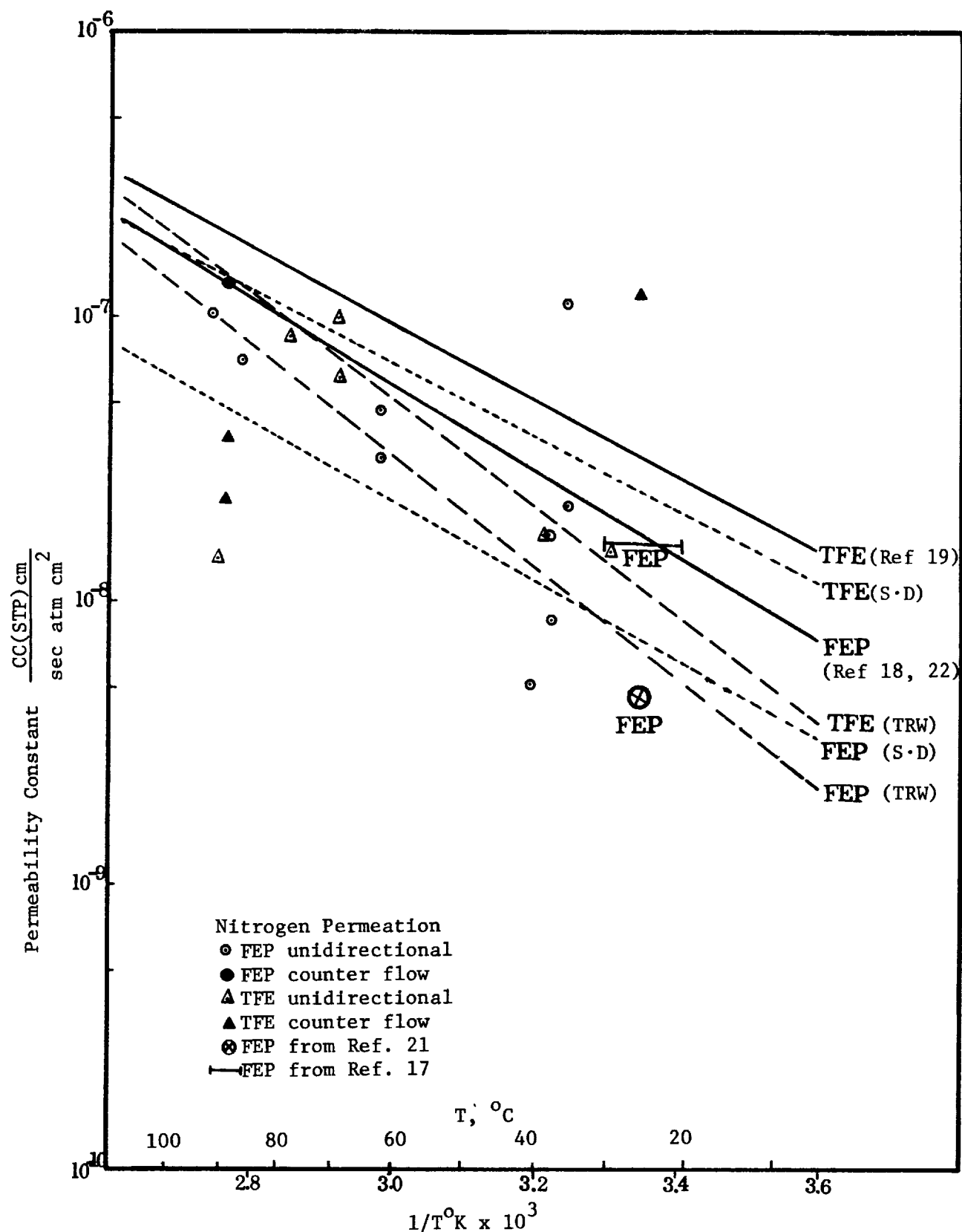


Figure 9.4 Experimental Permeation of Nitrogen

Redel (Reference 22) reported leakage rates of 1.7 to 4.7×10^{-2} g/hr in² through single 2 mil sheets of FEP at 24°C and 7×10^{-3} g/hr in² through double 2 mil sheets of FEP. These leakage rates permitted permeability constants to be calculated ranging from 3.0×10^{-9} to 1.0×10^{-8} g cm/sec atm cm².

Rocketdyne reported the results of a large number of tests using several test procedures and several pure and composite samples. The data for pure materials are given in Table 9-8 together with the calculated permeability constants.

Table 9-8

NTO Permeability (Reference 21)

| <u>Material</u> | <u>T, °C</u> | <u>Q/A, lbs/hr in²</u> | <u>p calc, g cm/sec atm cm²</u> |
|-----------------|--------------|-----------------------------------|--|
| 10 mil FEP | 74 | 6.76×10^{-5} | 4.0×10^{-9} |
| 10 mil FEP | 74 | 6.13×10^{-5} | 3.7×10^{-9} |
| 10 mil FEP | 74 | 13.7×10^{-5} | 8.2×10^{-9} |
| 10 mil FEP | 74 | 13.6×10^{-5} | 8.2×10^{-9} |
| 15 mil TFE | 74 | 4.67×10^{-5} | 4.2×10^{-9} |
| 15 mil TFE | 25 | 0.29×10^{-5} | 2.2×10^{-9} |
| 10 mil FEP | 21 | 0.43×10^{-5} | 8.0×10^{-10} |

All nitrogen permeability data obtained to the experimental program and calculated from the literature are given in Figure 9.5. The unidirectional and counter flow data were discussed in detail in the previous section but it is more evident from the figure that unidirectional tests gave permeation constants up to an order of magnitude higher than the counter flow tests. The S·D product, shown by the dotted lines is in better agreement with the unidirectional data as would be expected from the nature of the adsorption test. Most of the literature values gave results higher than all but the high pressure unidirectional tests of this study. It was not always possible to determine whether the literature test represented counter flow or unidirectional. The JPL data and apparently the Redel data and some of the Rocketdyne data are counter flow

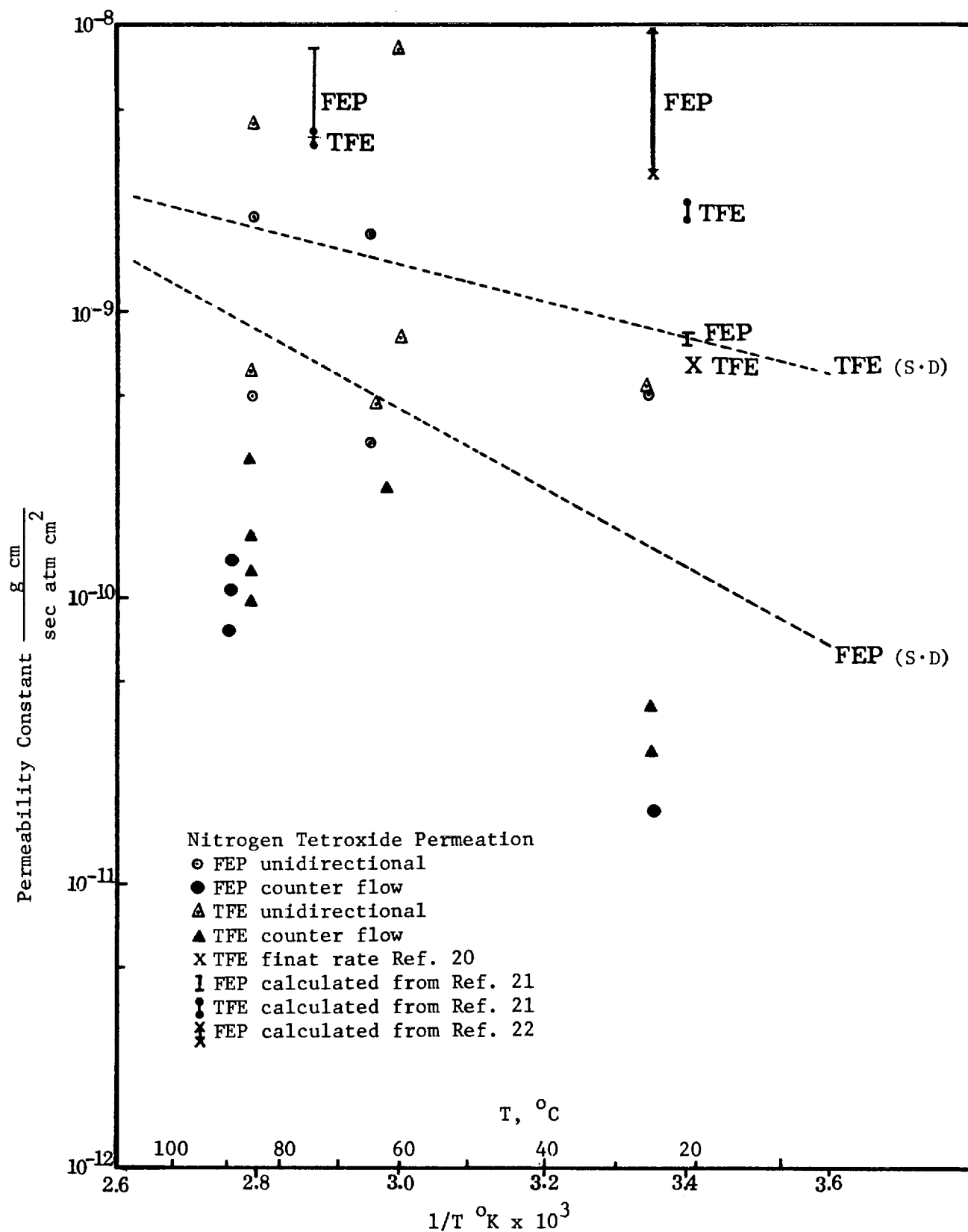


Figure 9.5 Experimental Permeation of Nitrogen Tetroxide

results. The high permeation rate data of Rocketdyne at 74°C are apparently counter flow but the remainder may be unidirectional. In all cases, the literature data seems to have liquid nitrogen tetroxide rather than vapor in contact with the membrane and therefore the test pressures at each temperature were above those of this study.

9.5 Leakage Through Holes

A final part of the test program involved counter flow tests with a laminated sample containing a selected hole area. The sample was made from 1 mil aluminum foil containing 100 ten mil diameter holes spaced on 0.1 inch centers of a 10 by 10 square pattern. To this foil 10 mils of TFE and FEP were applied to opposite faces. The sample was placed in the permeation cell and run in the counter diffusion mode with nitrogen tetroxide on the TFE side of the sample and helium on the FEP side.

During the first of three tests, the sample was evacuated at 187°F and when thoroughly degassed nitrogen tetroxide vapor and helium gas were introduced to a total pressure of 145 psia on each side of the sample. The cell was closed off and after 2 hours the gases on each side of the membrane were withdrawn for analysis. This test gave a helium leakage rate of 1.5×10^{-5} CC(STP)/sec, but an undetectably low concentration of NO₂. Equilibrium clearly was not attained during this time period.

The two later tests were conducted with a modified procedure. After evacuating the sample, the nitrogen tetroxide and helium were slowly flowed past the membrane at approximately the pressure to be used during the test. After a period of several hours, the cell was closed off as in the first test and allowed to remain for the specified test duration. The gas from each side was withdrawn for analysis as in the first test. Helium analyses in nitrogen tetroxide were by a gas chromatographic method with nitrogen as a carrier gas and nitrogen tetroxide analyses in helium were by an infrared technique.

The results of these tests are as follows:

| | <u>Test 2</u> | <u>Test 3</u> |
|---------------------------------------|----------------------|----------------------|
| Temperature, °C | 86 | 93 |
| Pressure, atm | 9.9 | 4.9 |
| Flow time, hours | 6 | 2 |
| Test time, hours | 64.5 | 44 |
| Helium leak rate, CC(STP)/sec | 8.6×10^{-8} | 1.6×10^{-5} |
| Nitrogen tetroxide leak rate g/sec | 3.1×10^{-8} | 1.6×10^{-8} |

The membrane was not inspected between tests, but at the conclusion of the tests the laminated sample was removed and examined. Several changes had occurred. The membrane was supported on the TFE side by a screen and on the FEP side by a porous metal sheet so that gross movement due to momentary pressure differentials was restrained. Nevertheless, at some time during the test series sufficient movement occurred to tear the aluminum foil near the flange. This may have occurred when flow rates were being adjusted at the start of Test 2 or Test 3, or possibly when the gas samples were taken at the end of any of the three tests. At any rate, the time at which this additional leakage path through the barrier occurred cannot be determined.

Another change also was evident. There was complete separation of the TFE and aluminum over the full 45.5 cm^2 area of the sample. This separation could have occurred at any time during the test series, but it is likely to have occurred during the initial test either during evacuation or during depressurization as the gas samples were withdrawn. Thus, very likely Tests 2 and 3 were made with only the FEP bonded to the foil. The sample as received had a weak bond at the TFE-foil interface. As in all the previous tests involving FEP membranes, the FEP was considerably lighter in color after exposure to nitrogen tetroxide but no significant effect was attributed to the bleaching. Earlier laminated samples which had insufficient hole areas were tested in the adsorption bomb with similar results relative to bleaching and delamination. It appears that improvements in bonding between TFE and aluminum foil are necessary.

10.0 REFERENCES

1. Jost, W., Diffusion in Solids, Liquids, Gases, Academic Press Inc., New York, 1960. Third Printing with Addendum.
2. DeGroot, S. R. and P. Mazur, Non-Equilibrium Thermodynamics, Interscience Publishers Inc., New York, 1962.
3. Landau, L. F. and E. M. Lifshitz, Statistical Physics, Addison Wesley Publishing Co., New York, 1960.
4. Sommerfeld, A., Thermodynamics and Statistical Mechanics, Academic Press Inc., New York, 1956.
5. Johnson, R. L., "An Approximate Calculation of the Leakage Rate Through a Laminated Bladder Structure When the Diffusion Barrier is Faulted," TRW Systems Report No. EM 16-12, October 1966.
6. Johnson, R. L., "Diffusion Through a Hole in an Otherwise Impermeable Boundary Between Two Semi-Infinite Slabs," TRW Systems Report No. EM 16-13, October, 1966.
7. Tranter, C. J., Integral Transforms in Mathematical Physics, John Wiley & Sons, Inc., New York, 1959.
8. Gradshteyn, I. S., and I. M. Ryzhik, Table of Integrals, Series, and Products, Academic Press, New York, 1965, Fourth Edition.
9. Johnson, R. L., "A Study to Analyze the Permeation of High Density Gases and Propellant Vapors Through Single Layer Teflon or Teflon Structure Materials and Laminations, Design Guide," TRW Systems Report 07282-0617-R000.
10. Milne-Thomson, L. M., Theoretical Hydrodynamics, The MacMillan Co., New York, 1961, Fourth Edition.
11. Copson, E. T., An Introduction to the Theory of Functions of a Complex Variable, Oxford University Press, Amen House, London, 1960.
12. Chang, E. T., and N. A. Gokcen, "Thermodynamic Properties of Gases in Propellants and Oxidizers, I. Solubilities of He, N₂, O₂, A_r, and N₂O₃ in Liquid N₂O₄," Journal of Physical Chemistry, 70, 2394, 1966.

13. Johnson, R. L., "Leakage Through a Circular Hole in an Impermeable Barrier Separating Two Soluble Phases," TRW Systems Report No. EM 17-12, August, 1967.
14. Prutton, C. F., and S. H. Maron, Fundamental Principles of Physical Chemistry, The MacMillan Co., New York, 1951.
15. Crank, J., The Mathematics of Diffusion, Oxford University Press, London (1956)
16. Rickles, R. N., "Molecular Transport in Membranes," Ind. Eng. Chem. 58 (6) 19 (June 1966).
17. Lebovits, A., "Permeability of Polymers to Gases, Vapors, and Liquids," Modern Plastics 43 (7) 139 (March 1966).
18. Stern, S. A., et al, "Helium Recovery by Permeation," Ind. Eng. Chem. 57 (2) 49 (Feb. 1965).
19. Stern, S. A., et al, "An Improved Permeability Apparatus of the Variable - Volume Type," Modern Plastics 42 (2) 154 (Oct. 1964).
20. Bauman, A. J. and C. H. Stenbridge, "A Continuous-Recording Automatic Permeameter, with Application to the Permeation of Nitrogen Tetroxide Through Teflon," JPL Space Programs Summary, No. 37-30, Vol. VI, p. 206.
21. Settle, J. P. and F. T. Schuler, "Permeation Tests of Candidate Gemini Oxidizer Expulsion Bladder Materials at Temperatures in the Range 15 - 165^oF," Rocketdyne Report MPR 3-253-020 (18 Feb. 1963).
22. "Teflon Sandwich Permeability Studies, Final Report," Redel Report RI #520-339-Final (14 Oct. 1963).
23. "Storable Liquid Propellants Nitrogen Tetroxide/Aerozine 50," Aerojet Report No. LRP 198 (June 1962).

Appendix A

Consider a laminated bladder structure separating two infinite half spaces. The upper half space contains gas, the lower liquid, and the laminated structure consists of two layers of material permeable to the pressurant gas separated by an impermeable barrier which has one circular hole in it. We wish to determine the leakage rate of the gas through the bladder and into the liquid taking into account the effect of the gas and liquid spaces. Let p_1 be the partial pressure of the pressurant gas in the gas mixture, c_1 the concentration (in mass fraction) of the gas in the first layer of Teflon, c_2 that in the second layer, and c_3 its concentration in the liquid propellant. Then from figure (A.1)

$$\nabla^2 p_1 = 0, \quad x > h$$

$$\nabla^2 c_1 = 0, \quad 0 < x < h$$

$$\nabla^2 c_2 = 0, \quad -b < x < 0$$

$$\nabla^2 c_3 = 0, \quad x < -b$$

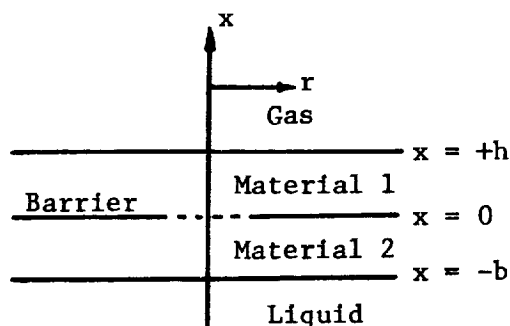


Figure A.1

Instead of p_1 we solve for $\psi = p_o - p_1$ where p_o is the total system pressure. Since p_1 goes to p at distances far removed from the opening, ψ vanishes for large $(x^2 + r^2)^{1/2}$. In cylindrical coordinates*

$$\nabla^2 \psi = \frac{\partial^2 \psi}{\partial r^2} + \frac{1}{r} \frac{\partial \psi}{\partial r} + \frac{\partial^2 \psi}{\partial x^2} = 0 \quad (\text{A.1})$$

The Hankel Transform of zero order of eq. (A.1) gives

$$\frac{d^2 \psi(k, x)}{dx^2} - k^2 \psi(k, x) = 0 \quad (\text{A.2})$$

as the equation satisfied by the Hankel Transform of $\psi(r, x)$. The solution which vanishes for large $\sqrt{x^2 + r^2}$ is

*We assume a circular shaped hole for convenience. The results are however valid for holes of any shape.

$$\psi(k, x) = A_1(k) e^{-kx} \quad (\text{A.3})$$

where, of course, $A_1(k)$ is an unknown function of k . Forming the Hankel inversion and using the definition of $\psi(r, x)$ gives

$$p_1(r, x) = p_o - \int_0^\infty k A_1(k) e^{-kx} J_0(kr) dk, \quad x > h \quad (\text{A.4})$$

For the Hankel Transform of $c_1(r, x)$ we find in the same manner

$$c_1(k, x) = A_2(k) \cosh kx + A_3(k) \sinh kx \quad (\text{A.5})$$

with inverse,

$$c_1(r, x) = \int_0^\infty k A_2(k) \cosh kx J_0(kr) dk + \int_0^\infty k A_3(k) \sinh kx J_0(kr) dk, \quad 0 < x < h \quad (\text{A.6})$$

The boundary conditions which must be satisfied at $x = h$ are

$$c_1(r, h) = \kappa_1 p_1(r, h) \quad (\text{A.7})$$

$$\text{and} \quad \rho_1 D_1 \frac{\partial c_1(r, h)}{\partial x} = \frac{M_g D_g}{RT} \frac{\partial p_1}{\partial x} \quad (\text{A.8})$$

In the first equation κ_1 is the solubility of pressurant gas in material 1 while in the second ρ_1 is density of material 1 and D_1 is the diffusivity of pressurant gas through material 1. Also M_g is the molecular weight of the pressurant, D_g the binary diffusion coefficient for the mixture of pressurant gas and propellant vapor, R is the gas constant and T the gas temperature. Applying eqs. (A.7) and (A.8) to equations (A.4) and (A.6) we obtain from (A.7)

$$\begin{aligned} \int_0^\infty k A_2(k) \cosh kh J_0(kr) dk + \int_0^\infty k A_3(k) \sinh kh J_0(kr) dk \\ = \kappa_1 p_o - \kappa_1 \int_0^\infty k A_1(k) e^{-kh} J_0(kh) dk \end{aligned} \quad (A.9)$$

and from (A.8)

$$\begin{aligned} \rho D_1 \left[\int_0^\infty k^2 A_2(k) \sinh kh J_0(kr) dk + \int_0^\infty k^2 A_3(k) \cosh kh J_0(kr) dk \right] \\ = \frac{M D}{\rho_1 D_1 RT} \int_0^\infty k^2 A_1(k) e^{-kh} J_0(kr) dk \end{aligned} \quad (A.10)$$

These equations hold for all r . We may, therefore, write from the second equation

$$A_2(k) \sinh kh + A_3(k) \cosh kh = \frac{M D}{\rho_1 D_1 RT} A_1(k) e^{-kh} \quad (A.11)$$

Using the representation of the delta function

$$\int_0^\infty r J_0(kr) dr = \frac{\delta(k)}{k} \quad (A.12)$$

we obtain, after multiplying equation (A.9) by $r J_0(k, r)$ and integrating over all r ,

$$A_2(k) \cosh kh + A_3(k) \sinh kh + \kappa_1 A_1(k) e^{-kh} = \kappa_1 p_o \frac{\delta(k)}{k} \quad (A.13)$$

From eqs. (A.11) and (A.13) we eliminate $A_1(k)$ and solve for $A_3(k)$ in terms of $A_2(k)$. Substituting the value of $A_3(k)$ in terms of $A_2(k)$ in eq. (A.5) we obtain

$$\begin{aligned} c_1(k, x) = \frac{\kappa_1 p_o}{\tanh kh + \beta} \frac{\sinh kx}{\cosh kh} \frac{\delta(k)}{k} \\ + A_2(k) \left[\cosh kx - \frac{1 + \beta \tanh kh}{\tanh kh + \beta} \sinh kx \right] \end{aligned} \quad (A.14)$$

where $\beta = \kappa_1 \rho_1 D_1 RT / M_g D_g$. If β is very small, that is, zero, eq. (A.14) reduces to

$$c_1(k, x) = \kappa_1 p_0 \frac{\sinh kx}{\sinh kh} \frac{\delta(k)}{k} + \frac{\sinh k(h-x)}{\sinh kh} A_2(k) \quad (A.15)$$

which, upon inversion gives

$$c_1(r, x) = \kappa_1 p_0 \frac{x}{h} + \int_0^\infty k A_2(k) \frac{\sinh k(h-x)}{\sinh kh} J_0(kr) dk \quad (A.16)$$

Putting

$$A_2(k) = \kappa_1 p_0 \frac{\delta(k)}{k} - A_2'(k)$$

gives finally

$$c_1(r, x) = \kappa_1 p_0 - \int_0^\infty k A_2'(k) \frac{\sinh k(h-x)}{\sinh kh} J_0(kr) dk \quad (A.17)$$

This is the same equation for A_2' as was found in section 2.1 for the case of constant concentration, $c_0 = \kappa_1 p_0$, on the boundary $x = h$. We conclude that when $\beta = 0$ the gas phase can be ignored and the problem reduces to that with a constant concentration on the gas phase boundary of the bladder.

Let us examine the order of magnitude of β under typical conditions. For Nitrogen gas the measured value of the solubility κ_1 is of the order of 10^{-4} [(gms N_2)/(cm³)]/[(gms Teflon)/(cm³)] atm⁻¹. At 300°K $RT/M_g = (82.05)(300)/28 = 0.88 \times 10^3$ while $D_1/D_g \sim 10^{-6}$ since the measured value of D_1 is about 10^{-7} and for binary gas solutions D_g is always about 10^{-1} . The density of Teflon is of the order of 1.0 so

$$\beta = \frac{\kappa_1 \rho_1 D_1 RT}{M_g D_g}$$

is of the order of 10^{-7} . Thus β is expected to be very small.

The leakage rate must, for a physically meaningful solution, be a continuous function of the parameters, for example β , upon which it depends. Therefore the leakage rate for very small values of β will differ only slightly from its value for $\beta = 0$. As we have shown above $\beta = 0$ corresponds to the assumption of a constant gas concentration on the interface between the bladder and the pressurant gas space. Therefore, the leakage rate through the structure can be calculated to good accuracy by ignoring diffusion in the gas space.

A similar analysis for the interface between bladder and liquid space gives the result that the concentration on this interface can be assumed to be zero provided $(\rho_\ell D_\ell \kappa_\ell) / (\rho_2 D_2 \kappa_2) \gg 1$. Here ρ_ℓ is the density of the liquid propellant, D_ℓ is the diffusivity of pressurant gas in liquid propellant, κ_2 is the solubility of the gas in material 2, ρ_2 is the density of material 2 and κ_ℓ is the solubility of the gas in liquid propellant. In this case $\rho_\ell \approx \rho_2$, $D_\ell \sim 10^{-5} \text{ cm}^2/\text{sec}$ (a best estimate from the literature, see reference 1) $\kappa_2 \sim 10^{-4}$ as above, $D_2 \sim 10^{-7}$ as above, and $\kappa_\ell \sim 10^{-4}$ according to the data of Chang and Gokcen⁽¹²⁾. Thus the magnitude of the ratio is about 10^2 . It appears that neglecting diffusion through the liquid is not so good an approximation as neglecting it through the gas. However, 10^2 is sufficiently large compared to 1.0 for us to expect that calculations based on assuming the concentration vanishes at the liquid-bladder interface will give a good engineering approximation to the leak rate.

Appendix B

In this section the integrals necessary for the calculation of the leakage rate through rectangular slits (Section 2.2) will be evaluated. From eq. (2.2.18) the integral is

$$\int_0^{\infty} \tanh kh J_0(ka) \sin ka \frac{dk}{k^2} = F \quad (B.1)$$

Let $ka = u$; $dk/k^2 = a(du/u^2)$; $kh = (h/a)u = \alpha u$ where $\alpha = h/a$. Then (B.1) is equivalent to

$$F(\alpha) = a \int_0^{\infty} \tanh \alpha u J_0(u) \sin u \frac{du}{u^2} \quad (B.2)$$

To evaluate the integral it is necessary to represent $\tanh \alpha u$ by its expansion in partial fractions⁽¹⁰⁾.

$$\frac{\tanh \alpha u}{u} = \frac{2}{\alpha} \sum_{n=0}^{\infty} \frac{1}{u^2 + (n + \frac{1}{2})^2 (\pi^2/\alpha^2)} \quad (B.3)$$

Using (B.3) in (B.2) gives, after interchanging the order of summation and integration

$$F(\alpha) = \frac{2a}{\alpha} \sum_{n=0}^{\infty} \int_0^{\infty} \frac{J_0(u) \sin u}{(u^2 + \gamma_n^2)} \frac{du}{u} \quad (B.4)$$

where $\gamma_n = (n + \frac{1}{2})\frac{\pi}{\alpha}$. Since the integrand is an even function of u , we can write eq. (B.4) as

$$F(\alpha) = \frac{a}{\alpha} \sum_{n=0}^{\infty} f_n(\alpha) \quad (B.5)$$

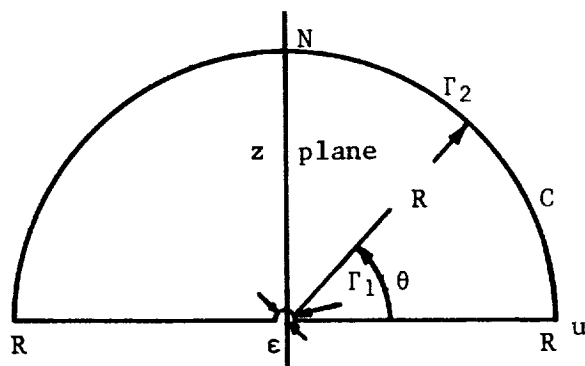
where

$$f_n(\alpha) = \int_{-\infty}^{+\infty} \frac{J_0(u) \sin u}{(u^2 + \gamma_n^2)} \frac{du}{u}$$

To evaluate the $f_n(\alpha)$ consider the complex integral

$$\int_C \frac{J_0(z) e^{iz}}{(z^2 + \gamma_n^2)} \frac{dz}{z}$$

where $z = u + iv$, and the contour C is a semi-circle in the upper half complex plane indented at the origin as shown.



By the theory of residues we have

$$\begin{aligned} \int_C \frac{J_0(z) e^{iz}}{(z^2 + \gamma_n^2)} \frac{dz}{z} &= \int_{-R}^{-\epsilon} \frac{J_0(u) e^{iu}}{u(u^2 + \gamma_n^2)} du + \int_{\Gamma_1} \frac{J_0(z) e^{iz}}{(z^2 + \gamma_n^2)} \frac{dz}{z} \\ &\quad + \int_{\epsilon}^R \frac{J_0(u) e^{iu}}{(u^2 + \gamma_n^2)} \frac{du}{u} + \int_{\Gamma_2} \frac{J_0(z) e^{iz}}{(z^2 + \gamma_n^2)} \frac{dz}{z} \\ &= 2\pi i \sum_n \rho_n \end{aligned} \quad (B.6)$$

where ρ_n denotes the n^{th} residue of the integrand within the contour. On Γ_2 (the large semi-circle) from the asymptotic expansion of $J_0(z)$ (11) we have

$$\begin{aligned}
e^{iz} J_0(z) &\approx z^{-1/2} e^{iz} \cos(z - \pi/4) \\
&= \frac{z^{-1/2} e^{iz}}{2} \left(e^{i(z-\frac{\pi}{4})} + e^{-i(z-\frac{\pi}{4})} \right)
\end{aligned}$$

Since on Γ_2 , $z = R(\cos \theta + i \sin \theta)$,

$$\begin{aligned}
|e^{iz} J_0(z)| &\leq \frac{1}{|z|^{1/2}} (e^{-2|z|\sin \theta} + 1) \\
&= \frac{e^{-2|z|\sin \theta}}{|z|^{1/2}} + \frac{1}{|z|^{1/2}}
\end{aligned}$$

Now $\sin \theta$ is positive in the interval $0 < \theta < \pi$ so that $e^{-|z|\sin \theta} \rightarrow 0$ as $|z|$ becomes large everywhere on the contour except possibly at $\theta = 0$ and $\theta = \pi$. Thus everywhere on Γ_2

$$|e^{iz} J_0(z)| < \frac{A}{R^{1/2}} \quad (\text{B.7})$$

where A is a finite constant and $R^{1/2} = |z|^{1/2}$. Then

$$\left| \frac{e^{iz} J_0(z)}{z(z^2 + \frac{1}{n})} \right| < \frac{A}{R^{7/2}} \quad (\text{B.8})$$

Since the length of the contour is πR , the integral over Γ_2 vanishes as $R \rightarrow \infty$ like $1/R^{5/2}$.

The only singularity of the integrand in the upper half plane is at a simple pole at $z = i\gamma_n$. The residue of the integrand there is

$$\frac{J_0(i\gamma_n)e^{-\gamma_n}}{-2\gamma_n^2} = -\frac{I_0(\gamma_n)e^{-\gamma_n}}{2\gamma_n^2} \quad (\text{B.9})$$

where $I_0(\gamma_n) \equiv J_0(i\gamma_n)$. Using the above results in eq. (B.6) gives the following preliminary results.

$$\begin{aligned} \int_{-R}^{-\epsilon} \frac{J_0(u)e^{iu}}{u^2 + \gamma_n^2} \frac{du}{u} + \int_{\Gamma_1} \frac{J_0(z)e^{iz}}{z^2 + \gamma_n^2} \frac{dz}{z} + \int_{\epsilon}^R \frac{J_0(u)e^{iu}}{u^2 + \gamma_n^2} \frac{du}{u} \\ = -2\pi i \frac{I_0(\gamma_n)e^{-\gamma_n}}{2\gamma_n^2} \end{aligned} \quad (\text{B.10})$$

On Γ_1 put $z = \epsilon e^{i\theta}$ $dz = \epsilon e^{i\theta} i d\theta$ to get

$$\int_{\Gamma_1} \frac{J_0(z)e^{iz}}{z^2 + \gamma_n^2} \frac{dz}{z} = \int_{\theta=\pi}^{\theta=0} \frac{J_0(\epsilon e^{i\theta})}{\epsilon^2 e^{2i\theta} + \gamma_n^2} i d\theta = -\frac{i\pi J_0(0)}{\gamma_n^2} = -\frac{i\pi}{\gamma_n^2}$$

for small ϵ , since $J_0(0) = 1$. Letting $\epsilon \rightarrow 0$ and $R \rightarrow \infty$, we obtain the result

$$P \int_{-\infty}^{+\infty} \frac{J_0(u)e^{iu}}{u^2 + \gamma_n^2} \frac{du}{u} = \frac{i\pi}{\gamma_n^2} - \frac{i\pi}{\gamma_n^2} I_0(\gamma_n)e^{-\gamma_n} \quad (\text{B.11})$$

Where the P denotes that the principal value of the integral is intended. On expanding the exponential in the integrand eq. (B.11) becomes

$$\begin{aligned}
P \int_{-\infty}^{+\infty} \frac{\cos u J_0(u)}{u^2 + \gamma_n^2} \frac{du}{u} + iP \int_{-\infty}^{+\infty} \frac{J_0(u) \sin u}{u^2 + \gamma_n^2} \frac{du}{u} \\
= i \left[\frac{\pi}{2\gamma_n} - \frac{\pi}{2} I_0(\gamma_n) e^{-\gamma_n} \right] \quad (B.12)
\end{aligned}$$

or

$$P \int_{-\infty}^{+\infty} \frac{\cos u J_0(u)}{u^2 + \gamma_n^2} \frac{du}{u} = 0 \quad (B.13)$$

and

$$f_n(\alpha) = \int_{-\infty}^{+\infty} \frac{J_0(u) \sin u}{u^2 + \gamma_n^2} \frac{du}{u} = \frac{\pi}{2\gamma_n} (1 - I_0(\gamma_n) e^{-\gamma_n}) \quad (B.14)$$

where the P has been omitted from the last integral since it exists in the ordinary sense.

From eq. (B.5)

$$F(\alpha) = \frac{\alpha\pi}{\alpha} \sum_{n=0}^{\infty} \frac{1}{\gamma_n^2} - \frac{\alpha\pi}{\alpha} \sum_{n=0}^{\infty} \frac{I_0(\gamma_n) e^{-\gamma_n}}{\gamma_n^2} \quad (B.15)$$

The first term is summable. From

$$\frac{\tanh \alpha u}{u} = \frac{2}{\alpha} \sum_{n=0}^{\infty} \frac{1}{u^2 + \gamma_n^2}$$

we have

$$\lim_{u \rightarrow 0} \frac{\tanh \alpha u}{u} = \alpha = \frac{2}{a} \sum_{n=0}^{\infty} \frac{1}{\gamma_n^2} \quad (\text{B.16})$$

Hence

$$F(\alpha) = \frac{a\pi\alpha}{2} - \frac{a\pi}{\alpha} \sum_{n=0}^{\infty} \frac{I_0(\gamma_n) e^{-\gamma_n^2}}{\gamma_n^2} \quad (\text{B.17})$$

Substituting the value of $\alpha = h/a$ and $\gamma_n^2 = (n + \frac{1}{2})^2 \frac{\pi^2}{a^2}$ gives

$$F(\alpha) = \frac{\pi h}{2} - \frac{h}{\pi} \sum_{n=0}^{\infty} \frac{I_0[(n + \frac{1}{2}) \frac{\pi a}{h}] e^{-(n + \frac{1}{2})^2 \frac{\pi a^2}{h^2}}}{(n + \frac{1}{2})^2} \quad (\text{B.18})$$

Using this result in eq. (2.2.19) and multiplying numerator and denominator by $2/\pi$ we obtain the result expressed in eq. (2.2.20). The function denoted by $G(\alpha)$ in section 2.2 is, of course, the second term on the right of eq. (B.18) multiplied by $2/\pi h$.

Appendix C

UNIDIRECTIONAL PERMEATION OF NITROGEN TETROXIDE

The permeability constant p is defined by the differential equation

$$\frac{dm}{dt} = \frac{A}{\ell} p \Delta P \quad (C.1)$$

where

m is the net mass transferred from time zero (a function of time)

$\frac{dm}{dt}$ is the net mass transfer rate (a function of time)

A is the area of the membrane (constant)

ℓ is the membrane thickness (constant)

ΔP is the pressure differential across the membrane ($P_H - P_L$)
(a function of time)

The pressure on each side of the membrane is a function of the volume, the temperature and the total number of mole of gas. The volume and temperature are fixed by the experimental conditions. The number of moles on each side however, varies with the mass. Using the high pressure side for example the relationship between pressure and mass can be developed. Defining:

T temperature, $^{\circ}K$

V_H volume on high pressure side, cm^3

R gas constant, $82.054 \text{ atm cm}^3/\text{g mole } ^{\circ}K$

P_H pressure, atm

n_1 g moles N_2O_4

n_2 g moles NO_2

n_T total moles ($n_1 + n_2$)

K_p equilibrium constant for reaction $N_2O_4 \rightleftharpoons 2NO_2$, atm
(defined by T)

m_H total mass of gas on the high pressure side, g

Perfect gas law

$$P_H V_H = n_T RT \quad (C.2)$$

Total Mass

$$m_H = 92.016n_1 + 46.008n_2 \quad (C.3)$$

$$m_H/46.008 = 2n_1 + n_2 \quad (C.4)$$

Equilibrium relationship

$$K_p = \frac{(P_{NO_2})^2}{P_{N_2O_4}} = \frac{(X_{NO_2})^2 (P_H)^2}{X_{N_2O_4} P_H} = \frac{(X_{NO_2})^2 P_H}{X_{N_2O_4}} \quad (C.5)$$

$$K_p = \frac{(n_2/n_T)^2 P_H}{(n_1/n_T)} = \frac{(n_2^2) P_H}{n_1 n_T} \quad (C.6)$$

The relationship defining pressure in terms of mass is derived as follows. Solving equation C.2 for n_T

$$n_T = \frac{P_H V_H}{RT} \quad (C.7)$$

and combining with equation C.6

$$K_p = \frac{n_2^2}{n_1} \frac{RT}{V_H} \quad (C.8)$$

Solving equation C.8 for n_1

$$n_1 = \frac{RT}{V_H K_p} n_2^2 \quad (C.9)$$

Substituting C.9 into C.4

$$\frac{m_H}{46.008} = \frac{2RT}{V_H K_p} n_2^2 + n_2 \quad (C.10)$$

and solving C.10 for n_2

$$n_2 = \frac{-1 + \left(1 + 8 \frac{RT}{V_H K_p} \frac{m_H}{46.008}\right)^{1/2}}{4 \frac{RT}{V_H K_p}} \quad (C.11)$$

Substituting C.11 and C.9 into C.2

$$P_H = \frac{K_p}{8} \left[\frac{4RT}{V_H K_p} \frac{m_H}{46.008} - 1 + \left(1 + 8 \frac{RT}{V_H K_p} \frac{m_H}{46.008}\right)^{1/2} \right] \quad (C.12)$$

A similar equation for the low pressure side may be written

$$P_L = \frac{K_p}{8} \left[\frac{4RT}{V_L K_p} \frac{m_L}{46.008} - 1 + \left(1 + \frac{8RT}{V_L K_p} \frac{m_L}{46.008}\right)^{1/2} \right] \quad (C.13)$$

Returning to equation C.1 the following definitions can be made

$$m_H = m_H^0 - m \quad (C.14)$$

$$m_L = m_L^0 + m \quad (C.15)$$

where m_H^0 is the total mass on the high pressure side at time zero and m_L^0 is total mass on the low pressure side at time zero.

m_H^0 and m_L^0 can be defined in terms of initial pressure using relationships defined in a manner similar to Equations C.12 and C.13. The differential Equation C.1 can be written now as follows:

$$\text{Letting } C_{1H} = C_{1L} = K_p/8. \quad (C.16)$$

$$C_{2H} = \frac{4 RT}{V_H K_p 46.008} \quad (C.17)$$

$$C_{2L} = \frac{4 RT}{V_L K_p 46.008} \quad (C.18)$$

$$\frac{dm}{dt} = \frac{A}{\ell} p \left\{ c_{1H} \left[c_{2H}(m_H^0 - m) - 1 + \sqrt{1 + 2c_{2H}(m_H^0 - m)} \right] \right. \\ \left. - c_{1L} \left[c_{2L}(m_L^0 + m) - 1 + \sqrt{1 + 2c_{2L}(m_L^0 + m)} \right] \right\} \quad (C.19)$$

This equation was solved numerically with various values of p using Milne's method to define $m = m(t)$. A computer program incorporating the solution of the equation and the generalized least squares determination of p was written for the analysis of the experimental data.